EMERGENCE AND STABILITY OF COMPLEX STRUCTURES FROM STOCHASTIC NEURONAL NETWORKS

BY

NANA ARIZUMI

DISSERTATION

Submitted in partial fulfillment of the requirements
for the degree of Doctor of Philosophy in Computer Science
in the Graduate College of the
University of Illinois at Urbana-Champaign, 2012

Urbana, Illinois

Doctoral Committee:

Adjunct Assistant Professor Todd Coleman, Chair
Assistant Professor Lee DeVille
Associate Professor Luke Olson
Professor Michael Heath
Professor William Gropp
Professor Mark Nelson

Abstract

A single neurons connectivity is the key to understanding the network of neurons in the brain. However, it is already a complicated system and many different approaches to understanding it have been taken over the years. One way is from anatomical study, which is to observe the morphology of each neuron and the organization of the neuronal connections. Another way is from physiological study, which describes the specific electrical outputs of the cells. Computational studies have been developed to fill the gaps between these studies. There are several stochastic computational models, but none of them is easy to analyze quantitatively and typically, the analysis resorts to simulations. Many of the previous studies were focused on physiological structures through Monte Carlo simulations, not on the model itself. This thesis introduces a general purpose stochastic model with mathematically rigorous assumptions, so that analysis of the model itself using a Markov chain is applicable. With specific input stimuli and parameters, the model demonstrates rich properties, such as selectivity of input structures and competition between input neurons. This method provides a well-positioned balance between neuro-biological relevance and theoretical tractability. The model is first studied quantitatively to prove theorems about the existence of a controlled Markov chain over an appropriate time scale. Using the Markov chain makes it possible to show the existence of an invariant measure with some convergence rates. In this context, other theorems are introduced to shed insight beyond the simple phenomenological approaches with simulations that others have developed. Then the system is studied qualitatively by simulating the neuronal physiology of visual neurons, which uses more complicated assumptions. This shows the emergence of direction and orientation selectivity, as the visual neurons properties. Hence, this selectivity could be an epiphenomenon of the assumptions chosen for the models. The key insight here is that the model

shows a robust phenomenon to the initial condition, but not to the input stimulus, which implies the importance of the initial condition and the noisy inputs. These dynamics may explain learning and reinforcement of the visual neurons and could predict results in future experiments.

Table of Contents

Part I

Introduction of Computational Neuroscience

Chapter 1

Introduction

1.1 Introduction

The brain is a complex system with many interacting stochastic components across many temporal and spatial scales. Through the study of neuroscience, it is known that the brain is a dynamically changing stochastic network of neurons. Anatomical study describes the morphology of each neuron and the organization of neurons. Physiological study, via single-unit recording, describes the specific outputs of the cells. The connectivity between neurons is difficult to observe, but the outputs from a single neuron indicate the existence of complex circuits that cannot be explained from simple predictionComputational studies have thus been developed to fill the gaps between anatomical and physiological study. There are several models which have been proposed to explain various properties of the brain over the years. Many of these models assume hard-wired neurons, without considering the development of the network. These models cannot encapsulate the possibility of modification through different inputs. In addition, these models have a stability problem, wherein if one neuron dies then the adjusting networks lose their structural properties. This is not the case in an actual neuronal circuit. We can address these problems through use of models with synaptic plasticities, i.e. the modification of chemical synapses between neurons. Recent experimental results have led to the formulation of well-regarded models of plasticity between neurons. Using a computational model, we can address the emergence of the properties from an abstract network with plasticity. If the model has enough abstraction then we can explain several properties from a single modeling framework.

Neuroscience has always had models to explain the nervous system. The introduction of com-

putational models expands the understanding of these older models of mathematical formulation, that otherwise could not be analyzed. One notable success of simulation using plasticity is the understanding of the specific neural network emergence, which could not be predicted without the help of large scale computation. The development of these properties has not been studied systematically in previous works, so we introduce a framework to understand the network of neurons that can develop and modify itself using a Markov chain. The model we present has a stable distribution that explains and accounts for the several classical network models which in turn explain various physiological properties. Via Markov chain analysis, we can study these stable distributions and learn their rate of convergence and stability conditions. We choose to use a Markov chain because it can retain the salient dynamical features, yet is perhaps simple enough to analyze. We believe this framework is a good balance between the neurobiological relevance and theoretical tractability.

1.2 Basic computational neuroscience

The basic component of the network that represents the brain is called a neuron, which is an electrically excitable cell. The neurons receive electrical signals from other neurons or exogenous stimuli through synapses, which translate chemical signals to electro signals. Typically, neurons have a cell body called a soma, dendrites, and an axon. The dendrites extend several branches toward other cells and the axon is a long filament that can also branch out. The neurons receive inputs from dendrites and outputs come from the axon. A typical neuron has an action potential that causes a spike from the electrical membrane potential of the cell depending on the input signal from synapses. There are two types of signals: one excitatory and the other inhibitory. The conceptual drawing of a single neuron is in Fig. 1.1.

We can use two kinds of experimental data to observe a single neuron. One is from the anatomy which tries to see the morphology of the neurons. The other is from electro-physiology in which a stimulus is given to the neuron and the responses are recorded from the other neurons. Electrophysiology is also divided into two different sections. One is in-vitro in which the neuron is outside of the living organism, so that the observer can give the electro signal directly into the system.

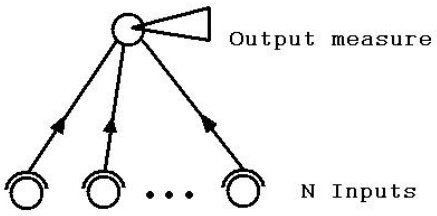

Figure 1.1: basic single neuron model with N synapses

The other is in-vivo which uses a single unit recording from living organisms, so that the observer can give biological stimuli to a subject. Electro-physiology in-vivo allows us to observe several interesting properties and electro-physiology in-vitro gives numerous mathematical models of each neuron. However, observation from the anatomy is more complicated. Specific connection of pre- and postsynaptic neurons network cannot be decided from this method at this point. The problem here is that we do not know the specifications of the circuits (anatomy), but we know the result (physiology). The computational model is connecting these two sets of data. We can consider the brain as a computational system of a network. The simulations of the circuits which do not contradict the anatomy information, but do not produce the expected biological property, can be eliminated, because we can conclude that the brain does not have these circuits. On the other hand, if our model produces the results as we expect and the model is simple enough, then it is likely that the circuit is the essence of the specific property. These assumptions lead the rapidly evolving field of computational neuroscience. In recent years, the model of synaptic plasticity has been constructed through electro-physiology. Including the idea of plasticity in the computational model, we can study the emergence and the development of the networks, which cannot be observed through classical experiments.

1.3 Synaptic plasticity

Synaptic plasticity is caused by the modification of chemical synapses, which is mainly observed by a phenomenon called long-term potentiation (LTP) and long-term depression (LTD). LTP is the long-lasting enhancement in signal transmission which occurs in synapses, and LTD is the long-

lasting depression in signal transmission. Both of these phenomena can last for hours and sometimes days. Therefore, these are the main candidates for the cellular mechanism of long-term memory and learning. LTP was first observed by Lømo and published in 1966 [91]. LTD was predicted in the 1960's but the technical difficulty of measuring inhibition caused its observation to be delayed until the late 1970's. Levy and Steward published this observation in 1979 [87].

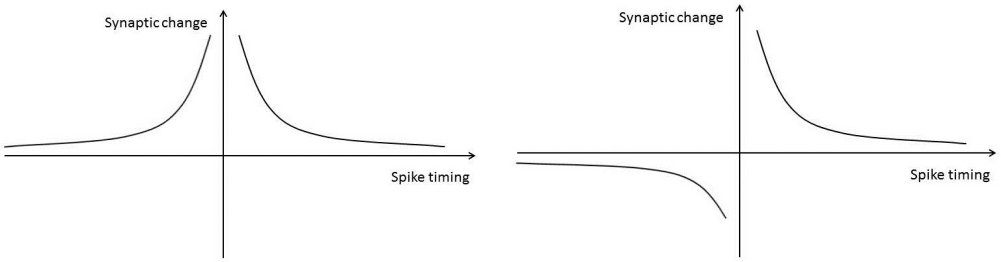

(a) Hebbian plasticity **(b)** STDP plastiticity

Figure 1.2: Window function

The plasticity of the neurons is believed to be the functionality behind the emergence of networks and it has been predicted since the late 1940's onward with Hebb's rule [60]. Hebbian learning uses the correlation between firing of pre- and postsynaptic neurons. It is usually summarized as "Cells that fire together, wire together." This was the classical explanation given to LTP and LTD. Several experiments confirmed this idea of correlated firing rate and long term changes in the synapses [39, 55, 88]. The idea of Hebbian learning is time symmetry over the difference of pre- and postsynaptic spikes as shown in Fig. 1.2a. However, Markram et al. observed that the synaptic strength was greatly weakened by presynaptic spikes, which came shortly after postsynaptic spikes. This work was published in 1997 [92]. Bell et al. also observed that the excitatory postsynaptic potential increases if the presynaptic spike happens before the postsynaptic spike and decreases if the presynaptic spike takes place after the postsynaptic spike. This work was also published in 1997 [13]. This was confirmed by several experiments in-vitro [14, 40, 45]and in-vivo in the Xenopus visual system [113, 162, 177] and rat visual system [108]. This led to a temporally asymmetric spike-timing-dependent plasticity (STDP) model. The main difference between Hebb's learning and the STDP is the time-plasticity window function, which takes the difference between pre- and postsynaptic

spiking time and returns the change of synaptic weights. The conceptual drawing of the window function is in Fig. 1.2. If presynaptic spikes happen after a postsynaptic spike, the STDP window function returns a negative synaptic weight as shown in Fig. 1.2b. The STDP window function is different for each neuron and is not always an odd function either. The important feature is that the temporal asymmetry can cause competition between synapses [151], which cannot be achieved by pure Hebbian learning [109]. There is ample evidence supporting the idea of an STDP model as the plasticity rule that can explain both LTP and LTD.

1.4 Computational Model studies

Even a single neuron is complex and has many models [63]. The simplest of all is the integrate-and-fire model, which has been studied since the early 1900's [82]. A neuron can be considered as a capacitor and once the membrane voltage reaches the threshold, then the output neuron fires. The influence of the presynaptic neurons does not decrease over time in this model. This shortcoming is accounted for in a leaky integrate-and-fire model, which adds a leak term in the voltage. This model still does not encapsulate the whole chemical and electrical synapses in the systems. There are many models that include specificity of neurons, however an actual neuron is a dynamical system with ionic conductance and a complicated morphology that cannot be fully described by a simple model. Even so, we need to choose a simple model so that it is feasible to analyze and evaluate. "Identifying the minimum set of features needed to account for a particular phenomenon and describing these accurately enough to do the job is a key component of model building" ([1]).

Model studies with STDP have started in recent years. The STDP rule is a fast time scale rule and is applied to individual groups of pre- and postsynaptic neurons, so it is easy to simulate on computers. The STDP model shows emergence of several properties, such as directional selectivity of the visual system and the hippocampus [25, 106, 144] and the orientation selectivity of the visual system [12, 175]. Using a simple model of constant firing probability, competition between presynaptic neurons emerges [151], and using the Fokka-Planck formulation, the equilibrium synaptic distribution in the final time can be induced [132]. Adding a time-varying presynaptic firing

probability, the STDP rule induces a good model for a fast time scale simulation.

The theoretical work of the stability, which explains the memory in the system, has been under emphasized in previous studies. The STDP can select particular mechanisms, but the issue of its maintenance is not trivial with the dynamically changing inputs. We introduce the Markov model analysis to investigate this problem. Because our simple plastic model can explain several properties, we can expand our stability analysis to the actual physiology.

1.5 Our approach

The goal is to introduce an abstract network with plasticity, so that we can propose quantitative analysis of the neuronal stability. The network with plasticity can become one of several stable distributions, which could explain different properties of biological physiology. For example, there is a property called directional selectivity (DS) in the visual system, which prefers one direction of movement in front of the eyes. One of the classical explanations is from the asymmetry in the network by Barlow and Levick [9]. The schematic is shown in Fig. 1.3, where the red arrows show the inhibition and the black arrows show the excitation. If the stimulus comes from the opposite of a preferred direction (called null direction) then the inter-neuron inhibits the output neurons before it gets excited. The reason behind this network was not the focus of the model. This asymmetry can be explained further by the competition of input neurons through STDP. If the network receives directed inputs, then it goes to a stable state as shown in Fig. 1.4, where the asymmetry of the network is caused by the strength of the synapses.

If the network is abstract enough, then many models can emerge. We have observed several stable distributions from this abstract model, some of which could qualitatively explain actual physiology. Continuing this pass with more neurons, following organization of anatomy, it should encapsulate more biologically feasible models. Specifically, a network to explain the visual system gives insight into the cortex and to the general neocortex.

To quantitatively understand the stability of the emerged model, it is important to introduce a mathematical formulation. We focus on Markov chain analysis, where we can find a stable

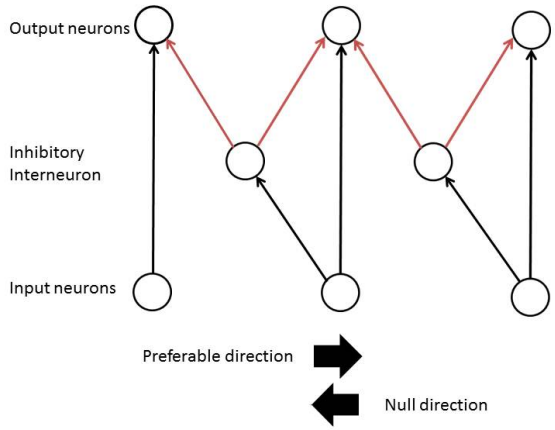

Figure 1.3: Classical Barlow and Levick's model

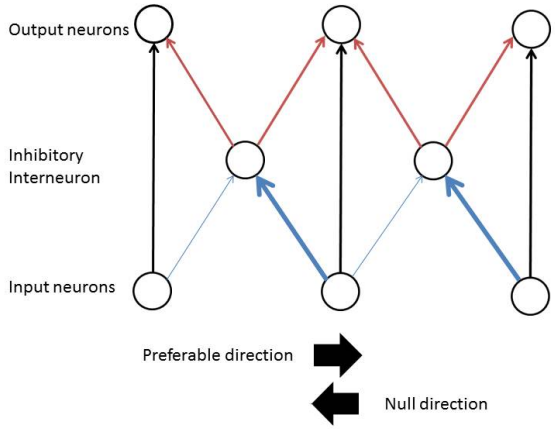

Figure 1.4: Emerged Barlow and Levick's model from STDP

distribution through invariant distribution of Markov matrix. Finding the eigenvalues of the Markov matrix can tell the stability of the whole system. The problem here is that the matrix becomes exponentially larger as the number of input neurons grows. Therefore, it is important to study the reduced problems. We have shown that some of the reduced problems still hold the interesting properties with smaller state space.

1.6 Thesis Outline

The thesis is divided into three parts. The first part is the introduction of computational neuroscience with an emphasis on neuronal physiology. The second part shows our approach and introduces our model. Also, it shows the basic structures that the model can produce. Rigorous mathematical study and the detailed structural study are in the third part. In detail, we start with an introduction in chapter 1, where we explain basic computational neuroscience and its importance, synaptic plasticity, STDP, and model studies. After that, we introduce our approach to the system. In chapter 2, we explain why the model is interesting by showing a specific part of the nervous system that has interesting properties of selectivity. The physiology we are interested in is observed by single cell recordings, so the focus is on the visual system and the limbic system, where the hippocampus is. Then, in chapter 3, we introduce a general model for STDP with definitions and assumptions. In this chapter, we show the model is in fact a Markov Chain. Also, we introduce the definition of the community formation. In chapter 4 we give specific rules for the assumptions and show the preliminary results from these rules. To study these results in chapter 4, we use the Markov Chains introduced in chapter 3. However, the state space is too large to deal with. Therefore, we perform space reductions in chapter 5. To do this, we show that a system with two different assumptions is also a Markov Chain. We examine specific cases of one dimensional constant time stimulus. First, we study the case where STDP modify the conductance level whenever the input fires but no modificiation otherwise (case 1). Second, we study the case where STDP modify the conductance level whenever the output fires but no modificiation otherwise (case 2). In case 1, we show the system is a Markov Chain and then study the properties of invariant distribution, i.e. the conditions for variables that produce the community formations. Also we study the eigenvalues of the Markov matrix to understand the convergence rate of the invariant distribution. In case 2, we show the system is a Markov Chain, and using the symmetry of the system, we show the smaller size Markov Chain can represent the same system. In the large network limit for case 2, we show the invariant distribution is in fact a convex function and represents community formation. In chapter 6, we study the one dimensional moving stimulus case using numerical analysis. Then we look at

more specific cases of two dimensional visual models, which show the properties of orientation- and direction-selectivity from specific stimuli. The conclusion and future directions are given in chapter 7.

Chapter 2

Relative Nervous System

2.1 Introduction

To understand neuronal circuits, we need to focus on the specific properties we can observe through the single-unit recording. The visual system and hippocampus/Entorhinal cortex (EC) are popular central nervous systems to study because of their simplicity in organization and the well-known functionality. The model studies are based on the large amount of experimental physiological data. The visual system interprets visual information received as light signals through the eyes. The Hippocampus/EC is a part of the brain that processes memory and spatial navigation. Each cell in the system has properties of its own. If we know the organization of the input stimulus then we can hypothesize the network. The visual system is topographically organized in the different parts of the brain: the stimulus in front of the eyes moves from one point to the other, while the corresponding cells in the visual system change continuously from one part to the other part of the cortex. For the Hippocampus/EC, there are still debates as to whether inputs are topographic or not. However, from the single-unit recordings, several input signals are induced. Since both the visual system and the Hippocampus/EC have been studied for a long time, there are numerous network models to explain each biological physiology. We would like to introduce an abstract model with plasticity, so that these classical models can emerge from our models. In fact, animals have "critical periods" for distinct visual mechanisms [62], and the assumption is that the STDP rule is the functionality behind the development. Even after development, an environment may change and the system may have been damaged within. The matured visual system can deal with input loss [76]. Also, the Hippocampus/EC can adapt to the new environment rapidly [56, 170]. These

modifications of the network could be explained through the STDP models.

2.2 Visual system

The visual system receives light signals with the eyes and processes the information in the cerebral cortex, which is the outermost layer of neural tissue of the cerebrum. The part focusing on the visual system in the cerebral cortex is called the visual cortex, which is in an evolutionarily recent part called the neocortex. All mammals have a neocortex which is a similar six-layered structure. The uniformity of the anatomical structure leads to the hypothesis that the neocortex performs the same basic operation using different inputs, which creates the different output [37, 95]. In fact, rewiring of a ferrets visual inputs to the auditory cortex during the developmental stage, led to the emergence of visual functions in the auditory cortex [141, 163]. The study of the visual cortex should help the understanding of the other part of the neocortex.

To study visual systems, we should start from understanding the anatomy. The light stimulus is translated into chemical and electro signals in the photoreceptor cells in the retina. The photoreceptor cells then send this information to horizontal and bipolar cells in the retina. Horizontal cells connected to the bipolar cells send information to retinal ganglion cells and amacrine cells, which send signals to ganglion cells. The ganglion cells become an optic nerve and send information to the lateral geniculate nucleus (LGN) which sends information to the visual cortex, called the primary visual cortex (V1). The visual cortex is divided into V1, V2, V3, V4, and V5. There are two main streams of visual pathways in the visual cortex. One, called the dorsal stream, is from V1 and goes to V2 then to V5, which is associated with motion, representation of object location, and eye-hand coordination. The other one, called the ventral stream, is also from V1 to V2, but then it goes to V4 and is associated with form recognition and object representation. Even though the information from the eyes are directly connected to LGN and LGN is directly sending information to V1, LGN and V1 receive information mainly from other cortical areas [5, 85, 124]. The conceptual drawing of the visual system is in Fig. 2.1

To understand the physiologies of cells in systems, experiments with single-unit recording are

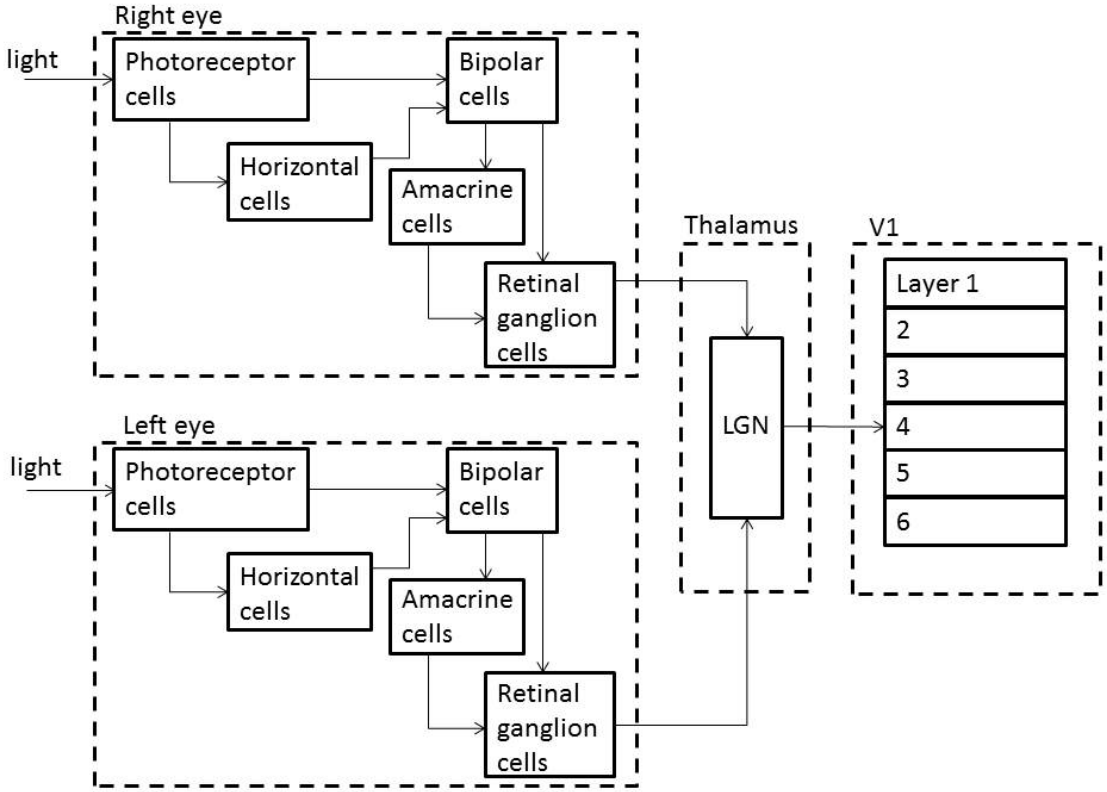

Figure 2.1: Visual circuit

useful. Each cell has a receptive field, which is a region that can affect firing of the cell by a stimulus. The receptive fields of the ganglion cells in the retina are of the on-center and off-center physiological type. On-center cells react to light on the center of the receptive field which is surrounded by no light sub field. Off-center cells react the other way around. This was first observed in the 1950's [81]. Bipolar-cells also have these types, and the measurement of the center is the size of connected photoreceptors' receptive fields. The surrounded section is believed to come from the horizontal cells. These properties of bipolar cells are the case of a wired network, since they appear before the eyes are open for the first time at birth [32, 35, 43]. LGN cells also have on-center and off-center types, but an animal's center shape has a slight tendency toward one orientation [152, 160]. The cells in V1 consist of simple and complex cell types. Both simple cells and complex cells prefer one orientation, and respond to oriented bars and gratings. This property is called orientation

selectivity (OS). Simple cells have a fixed excitatory and inhibitory sub field, but the complex cells do not have these and respond to larger receptive fields. These were first observed by Hubel and Wiesel [69, 70] in the later part of the 1950's. If the receptive field receives moving bars on the specific orientation, both simple and complex cells prefer one direction [69]. This property is called direction selectivity (DS) and has been observed in several regions of the visual system, i.e. ganglion cells in the retina of rabbits [8], mice [176], and pigeons [100], as well as frogs' tectum [83].

2.2.1 Model study of direction selectivity

There are many models to explain DS. One is from asymmetry of the receptive field observed in the simple cell [70], but not all the DS simple cells have an asymmetric receptive field. Furthermore, this does not explain DS in the complex cell. However, cortical connections could expand asymmetric DS to the other neurons, which is modeled with STDP in [144, 166]. Barlow and Levick expanded asymmetry to each cell in the network, which uses inhibitory innerneurons in 1965 [9]. This way, the complex cells and the retinal ganglion cells can also have directionality. Another explanation is from a non-separable spatio-temporal receptive field [4, 165], which was published in 1985. This was anatomically explained in 1990 [135] by lagged and non-lagged cells in LGN, which can be emerged using rate-based Hebbian learning [171]. There are several network models with STDP that produce an asymmetric receptive field [25, 140, 144]. Before STDP was experimentally shown, many of the models with emergence were based on the short-term synaptic depression models [33, 143]. The asymmetric receptive field model is especially important to the development of Xenopus retinotectal systems, since its receptive field can be trained to become asymmetric DS which was first observed in 2002 [44]. Further experiments on Xenopus show that blockage of GABAergic transmission alter STDP [130], which shows the importance of inhibitory neurons. This particular Xenopus experiment is modeled with inhibitory innerneurons in [68].

DS of mice's and rabbits' retinal ganglion cells emerge even in dark-reared animals [32, 35, 43]. On the other hand, ferrets require early visual stimuli [89]. DS in retinal ganglion cells is induced by inhibitory inputs, since losing an inhibitory transmitter causes no DS [30, 79]. Starburst amacrine cells, which are inhibitory interneurons, could be the source of GABA [123]. Starburst amacrine cells

do not have axons, instead the dendrites synaptic site has both input and output features. Action potential in the dendrite is suppressed by local application of GABA [174]. Starburst amacrine cells also have DS that provides more inhibition with null direction, which is the opposite of the preferred direction of the ganglion cells [50]. This may cause the DS in the ganglion cells, however laser ablation of starburst cells of rabbits did not erase DS [59]. Though, removing starburst cells of mice using a neurotoxin did erase DS [176]. Before the first eye opening, the retinal waves are the main stimulus in the retina. It is believed to have a important role for the development of retinal circuits [173]. In particular, it activates starburst amacrine cells during first and second postnatal weeks [164, 178]. The retinal wave is directional and has significant bias in wave propagation in first postnatal week [153], so this could lead to the DS network. However a recent experiment showed that DS in the ganglion cell was not dependent on the propagation direction [42]. Still, more detailed experiments are necessary to understand the network in the retina.

2.2.2 Model study of orientation selectivity

Hubel and Wiesel proposed that OS is derived from the oriented arrangement of the input neurons [70]. This model only requires feed-forward excitatory inputs from LGN cells. Cross-correlation experiments show that the simple cell's sub field overlaps similar response type with connected LGN cells on-center and off-center receptive fields [6, 129, 154]. Oriented connection was confirmed experimentally, however this is not the only factor for the origin of OS. In fact, it has been shown that removing inhibition causes significant decrease of OS [145, 157]. Also, the feed-forward model is insufficient to explain the contrast-invariant width of orientation tuning [138, 146]. In the simple cell experiments, if the contrast of stimulus become greater, then the firing rate increases, but the width of the preferable orientation is invariant. However, the width of the tuning curve increases as the threshold of firing increases with the feed-forward model, this issue is called the iceberg problem. The easiest way to fix this problem is to modify the threshold for each contrast, but experiments show that the threshold is invariant with contrast [31]. If the feed-forward model has inhibition in the preferable location, then a stimulus at the non-preferable location gets more inhibition and the model has contrast-invariance [155]. The ratio of inhibition and excitation

strength becomes important in making the correct OS. This model is called push-pull inhibition and was first discussed in [70] without going into the significance of contrast-invariance. There are recordings of inhibition in the simple cell sub fields and they tend to be the largest in the preferable orientation [7, 17, 46, 61, 66, 97, 111]. The inhibition is thought to be used for orientation tuning. However no physiological evidence for feed-forward inhibition from direct physiological experiment was found [48, 96, 148]. It is more likely to have inhibitions from intercortical connections [155, 156]. There are several models of OS with inhibitory inputs [47, 49, 148, 149, 161]. These models assume that the inhibition is recurrent from the cortex and/or feed-forward from the interneurons, which could come from the thalamus or other part of the cortex. Recurrent network models with STDP were proposed to explain development of OS [12, 175].

2.2.3 Column structure in visual cortex

The cortex is like a 2mm thick sheet on top of the cerebrum. Neurons with similar functionality are grouped vertically from the surface, which is called a cortical column [112]. In the visual cortex, preference for the left or right eye is organized in ocular dominance columns, first observed in a macaque monkey [72], and also observed in humans [67]. In cats, the pattern is less regular [86] and rodents and squirrel monkeys do not have this structure [2, 3, 53, 158]. Orientation columns were first studied by Hubel and Wiesel [70, 71], and they proposed an ice-cube model in which the orientation preference is gradually changing slabs which are intersecting with several ocular dominant columns. Using optical recording experiments, the ice-cube model was modified with a pin-wheel model [16]. The orientation columns are not organized in parallel but have many different organizations of columns including a point at which all the orientations come together like a pinwheel. The ocular dominant columns are closer to the original ice-cube model and intersect orthogonally with the orientation columns. The property of OS is different in the center of the pinwheel in that the response amplitude between preferred and non-preferred orientation is less than the iso-oriented domain [137]. There is also an organization, that is shorter than the columns, called blobs, which prefer color [90, 172].The theoretical one-dimensional feed-forward model with STDP shows that two different correlated inputs are given then the conductance chooses one of

correlated inputs to be the maximum and the other to be minimum [150]. This could be the origin of the competition of the ocular dominance columns. The same model with additional recurrent inhibitory inputs with STDP shows organization of the same preferable location and adding one more layer shows the tuning of the preferable location [150]. A recursive two-dimensional model with STDP also shows a pinwheel structure [166].

2.3 Hippocampus/Enthorhinal cortex

The hippocampus is the brain structure, which plays an important role in short term episodic memory and spatial navigation. It is in the limbic system and lies beneath the cerebral cortex. The functionality of the hippocampus was first discovered through patient H.M., whose hippocampus and neighboring medial temporal structures had been removed. H.M. was widely studied beginning in 1957 [139]. His case helped advance the theories of memory. Through animal testing, significant improvement occurred after the discovery of the"place cell" in 1971 [119]. The place cell is a cell in hippocampus that reacts if the animal is in one or sometimes two preferable locations. It was first discovered in rats, but later a similar property was discovered in humans [41]. This is a key feature for animals to integrate self position, which is a known property of animals from Darwin's time and referred as "path integration" in recent years. Animals can return directly to their starting points even without visual signals. This shows that the animals have mechanisms to integrate linear and angular self-motion [10, 110]. The place cell can form a cognitive map of the environment [120] and an animal can use this to navigate itself. Furthermore, removal of rats hippocampus causes severe navigational memory loss [136]. In 1993, the "phase precession" effect was also discovered [121], which explained the relationship between the EEG theta wave and the place cell firing. The spikes in the place field advance progressively during the theta-cycle as rats run through the field. This shows that the animal can integrate self-position even within the place field.

The hippocampus is older and more primitive than the neocortex and has only three layers. This is another reason why we should study the hippocampus contrary to the more complicated six layered neocortex, which includes the visual cortex. The inputs of the hippocampus are mainly

from the second and third layer of the entorhinal cortex (EC). The dantate gyrus (DG) in the hippocampus receives information from the second layer of the EC (EC II) and sends information to CA3, which further sends information to CA1. CA1 and CA2 receive information from ECII and the third layer of the EC (ECIII) accordingly. The DG and CA3 have many lateral connections. The output of the hippocampus is mainly from CA1 and information travels to the subculum, which also receives information from the ECIII. A conceptual drawing of the Hippocampus/EC circuits is in Fig. 2.2.

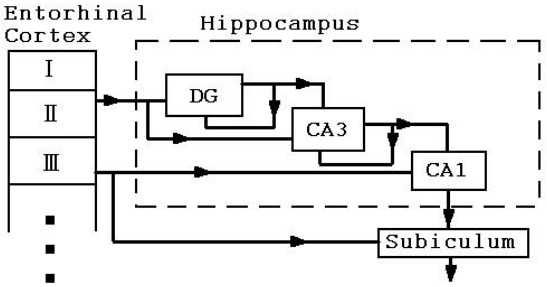

Figure 2.2: basic circuit of hippocampus

The DG is mainly constructed by granule cells, while CA1 and CA3 are constructed of pyramidal neurons. The DG, CA1 and CA3 all have place cells. Even cutting a pathway between CA3 and CA1 does not erase the place cells of CA1[22]. Because of this, it is believed that place cells originate in the EC. "Grid cells" in the EC, which were discovered in 2005 [56], preferred locations, which are organized as vertices regular triangle grids. It also has a phase precession effect [57] like the place cells. The spacing between grids and size of the preferable location increase monotonically from the dorsomedial pole to ventrolateral positions [23, 56], which can be speculated from the place cell properties that the size of place fields increases and sharpness of signal to noise ratio decreases toward ventral pole from dorsal pole [75]. From this the place cells could be emerged from a combination of grid cells [131, 147]. However, the memory loss after removing the EC is not always severe [52, 116, 136].

The EC is located in the medial temporal lobe, which is divided into the lateral entorhinal cortex (LEA) and the medial entorhinal cortex (MEA). The grid cells are located in the MEA, which is closer to the hippocampus. The EC has six layers. Both the MEA and LEA are inputs to

the hippocampus, and receive inputs from CA1 in layer five. The main inputs to the LEA are from the perirhinal cortex (PER) and the inputs for the MEA are from the postrhinal cortex (POR). Both receive inputs from parahippocampal cortices. More specific anatomy is in the review [159]. Many of the inputs of the EC deal with some sort of sensory information, and may have spatial selectiveness. More than half of the POR exhibits positional correlation [28], and one third of the PER also has spatial selection [29].

There are significantly, many close relationship with the visual systems properties [104]. A good example is directional selectivity. As with the visual system, the place cell has a selectivity of for the animal's movement. ECIII, ECV, and ECVI also have direction selectivity [134]. They have a property of both grid cells and head direction cells, which activate only if the animal has a specific head direction in the environment, not related to body position. The head direction cells are in several parts of the brain, and are likely to be one of the inputs to the hippocampus/EC system. On the contrary, ECII does not have directionality [134].

2.3.1 Properties of place cell and grid cell

We need to consider some measuring parameters for the place cells and the grid cells. Both need to measure the size of the preferable location and the spatial phase for displacement relative to an external reference point. Grid cells also need to measure the spacing between fields, and the orientation of the grid related to an external reference axis. Neighboring grid cells have similar size, spacing and orientation [56]. However, the spatial phases of place cells and grid cells are distributed [51, 56, 170].

The place cells can have a place field in different environments [118], and if the animal stays in the same environment the place field will be stable for days [115]. However, if the environment is modified, then the place field may disappear in a second or appear in a different place [114]. It is strongly dependent on the distal cue. When rats are moving in a circular cylinder, a rotating circumferential cue causes the same rotation in the place cell [114, 118, 122]. The grid cells also rotate with landmark rotation [56]. This rotation is related to the head direction cells. If the rotation of cue causes the place cell to rotate, then the thalamatic head direction cells also rotate

[80]. If the grid cells have a directionality and rotate with the cue card, then the directionality also rotates [134]. If the distal cue is removed from the familiar environment, place cells and grid cells do not change their preferable location [56, 114]. Moving from the cylindrical environment to a rectangular environment cause half of the place cells to lose the place field and the other half to have an unpredictable place field [114]. On the other hand, the grid cells keep size, spacing, and orientation, but change their spatial phase [51]. If the environment is smoothly transformed to the familiar environment from the familiar environment then the place field also gradually changes to the well-learned end representation [84]. An extension of the edges of the environment also stretches or splits the place field [117]. The grid fields are also distorted by the extension of the edges [11]. If the environment's light is removed, then the place cells keep the same place field [102, 125], but are less reliable [93]. The grid cells also keep preferable locations in the dark environment and decrease spatial correlation of the rate map [56]. Rats were released from a movable box in a linear track with a fixed goal. When changing the position of the box, in the beginning the place field was related to the distance from the box, then later modified to a fixed position related to an external landmark [54, 128]. Also, the place field can be modified through reward, even if the environment is same [94, 103].

How the place/grid cells achieve a stable state in the new environment is an interesting question. It was first addressed by Hill using twelve place cells [64]. Ten of them had a firing field in a new environment without learning, and two of them learned within ten minutes. Other experiments were done using black and white cue cards in a cylindrical environment [18]. After changing cue cards, the place field change does not come abruptly. Using ensemble code to record several place cells from the same experiment improved the outcome, that the animal's place field is less robust in the first ten minutes but improves rapidly [170]. The grid cells also have the same property that, that the spatial correlation is weaker in the early stage of environment modification [56]. For the linear track experiments, the place field expands and the center of mass shifts opposite to the animal's movement in the first few laps [105, 106].

2.3.2 Model study of place cell and grid cell

The inputs to the hippocampus and the EC system are not as clear as the visual systems inputs. This is one of the reasons why modeling is difficult. There are also arguments about where the path integration exactly occurs. The inputs of the hippocampus and EC are highly integrated stimuli, and thus may already contain information about speed and orientation of self-movement. Further analysis of the place cell through phase precession experiments produced several models with inputs. The oscillatory interference model considers inputs as several waves with different frequencies, so that the combination of these causes the phase precession. It was first introduced in the one dimensional case [121]. Theoretical study was done by [73]. A two dimensional model was introduced with preliminary computational experiments [27]. Different ways of combining waves were introduced by [26]. The computational analysis of this model was done by [74]. The model assumes that the dendrites have different oscillations and that the soma's membrane potential oscillations do synchronize with the theta-wave [77]. The model assumes both dendrites and the soma are dependent on their speed and the angle relative to a reference point. The model uses a few inputs, considering large scale self-organization [74]. the animal runs through the environment the corresponding dendrites are stimulated systematically. One piece of evidence is that the phase precession occurs even with non-spatial behavior of rats moving in a wheel [58]. The other is that there is asymmetry of spike numbers within the place field. Combining this asymmetry with theta-wave could be the source of the phase-precession [58, 107]. However, [73] reported that this asymmetry was not observed. The grid cells have this kind of asymmetry of the field [57], and both models can explain the grid cell properties.

2.3.3 Direction selectivity

Direction selectivity in the place cell was first observed in linearly moving rats in 1983 [101]. For randomly moving animal's 20% of the place cells have direction selectivity [94]. There are several models for DS, since it can be extended from the visual system DS. There are several theoretical models using attractor dynamics without going into explicit network of neurons [127, 133]. The

place cell can be considered to hold directionality and unsupervised Hebbian learning with recurrent connections can remove this property [24]. Also, the STDP rule can produce asymmetric receptive field [106] as the case of the visual system.

Part II

Model Study and Preliminary Results

Chapter 3

An Abstract Model Of A Single Neuron

3.1 Introduction

We have chosen a simple single-neuron model in which the postsynaptic neuron follows the leaky integrate-and-fire model and the STDP rule for the plasticity between neurons. Neurons are connected with other neurons by synapses, so for simplicity we consider N synapses connecting N different presynaptic neurons, all of them with the same dendrite conditions, as shown in Fig. 1.1.

In this section, we start with addressing all definitions for modeling, then give general assumptions. Using these definitions and assumptions, we show the system is in fact a Markov chain. Then, we set the specific conditional probability rules that follow those assumptions. We simulate the system with these rules and show the emergence of community formation and place selectivity. We analyze the emergence of community formation by reducing the state space, because large state space is not feasible to study. In the reduced case, the conductance level is modified given the input neuron's firing or the output neuron's firing. In both cases, we show analytically the emergence of community formation. We also show numerically that it takes a long time to converge to the invariant distribution, and also there are long-lived distributions that are not invariant.

The previous works [78, 98, 99, 150, 151] assume the convergence. We point out potential pitfalls of numerical analysis. Observing one or even many numbers of realizations can be different from the total distribution, because stability is only observed with the distribution not from the states. To see the distribution from one realization, we require infinite number of input neurons, but that also causes infinite influence in the output neuron. Therefore, taking the limit cannot be the solution. We need an infinite number of realizations to find the distribution through numerical simulation,

which can be approximated by many number of simulations, but is still not precise. This is why analytical study is important.

3.2 Definitions

We assume our observation interval to be the time axis $[0, T]$ where T is in milli seconds. We use the index $t \in [0, T]$ when discussing continuous time units. Assume we discretize $[0, T]$ into $T/\Delta t$ intervals where $\Delta t > 0$ but $\Delta t \ll 1$. Any continuous-time process in discrete-time will be given the index k, where

$$x_k \equiv x_t \text{ where } t = k\Delta t.$$

Denote $K = \lfloor T/\Delta t \rfloor$. We denote $a_j^K \triangleq (a_j, \ldots, a_K)$ and $a^K \equiv a_1^K$. We say that $g(s) = o(s)$ if $\lim_{s\to 0} g(s)/s = 0$.

Because of the inherent stochasticity of neural systems, we will model everything with a probabilistic framework. We denote a random process R as a time-indexed set of random variables $R = (R_k : \ k \geq 1)$. The applied probability definitions we will use throughout the manuscript are as follows.

Definition 3.2.1. *A random process $S = (S_k : k \geq 1)$ is termed a time-homogeneous Markov chain if*

$$\mathbb{P}\left(S^K = s^K\right) = \prod_{k=1}^{K} \mathbb{P}\left(S_k = s_k | S_{k-1} = s_{k-1}\right) = \prod_{k=1}^{K} Q(s_k|s_{k-1}). \tag{3.1}$$

Note that the latter equality explicitly denotes that this transition law does not depend on time k. Analogously, we have a definition for a controlled Markov chain:

Definition 3.2.2. *A random process $S = (S_k : k \geq 1)$ is termed a time-homogeneous controlled Markov chain with respect to random process $X = (X_k : k \geq 1)$ if*

$$\mathbb{P}\left(S^K = s^K | X^K = x^k\right) = \prod_{k=1}^{K} \mathbb{P}\left(S_k = s_k | S_{k-1} = s_{k-1}, X_k = x_k\right) = \prod_{k=1}^{K} Q(s_k|s_{k-1}, x_k). \tag{3.2}$$

The primitive random processes are X, Y, G, V, Z, which all have a time axis. The basic diagram describing the interaction between the primitive random processes is given in Figure 3.1.

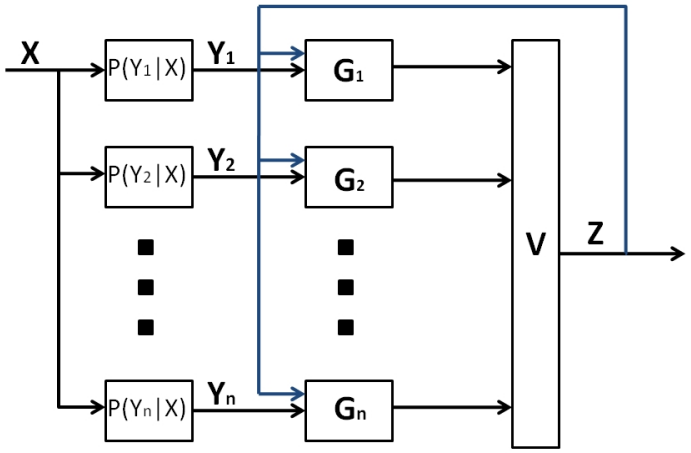

Figure 3.1: basic circuit

X_k denotes the location of an input stimulus at time k. The likelihood of any neuron $i \in \{1, \ldots, N\}$ to fire at time k is proportional to $\rho_i(x_k)$, which is the relationship between the stimulus and the center of neuron i's receptive field. The firing activity of neuron i is specified by the random process $Y_i = (Y_{k,i} : \ k \geq 1)$. We express Y_i in its point process counting function notation [20, 21].

In short, $Y_{k,i}$ denotes the total number of spikes generated by neuron i up to and including time k. See Figure 3.2.

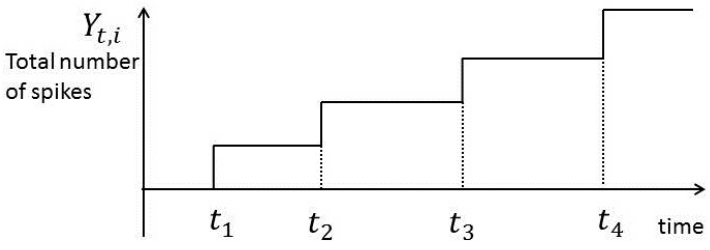

Figure 3.2: Counting function.

We also use the notation $dY_{k,i} \in \{0,1\}$[1] to denote whether or not the neuron fired at time k:

$$dY_{k,i} \triangleq Y_{k,i} - Y_{k-1,i}.$$

Note that there is bijection between $(dY_{1,i}, \ldots, dY_{K,i})$ and $(Y_{1,i}, \ldots, Y_{K,i})$.

There are N such neurons in parallel, all of whose spiking activity will affect the neural activity of the output neuron, whose spiking activity will be denoted by $Z = (Z_k : \ k \geq 1)$. Z will also be expressed in its point process counting function notation. We use the analogous notation $dZ = (dZ_k : \ k \geq 1)$ for the output neuron.

The relationship between the neural activity $(Y_1, \ldots, Y_N)$ of the N 'input neurons' and the output neuron's activity Z is manifested through internal variables pertaining to synaptic weights and the output neuron's membrane potential. Synaptic weights are manifested in terms of conductance levels $G = (G_1, \ldots, G_N)$. $G_i = (G_{k,i} : \ k \geq 1)$ denotes the conductance levels of the ith neuron at time k, which are in between $g_{\max}$ and $g_{\min}$. In general, $G_{k,i}$ is modulated by the recent firing of both input and output neurons. This explains the feedback loop in Figure 3.1. The conductance levels, in conjunction with the spiking of the input neurons $(Y_1, \ldots, Y_n)$ affect the output neuron's membrane potential process $V = (V_k : \ k \geq 1)$, which affects the propensity for spiking Z of the output neuron.

Primitive random variables	
X_k	Stimulus location at time k
$Y_{k,i}$	ith input neuron's spike train at time k
$G_{k,i}$	Conductance between ith input neuron to the output neuron at time k
V_k	Membrane potential of the output neuron at time k
Z_k	Output neuron's spike train at time k

[1] provided that Δt is small enough (e.g. less than 1ms), from the Hodgkin-Huxley effect, we know that this is a valid assumption.

Denote 'everything' E_k as all primitive random variables except the input stimulus at time k:

$$E_k = (dY_k, G_k, V_k, dZ_k).$$

Definition 3.2.3. *To say that the conductance G_k at time k has a 'community formation' means that the probability density function of the normalized conductance level $q(g)$ has following condition*

- *convex*
- *the minimum of q is at g^*, and g^* is not g_{max} nor g_{min}*

Larger α and β means stronger community formation, where

$$\begin{aligned} \alpha &= \frac{min\{q(g_{max}), q(g_{min})\}}{q(g^*)} \\ \beta &= 1 - \int_{g^*-\gamma}^{g^*+\gamma} q(g)\, dg, \quad \textit{for some } \gamma. \end{aligned}$$

3.3 Statistical Dependence Assumptions Between Processes

In this section, we introduce more detailed stochastic assumptions about the statistical inter dependencies between the interacting random processes. These assumptions are all based on physiological mechanisms that are known to be approximately accurate in the limit as $\Delta t \to 0$.

1. We will always assume that the input stimulus X evolves stochastically continuously (i.e. as a Markov process), independently of the past activity of the other primitive random processes:

   Assumption 1. *The input stimulus position X_k at time k is conditionally independent on E^k given X_{k-1}:*

   $$\mathbb{P}\left(X_k = x_k | E^K = e^K, X^{k-1} = x^{k-1}, X_{k+1}^K = x_{k+1}^K\right) = \mathbb{P}\left(X_k = x_k | X_{k-1} = x_{k-1}\right).$$

2. The firing rate of input neuron i depends only on the input stimulus:

Assumption 2. *The point process $dY_{k,i}$ for the ith input neuron at time k is conditionally independent on everything given stimulus X_k:*

$$\begin{aligned}\mathbb{P}\left(dY_k = dy_k | E^{k-1} = e^{k-1}, X^K = x^K\right) &= \mathbb{P}\left(dY_k = dy_k | X_k = x_k\right) \\ &= \prod_{i=1}^{n} \mathbb{P}\left(dY_{k,i} = dy_k | X_k = x_k\right), \\ \mathbb{P}\left(dY_{k,i} = 1 | X_k = x_k\right) &= \rho_i(x_k)\Delta t + o(\Delta t)\end{aligned}$$

Note that $\rho_i(x)$ pertains to the receptive field of neuron i, the idea being that $x_i^* \triangleq \arg\max_x \rho_i(x)$ is the 'center' of the receptive field, where the neuron is most likely to spike. Also note that as a consequence of the product in the above formula, we have that for small Δt, it is very unlikely for more than one neuron to spike in bin k:

Proposition 1. *Under Assumption* (2)*, for any k,*

$$\mathbb{P}\left(\sum_{i=1}^{n} dY_{k,i} > 1 | X^k = x^k\right) = o(\Delta t).$$

3. Considering Hebbian learning including STDP, conductance change depends on the previous inputs, the output neuron's firing timings and the previous conductance level. We choose cutoff L for the longest time to consider for the influence in the conductance update rule. From these, we assume:

Assumption 3. *The conductance level $G_{k,i}$ of the ith input neuron at time k is conditionally independent on $E^{k-1}, X^k, dY_k, G_k/G_{k,i}$ given the conductance level of the previous time step and L time step history of the input neurons and the output neuron:*

$$\begin{aligned}&\mathbb{P}\left(G_{k,i} = g_{k,i} | E^{k-1} = e^{k-1}, X^k = x^k, dY_k = dy_k, \bigcap_{j \neq i} G_{k,j} = g_{k,j}\right) \\ = \;& \mathbb{P}(G_{k,i} = g_{k,i} | G_{k-1,i} = g_{k-1,i}, dY_{k-(L+1),i}^{k-1} = dy_{k-(L+1),i}^{k-1}, dZ_{k-(L+1)}^{k-1} = dz_{k-(L+1)}^{k-1}).\end{aligned}$$

4. The membrane potential of the output neuron is dependent on its own voltage and influence from the input neurons. The influence is caused by the input neuron's firing and the conductance level between the fired input neuron and the output neuron. Choose cutoff L, so that the input neuron's firing before the L time steps is independent of the membrane potential. From these, we assume:

   Assumption 4. *The output neuron's membrane potential V_k at time k is conditionally independent on E^{k-1}, X^k, dY_k, G_k given the previous time membrane potential and L time step history with the current input neurons' accumulative influence h_k:*

$$\begin{aligned} & \mathbb{P}(V_k = v_k | E^{k-1} = e^{k-1}, X^k = x^k, dY_k = dy_k, G_k = g_k) \\ = \quad & \mathbb{P}(V_k = v_k | V_{k-1} = v_{k-1}, G^k_{k-L} = g^k_{k-L}, dY^k_{k-L} = dy^k_{k-L}). \end{aligned}$$

5. If the membrane potential exceeds the maximum then the output neuron fires so we assume:

   Assumption 5. *The point process dZ_k of the output neuron's firing at time k is conditionally independent on $E^k/dZ_k, V_k$ given the membrane potential V_k:*

$$\mathbb{P}(dZ_k = dz_k | E^{k-1} = e^{k-1}, X^k = x^k, dY_k = dy_k, V_k = v_k, G_k = g_k) = \mathbb{P}(dZ_k = dz_k | V_k = v_k)$$

3.4 State Space and Controlled Markov Chain

The purpose of this section is to define the "minimal" state space for which the future is independent of the past, given the present. In our case, we care about conditional independence given exogenous inputs.

We now denote the random process S pertaining to the state in our model as:

$$S_k = \left\{ dY^k_{k-L}, dZ^k_{k-L}, G^k_{k-L}, V_k \right\} \tag{3.3}$$

We have the following property of the 'state' random process:

Lemma 3.4.1. *The random process S as defined in* (3.3) *satisfies*

$$\mathbb{P}(S_k = s_k | S^{k-1} = s^{k-1}, X^k = x^k) = \mathbb{P}(S_k = s_k \, | S_{k-1} = s_{k-1}, X_k = x_k)$$

Proof. Note that

$$
\begin{aligned}
& \mathbb{P}(S_k = s_k | S^{k-1} = s^{k-1}, X^k = x^k) \\
= \quad & \mathbb{P}(dY_{k-L}^k = dy_{k-L}^k, G_{k-L}^k = g_{k-L}^k, dZ_{k-L}^k = dz_{k-L}^k, V_k = v_k | S^{k-1} = s^{k-1}, X^k = x^k) \\
= \quad & \mathbb{P}(dY_{k-L}^{k-1} = dy_{k-L}^{k-1} | S^{k-1} = s^{k-1}, X^k = x^k) \\
& \mathbb{P}(dY_k = dy_k | S^{k-1} = s^{k-1}, X^k = x^k) \\
& \mathbb{P}(G_{k-L}^{k-1} = g_{k-L}^{k-1} | S^{k-1} = s^{k-1}, X^k = x^k, dY_k = dy_k) \\
& \mathbb{P}(G_k = g_k | S^{k-1} = s^{k-1}, X^k = x^k, dY_k = dy_k) \qquad (3.4) \\
& \mathbb{P}(V_k = v_k | S^{k-1} = s^{k-1}, X^k = x^k, dY_k = dy_k, G_k = g_k) \\
& \mathbb{P}(dZ_{k-L}^{k-1} = dz_{k-L}^{k-1} | S^{k-1} = s^{k-1}, X^k = x^k, dY_k = dy_k, V_k = v_k, G_k = g_k) \\
& \mathbb{P}(dZ_k = dz_k | S^{k-1} = s^{k-1}, X^k = x^k, dY_k = dy_k, G_k = g_k, V_k = v_k) \\
= \quad & \mathbb{P}(dY_{k-L}^{k-1} = dy_{k-L}^{k-1} | S_{k-1} = s_{k-1}, X_k = x_k) \qquad (3.5) \\
& \mathbb{P}(dY_k = dy_k | S^{k-1} = s^{k-1}, X^k = x^k) \\
& \mathbb{P}(G_{k-L}^{k-1} = g_{k-L}^{k-1} | S_{k-1} = s_{k-1}, X_k = x_k, dY_k = dy_k) \qquad (3.6) \\
& \mathbb{P}(G_k = g_k | S^{k-1} = s^{k-1}, X^k = x^k, dY_k = dy_k) \\
& \mathbb{P}(V_k = v_k | S^{k-1} = s^{k-1}, X^k = x^k, dY_k = dy_k, G_k = g_k) \\
& \mathbb{P}(dZ_{k-L}^{k-1} = dz_{k-L}^{k-1} | S_{k-1} = s_{k-1}, X_k = x_k, dY_k = dy_k, G_k = g_k, V_k = v_k) \qquad (3.7) \\
& \mathbb{P}(dZ_k = dz_k | S^{k-1} = s^{k-1}, X^k = x^k, dY_k = dy_k, G_k = g_k, V_k = v_k) \\
= \quad & \mathbb{P}(dY_{k-L}^{k-1} = dy_{k-L}^{k-1} | S_{k-1} = s_{k-1}, X_k = x_k) \\
& \mathbb{P}(dY_k = dy_k | S_{k-1} = s_{k-1}, X_k = x_k) \qquad (3.8) \\
& \mathbb{P}(G_{k-L}^{k-1} = g_{k-L}^{k-1} | S_{k-1} = s_{k-1}, X_k = x_k, dY_k = dy_k) \\
& \mathbb{P}(G_k = g_k | S_{k-1} = s_{k-1}, X_k = x_k, dY_k = dy_k) \qquad (3.9) \\
& \mathbb{P}(V_k = v_k | S_{k-1} = s_{k-1}, X_k = x_k, dY_k = dy_k, G_k = g_k) \qquad (3.10) \\
& \mathbb{P}(dZ_{k-L}^{k-1} = dz_{k-L}^{k-1} | S_{k-1} = s_{k-1}, X_k = x_k, dY_k = dy_k, V_k = v_k, G_k = g_k) \\
& \mathbb{P}(dZ_k = dz_k | S_{k-1} = s_{k-1}, X_k = x_k, dY_k = dy_k, V_k = v_k, G_k = g_k) \qquad (3.11) \\
= \quad & \mathbb{P}(S_k = s_k | S_{k-1} = s_{k-1}, X_k = x_k) \qquad (3.12)
\end{aligned}
$$

where (3.4) follows from the chain rule; (3.5), (3.6), and (3.7) follows since

$$\mathbb{P}(A_t = a_t | A_t = \alpha_t) = \mathbb{P}(A_t = a_t | A_t = \alpha_t, B^T = b^T) = 1_{a_t = \alpha_t},$$

hold for any B; (3.8) follows from Assumption 2, each $dY_{k,i}$ is conditionally independent of each other; (3.9) follows from Assumption 3, each $G_{k,i}$ is conditionally independent of each other; (3.10) follows from Assumption 4; (3.11) follows from Assumption 5, each $dZ_{k,i}$ is conditionally independent of each other;(3.12) follows from the chain rule. □

This leads to the following theorem, which justifies our use of calling S a 'state':

Theorem 3.4.2. *The random process S as defined in* (3.3) *is a time-homogeneous controlled Markov chain with respect to X.*

Proof. Note that

$$\begin{aligned}
& \mathbb{P}\left(S^K = s^K | X^K = x^K\right) \\
= \quad & \frac{\mathbb{P}\left(S^K = s^K, X^K = x^K\right)}{\mathbb{P}\left(X^K = x^K\right)} && (3.13) \\
= \quad & \prod_{k=1}^{K} \frac{\mathbb{P}\left(S_k = s_k, X_k = x_k | S^{k-1} = s^{k-1}, X^{k-1} = x^{k-1}\right)}{\mathbb{P}\left(X_k = x_k | X^{k-1} = x^{k-1}\right)} && (3.14) \\
= \quad & \prod_{k=1}^{K} \frac{\mathbb{P}\left(S_k = s_k | S^{k-1} = s^{k-1}, X^k = x^k\right) \mathbb{P}\left(X_k = x_k | S^{k-1} = s^{k-1}, X^{k-1} = x^{k-1}\right)}{\mathbb{P}\left(X_k = x_k | X^{k-1} = x^{k-1}\right)} && (3.15) \\
= \quad & \prod_{k=1}^{K} \mathbb{P}\left(S_k = s_k | S^{k-1} = s^{k-1}, X^k = x^k\right) && (3.16) \\
= \quad & \prod_{k=1}^{K} \mathbb{P}\left(S_k = s_k | S_{k-1} = s_{k-1}, X_k = x_k\right) && (3.17) \\
& && (3.18)
\end{aligned}$$

where (3.13) follows from the law of conditional probability; (3.14) follows from the chain rule; (3.15) follows from the law of conditional probability;(3.16) holds because the RHS of the numerator and the denominator cancel from Assumption 1; and (3.17) holds from Lemma 3.4.1. □

It is the purpose of this section to carefully define the 'state space' over which we can speak of how the past is independent of the future given the present. As of now, this space is very large. Under different assumptions or reductions to get intuition, we will set certain parameters which lead to a reduction in the state space. With this framework, we will be able to apply advanced stochastic Markov chain analysis to elucidate certain emergent properties of this complex stochastic network.

3.5 Detailed Rules

Given the above statistical inter-dependence assumptions, we can now fill in some of the details about the rules of the model for assumptions pertaining to possible input stimulus locations, receptive fields, conductance strength of synapses, possible voltage levels, etc. Each rule also has several parameters for specification.

Each assumption has details that will be instantiated under different modeling scenarios in the manuscript. As such, when we speak to simulation results or quantitative analysis in the later Chapters, we will refer to Assumptions (1a,2b,3c, .., 4a) so that it is clear which rules are used and how the parameters were aligned.

1. For Assumption 1: Consider input neurons to be organized as in Fig. 3.3, where input neurons are organized in a line and separated by 1mm. The stimulus moves with some speed s_t on this line.

   (a) Consider the stimulus to be outside of the receptive field of all input neurons for all time, meaning the speed of the stimulus $s_t = 0$ (m/s) for all t. So the stimulus does not influence any input neuron.

   (b) Consider there to be an infinite number of stimuli moving at a fixed speed $s_t = s$ (m/s) and each stimulus to be separated by a fixed distance ns (mm). The position of the

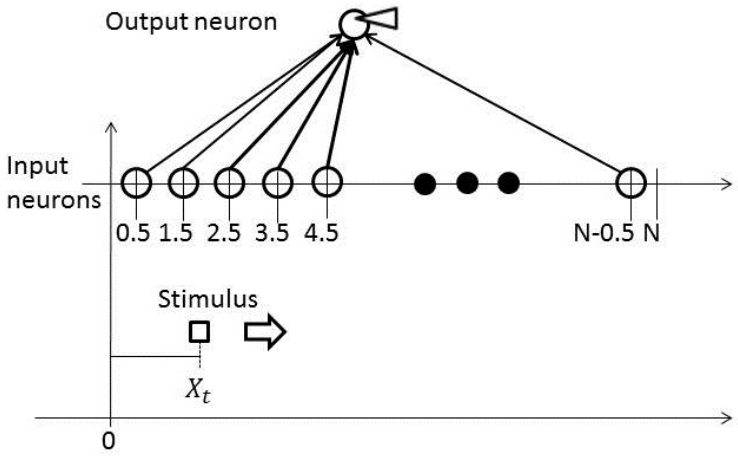

Figure 3.3: Input neurons are equally distanced and organized in the line. The stimulus also moves on the same line.

stimulus within the interval $[-W, N+W]$ is

$$x_t = (t/n - \lfloor t, n \rfloor)v - W.$$

If $n \leq (N+2W)/s$, then there is more than one stimulus in the receptive field of the output neuron.

2. For Assumption 2: Again, consider input neurons to be organized as Fig. 3.3, and each input neuron i to have probability function $\rho_{k,i}$ at time k as shown in Fig. 3.4.

   (a) Consider the case of Rule 1a, then the input neuron's propensity to fire is unaffected by the stimulus:

   $$\rho_i(x) \equiv \rho.$$

   (b) Consider the input neurons to be organized topographically on a line as shown in Fig. 3.3 , where $\rho_i(\cdot)$ is a slightly shifted version of $\rho_{i+1}(\cdot)$. These are all shifted versions of a 'base canonical receptive field' $\rho(\cdot)$ given in Figure 3.4.

   Note that the base receptive field $\rho(\cdot)$ is a triangular structure that has a base firing rate B, a maximum firing rate H, and a width of W. As such, $\rho(\cdot)$ is in one-to-one

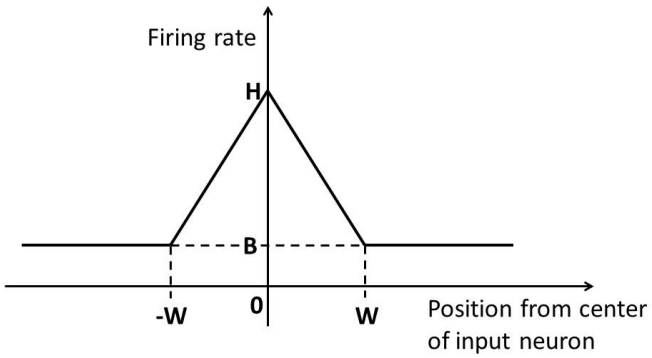

Figure 3.4: Each input neuron has a receptive field spanning $-W$ to W. The probability function is according to the hat function with maximum H with base line B.

correspondence with the parameters (B, H, W). In simulations, we will specify these three quantities.

We demonstrate the topographic relationships by describing a base receptive field centered at 0, given by $\rho(\cdot)$. Then we have that

$$\rho_i(x) = \rho(x - \alpha_i) = \begin{cases} B + \dfrac{H-B}{W}(W - x + \alpha_i) & \text{if } W > x - \alpha_i > 0 \\ B + \dfrac{H-B}{W}(W + x - \alpha_i) & \text{if } -W < x - \alpha_i < 0 \\ B & \text{else} \end{cases} \tag{3.19}$$

where α_i is the center of the ith receptive field. We set $\alpha_1 = 0.5, \alpha_2 = 1.5, \alpha_3 = 2.5, \cdots, \alpha_N = N - 0.5$, as shown in Fig. 3.3. As such, the center of input neuron i's receptive field is close to the center of neuron $i+1$'s receptive field.

3. For Assumption 3 we consider STDP rules:

   (a) Consider $g_{k,i}$ to be calculated through the deterministic function:

$$g_{k,i} = g_{k-1,i} + \hat{f}(g_{k-1,i}, dy_{k-1,i}, dy_{k-2,i}, \cdots, dy_{k-(L+1),i}, dz_{k-1,i}, dz_{k-2,i}, \cdots, dz_{k-(L+1),i}),$$

where the update function $\hat{f}$ has to deal with the boundary conditions:

$$\begin{aligned}
&\hat{f}(u_g, u_y, u_{y1}, \cdots, u_{y(L+1)}, u_z, u_{z1}, \cdots u_{z(L+1)}) \\
&= \begin{cases} g_{\max} - u_g & \text{if } u_g + f(\Delta s) > g_{\max} \\ g_{\min} - u_g & \text{if } u_g + f(\Delta s) < g_{\min} \\ f(\Delta s(u_{y1}, u_{y2}, \cdots, u_{y(L+1)}, u_{z1}, u_{z2}, \cdots, u_{z(L+1)})) & \text{else} \end{cases},
\end{aligned}$$

where the update function f uses STDP rule with parameters A_+, A_- for the size of change in conductance and τ_+, τ_- for the exponential decaying influence over time:

$$f(u) = g_{max} \begin{cases} A_+ \exp(\frac{u}{\tau_+}) & \text{if } u < 0 \\ A_- \exp(\frac{-u}{\tau_-}) & \text{if } u > 0 \\ 0 & \text{if } u = 0 \end{cases},$$

and the time asymmetry influence Δs has to deal with the exception from the time discretization, that both input and output neurons fired in the same time. If an input neuron fires then this causes the output neuron to fire but not the other way around, so we choose $\Delta s = -\Delta t$:

$$\begin{aligned}
&\Delta s(u_y, u_{y1}, \cdots, u_{y(L+1)}, u_z, u_{z1}, \cdots u_{z(L+1)}) \\
&= \begin{cases} -\Delta t & \text{if } u_y = 1 \text{ and } u_z = 1 \\ \Delta t(1 - MRS(u_{z1}, u_{z2}, \cdots, u_{z(L+1)})) & \text{if } u_y = 1 \text{ and } u_z = 0 \\ \Delta t(MRS(u_{y1}, u_{y2}, \cdots, u_{y(L+1)}) - 1) & \text{if } u_y = 0 \text{ and } u_z = 1 \\ 0 & \text{else} \end{cases},
\end{aligned}$$

where the most recently spiked time function MRS is

$$MRS(u_1, u_2, \cdots, u_{L+1}) = \begin{cases} \infty & \text{if } \sum_{i=1}^{L} u_i = 0 \\ (min_x\{u_x = 1\})\Delta t & \text{else} \end{cases}.$$

(b) If conductance is discretized, then the value of f has to be discretized with the size of Δg.

(c) If $L = 0$ then the previous rule cannot reduce the conductance values, so we need to have different rules.

4. For Assumption 4, we choose the membrane potential V_t of the output neuron at time t to obey the leak integrate-and-fire model:

$$C_0 \frac{dV_t}{dt} = I_t + g_{\text{leak}}(V_{\text{rest}} - V_t), \tag{3.20}$$

where C is the capacitance, I_t is the current, g_{leak} is the parameter for leakage, and V_{rest} is the resting potential. Normalize this with g_{leak}, then we have

$$C \frac{dV_t}{dt} = h_t(V_{\text{ex}} - V_t) + (V_{\text{rest}} - V_t), \tag{3.21}$$

where V_{ex} is the extension level, and h_t is the accumulative influence from input neurons spikes:

$$h_t = \sum_{i=1}^{N} \int_{\tau=0}^{t} g_{\tau,i}/g_{\text{leak}} \exp\left(-\frac{t-\tau}{b}\right) dy_{\tau,i}.$$

This explains why V_t grows faster when several inputs fire in a close interval.

(a) Choose the forward Euler method for discrete time model (3.21) with the boundary condition:

$$V_k = \begin{cases} (V_{k-1} - V_{\max} + \dfrac{\Delta t}{C}(V_{\text{rest}} - V_{k-1}) + \dfrac{\Delta t}{C} h_k(V_{\text{ex}} - V_{k-1}) & \text{if } V_{k-1} > V_{\max} \\ V_{k-1} + \dfrac{\Delta t}{C}(V_{\text{rest}} - V_{k-1}) + \dfrac{\Delta t}{C} h_k(V_{\text{ex}} - V_{k-1}) & \text{else} \end{cases} \tag{3.22}$$

where the accumulative influence h_k is the fired input neurons' conductance with the decaying parameter b over L:

$$h_k = \sum_{i=1}^{N} \sum_{l=0}^{L} g_{k-l,i}/g_{\text{leak}} (\exp(-\Delta t/b))^l dy_{k-l,i}.$$

(b) To make a discretization of membrane potential for Markov chain analysis, consider the probability of incrementing Δv as $U(v,h)$ and decrementing Δv as $D(v,h)$.

Lemma 3.5.1. *Choose the following functions:*

$$\begin{aligned} U(v,h) &= (hV_{ex} + V_{rest}) \,/\, (hV_{ex} + V_{rest} + v(h+1)) \\ D(v,h) &= (v(h+1)) \,/\, (hV_{ex} + V_{rest} + v(h+1)) \\ \Delta v &= (\Delta t/C)(hV_{ex} + V_{rest} + v(h+1)) \end{aligned}$$

These represent Eq. (3.22) *without the boundary condition in the limit of* Δt *going to 0.*

Proof. Consider the expected value of the next voltage value:

$$\begin{aligned} \mathbb{E}(v_{k+1}) &= v_k(1-U-D) + (v_k + \Delta v)U + (v_k - \Delta v)D \\ &= v_k + \Delta v U - \Delta v D \end{aligned}$$

Because U and D are normalized, applying the values of U, D, and Δv leads to the Eq. (3.22) without the boundary conditions. The result follows from the Central Limit Theorem. □

Using this lemma, the probability of voltage level change is evaluated as

$$\begin{aligned} &\mathbb{P}\left(V_k = v_k | V_{k-1} = v_{k-1}, dY_k = dy_k, G_{k-L}^{k-1} = g_{k-L}^{k-1}, dY_{k-L}^{k-1} = dy_{k-L}^{k-1}\right) \\ &= \begin{cases} 1 - U(V_{\min}, h_k) & \text{if } v_k = V_{\min} \text{ and } v_{k-1} = V_{\min} \text{ or } v_{k-1} = V_{\max} \\ 0 & \text{if } v_k = V_{\max} - \Delta v \text{ and } v_{k-1} = V_{\max} \\ U(V_{\min}, h_k) & \text{if } v_k = V_{\min} + 1 \text{ and } v_{k-1} = V_{\max} \\ D(v_{k-1}, h_k) & v_{k-1} = v_k + \Delta v \\ U(v_{k-1}, h_k) & v_{k-1} = v_k - \Delta v \\ 1 - D(v_{k-1}, h_k) - up(v_{k-1}, h_k) & v_{k-1} = v_k \text{ and } v_k \neq V_{\min} \end{cases} \end{aligned}$$

When the voltage is $V_{\max}$, it means the output neuron has already fired. However, we

cannot reset it to $V_{\min}$ before updating output firing dZ_k.

5. For Assumption 5, consider the firing rate to be deterministic and

$$\mathbb{P}(dZ_k = 1 | V_k = v_k) = 1_{v_t \geq V_{\max}}.$$

3.6 Summary

The rules in the previous section is summarized in Tab. 3.1. For the computational experience we choose Rules from here and parameter values from Tab. 3.2 and 3.3. Empty values are set according to each simulations. τ_+ are closer to τ_- in some experiments [14, 92, 177] and some cases τ_- are much bigger than τ_+ [40, 45]. We chose same values for τ_+ and τ_-. [150] observed the value of $A_-\tau_-/(A_+\tau_+)$ makes significant impact on their simulation, however we did not see the difference and used same value for A_+ and A_-. There are different STDP window functions depend on the cells and [150] chose $b = 0.005$(ms) for their experiments. We chose either $b = 0.005$(ms) or $b = 0.001$(ms) for different simulations. $V_{\text{rest}} = -74$(mV), $V_{\text{ex}} = 0$(mV), $V_{\max} = -54$(mV), and the output neuron's reset value is set to -60(mV) in [155]. For simplicity, we remove refractory period of the output neuron's firing and also use same value for V_{rest} and the reset value of the output neuron. We also shift the membrane potential of the output neuron to make minimum value to be 0. Since the system is theoretical model, it is difficult to use the number of input neurons and the range of conductance level from biological experiments. The number of input neurons are depends on the network of the neurons at specific locations. [150] chose $N = 1000$, and we chose $N = 200$. This difference change the influence of input neurons h, which depends on N as $h_k = \sum_{i=1}^{N} \sum_{l=0}^{L} g_{k-l,i}/g_{\text{leak}}(\exp(-\Delta t/b))^l dy_{k-l,i}$.. Also, the conductance level change h. [150] chose $g_{\max}/g_{\text{leek}} = 0.015, 0.02$ and $g_{\min}/g_{\text{leek}} = 0.0$. [150] chose $C = 0.02$(s) following [155]. We chose either $C = 0.02$(s) or $C = 2.0$(s). When choosing $C = 0.02$(s), we set $g_{\max}/g_{\text{leek}} = 1.4, 0.6.$ and $g_{\min}/g_{\text{leek}} = 0.01$ to show the community formation. When choosing $C = 2.0$(s), we set $g_{\max}/g_{\text{leek}} = 20.0$ and $g_{\min}/g_{\text{leek}} = 1.0$ for the excitatory input neurons and $g_{\max}/g_{\text{leek}} = 19.0$ and $g_{\min}/g_{\text{leek}} = 1.0$ for inhibitory input neurons to show the properties of selectivity. We did not set

Rule	Equation	Description
1.(b)	$x_t = (t/n - \lfloor t, n \rfloor)v - W$	stimulus position at time t
2.(a)	ρ	Firing rate without stimulus
2.(b)	$\rho_i(x) = \begin{cases} B + \frac{H-B}{W}(W - x + \alpha_i) & \text{if } W > x - \alpha_i > 0 \\ B + \frac{H-B}{W}(W + x - \alpha_i) & \text{if } -W < x - \alpha_i < 0 \\ B & \text{else} \end{cases}$	Firing rate
3.(a)	$f(u) = g_{max} \begin{cases} A_+ \exp(\frac{u}{\tau_+}) & \text{if } u < 0 \\ A_- \exp(\frac{-u}{\tau_-}) & \text{if } u > 0 \\ 0 & \text{if } u = 0 \end{cases}$,	STDP window function
4	$C\frac{dV_t}{dt} = h_t(V_{\text{ex}} - V_t) + (V_{\text{rest}} - V_t)$,	Integrate and Fire model
	$h_t = \sum_{i=1}^{N} \int_{\tau=0}^{t} g_{\tau,i}/g_{\text{leak}} \exp\left(-\frac{t-\tau}{b}\right) dy_{\tau,i}$	accumulate influence
4.(a)	$V_k = \begin{cases} (V_{k-1} - V_{\max} + \frac{\Delta t}{C}(V_{\text{rest}} - V_{k-1}) + \frac{\Delta t}{C} h_k(V_{\text{ex}} - V_{k-1}) & \text{if } V_{k-1} > V_{\max} \\ V_{k-1} + \frac{\Delta t}{C}(V_{\text{rest}} - V_{k-1}) + \frac{\Delta t}{C} h_k(V_{\text{ex}} - V_{k-1}) & \text{else} \end{cases}$	Integrate and Fire model
	$h_k = \sum_{i=1}^{N} \sum_{l=0}^{L} g_{k-l,i}/g_{\text{leak}}(\exp(-\Delta t/b))^l dy_{k-l,i}$	accumulate influence
5	$\mathbb{P}(dZ_k = 1 \mid V_k = v_k) = 1_{v_t \geq V_{\max}}$	output neuron's firing rate

Table 3.1: Rules

parameter	unit	description	our value	values from [150, 151]
τ_+	s	damping ratio for STDP rule	0.02	0.02
τ_-	s	damping ratio for STDP rule	0.02	$\tau_- = \tau_+$, $\tau_- = 5\tau_+$
A_+		magnitude of STDP rule	0.005	0.005, 0.001, 0.02
A_-		magnitude of STDP rule	0.005	$A_-\tau_-/(A_+\tau_+) = 1.05$
V_{rest}	mV	resting potential of voltage V	0	-74, -70
V_{ex}	mV	extension level of voltage V	25	0
$V_{\max}$	mV	maximum voltage	20	-54
C	s	integrate-and-fire model parameter		0.02
b	s	damping ratio of influence		0.005
g_{leak}	$1/\Omega$	ratio of leakage	1.0	
$g_{\max}$	$1/\Omega$	maximum conductance value		$\frac{g_{\max}}{g_{\text{leak}}} = 0.015, 0.02, 0.035$
$g_{\min}$	$1/\Omega$	minimum conductance value		0
N		number of input neurons	200	1000

Table 3.2: Parameters

minimum conductance to be 0, because we would like to have non-stable state when the network has all minimum conductance. The step size of output membrane potential Δv is $(\Delta t/C)(hV_{\text{ex}} + v(h+1))$, therefore the larger C and the larger g in h does not cause larger voltage step.

parameter	unit	description	value we used
Δt	s	time step	
N_0	mm	linear space where input neurons are spanned	200
s	mm/s	speed of stimulus	$1/\Delta t$
n	s	time between two peaks of stimuli	$(N + 2W)/s$
Δg	$1/\Omega$	conductance step size	$(g_{\max} - g_{\min})/10000$
Δv	mV	output neuron's membrane potential step size	$(V_{\max} - V_{\text{rest}})/10000$
$\rho_{k,i}$	1/s	firing rate at time k for ith input neuron	
H	1/s	maximum firing rate	
B	1/s	base firing rate	
W	mm	maximum distance of input neuron's receptive field	
L		number of look back	
M		number of conductance level	

Table 3.3: Parameters

Chapter 4

Phenomenology and Numerical Simulation

4.1 Introduction

In this section, we run the simulation using the specific rules from the previous section and show the emergence of community formation and place selectivity. The purpose of this section is to show that our model is sufficient to represent the results from the previous works [150, 151], and also show the convergence of the conductance levels. The computational results are often taken by a snapshot of the simulation, however we have to be careful about this, because of the stochasticity in the system. One snapshot only represents a state in the system, and does not become completely stable. We show this point by showing the average of the conductance level over time. Even though the average of conductance level becomes stable, it does not become constant in our simulation time.

The system is complex, so the parameters are important. For all simulations we use values from Table 3.2, except where specified otherwise. Other parameters used in these models are given in Table 3.3.

4.2 Stimulus out of receptive field

Choose an infinite number of looks back $L = \infty$ with continuous space from Rule 3a and 4a, and choose parameters as in Table 3.2 and all input firing to be $\rho_{k,i} = 10.0$ (1/s) independent from input location as in Rule 1a and 2a. Starting from a medium value of conductance levels, we see the maximum and minimum conductance levels after one simulation as shown in Fig. 4.1, which shows

the value of the conductance level after the simulation. It is the same result from [151]. This also shows the average conductance level over time. Note, it fluctuates within a small value, but is not a single value. That means, the state is not the realization of the invariant distribution, but it is in the other long-lived distribution. In this simulation, we chose $g_{\min} = 0.01(1/\Omega)$, $g_{\max} = 0.6(1/\Omega)$, $dt = 10^{-4}$ (s). Shorter time step of $dt = 10^{-5}$ (s) does not make much difference as shown in Fig. 4.2

We also choose systematic discretized voltage and conductance levels for the same parameters with Fig. 4.1. 10^4 conductance steps and 10^4 voltage steps were chosen for its discretization. Fig. 4.3 shows community formation same with the continuous case.

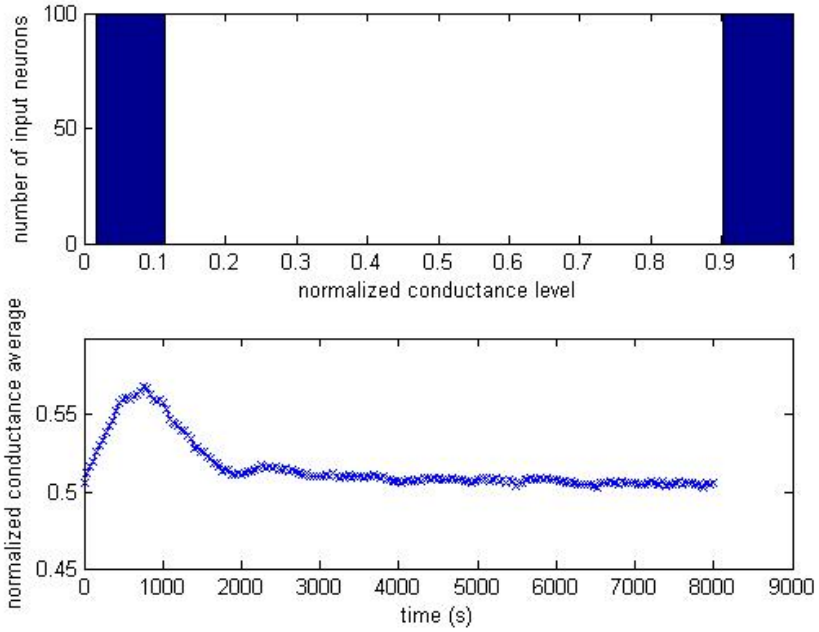

Figure 4.1: Continuous voltage and conductance case: Emergence of community formation of group of neurons for constant stimulus from Rule 1a, 2a, 3a, 4a, and 5. Parameters are chosen as $L = \infty$, $C = 0.05$(s), $b = 0.005$(s), $g_{\min} = 0.01(1/\Omega)$, $g_{\max} = 0.6(1/\Omega)$, $dt = 10^{-4}(s)$, and $\rho_{k,i} = 10.0$ (1/s).

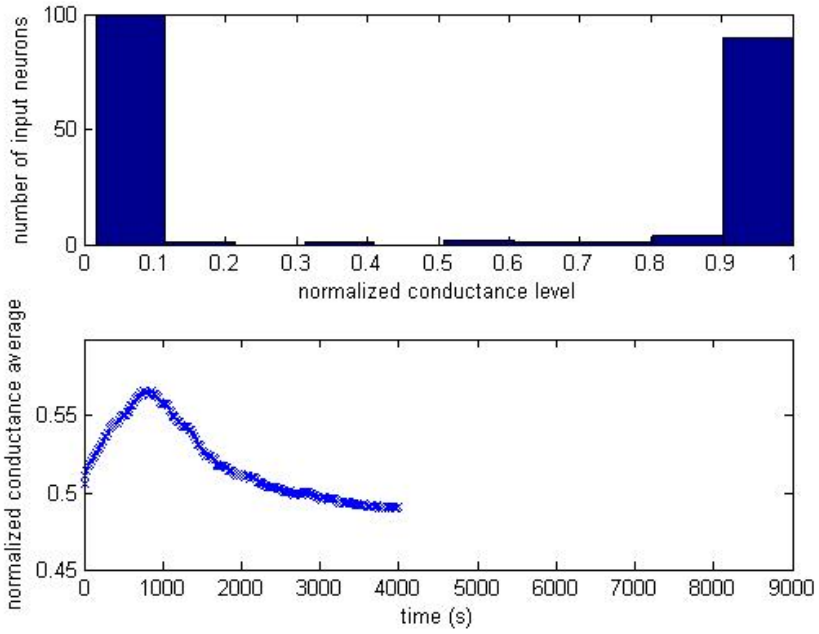

Figure 4.2: Continuous voltage and conductance case: Emergence of community formation of group of neurons for constant stimulus from Rule 1a, 2a, 3a, 4a, and 5. Parameters are chosen as $L = \infty$, $C = 0.05$(s), $b = 0.005$(s), $g_{\min} = 0.01(1/\Omega)$, $g_{\max} = 0.6(1/\Omega)$, $dt = 10^{-5}(s)$, and $\rho_{k,i} = 10.0$ (1/s).

4.3 Stimulus moves in receptive field

In this section, the input stimulus moves over the receptive field. Here, we show that the different receptive field parameters lead to a different type of place selectivity.

Choose an infinite number of looks back, and continuous voltage and conductance levels with the same parameters as in Table 3.2. This time, we choose a moving input stimulus from Rule 1b and 2b, where $s = 1000$(mm/s) and periodic boundary condition. Other parameters are $C = 0.05$(s), $b = 0.005$(s), $g_{\min} = 0.01(1/\Omega)$, $g_{\max} = 1.4(1/\Omega)$, and $dt = 10^{-4}(s)$. We consider two cases, $(H, B, W) = (70$ (1/s), 1 (1/s), 10 (mm)), and $(H, B, W) = (70$ (1/s), 0.9 (1/s), 6 (mm)). The conductance levels also become maximum and minimum with the constant input firing case as shown in Fig. 4.4 and 4.5, but this time, we also observe clustering of maximum conductance levels as shown in Fig. 4.6a and 4.6b, which represents the conductance level by color for each input

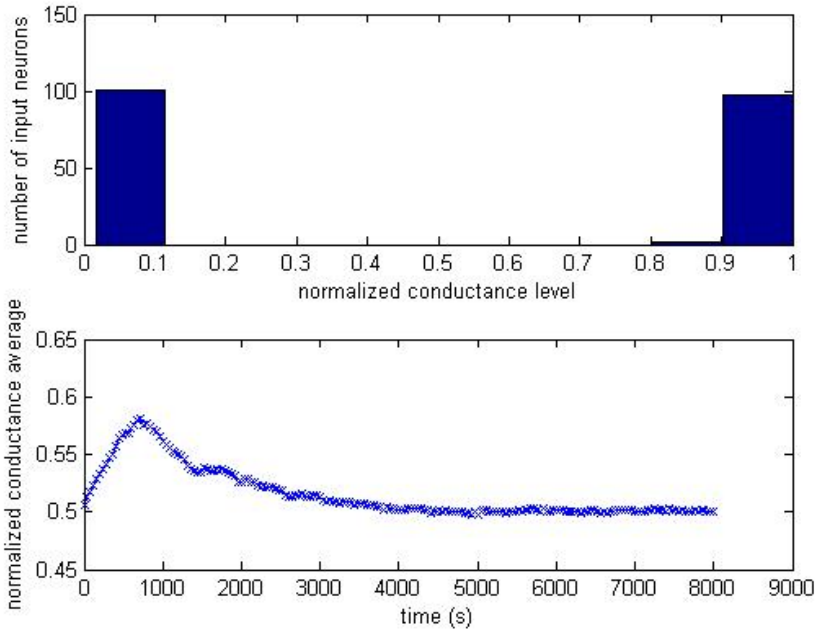

Figure 4.3: Discrete voltage and conductance case: Emergence of community formation of group of neurons for constant stimulus from Rule 1a, discretized space from Rule 3b, 4b, also Rule 2a and 5. Parameters are chosen as 10^4 conductance steps, 10^4 voltage steps, $L = \infty$, $C = 0.05$(s), $b = 0.005$(s), $g_{\text{min}} = 0.01(1/\Omega)$, $g_{\text{max}} = 0.6(1/\Omega)$, $dt = 10^{-4}(s)$, and $\rho_{k,i} = 10.0$ (1/s).

neuron over time. Fig. 4.6a has moving preferable locations, which are caused by the resonance of a periodic input stimulus. This is not observed in the constant stimulus case. Note that even though the average of the conductance level is almost constant for a long time, the position of the maximum conductance level is not. The stable distribution is not necessarily represented by the case of stable state.

4.4 Orientation and Direction Selectivity

Our simple model is capable of several types of selectivity. We focus on the visual system here and show the orientation and direction selectivity emerging from our model.

Consider both inhibitory and excitatory input neurons to be randomly scattered in the circle

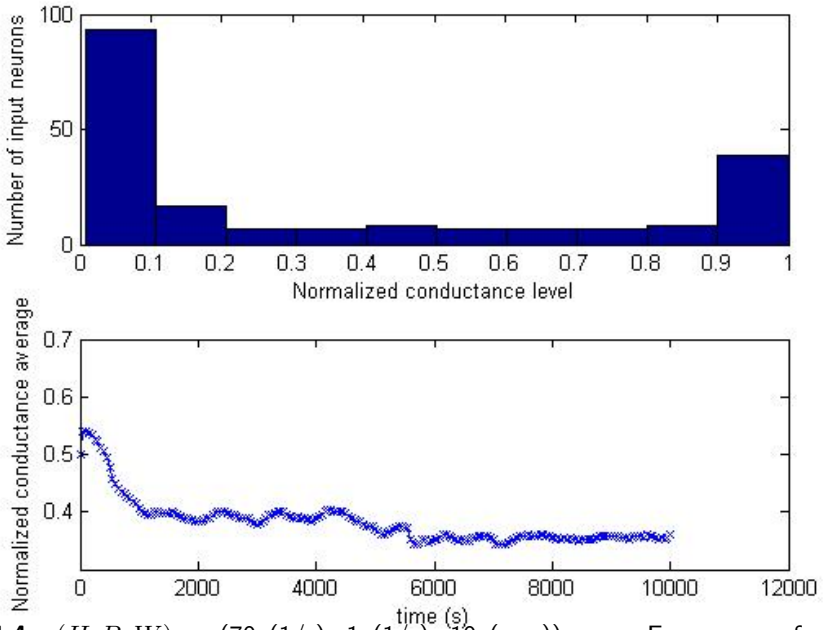

Figure 4.4: (H, B, W) = (70 (1/s), 1 (1/s), 10 (mm)) case: Emergence of community formation of group of neurons for moving input stimulus from Rule 1b, 2b, 3a, 4a, and 5 with $L = 0$, $s = 1000$ (mm/s), and periodic boundary condition.

with 1mm diameter, and a bar stimulus moving over this circle. Then we can demonstrate that orientation and direction selectivity emerge from training by several swipes with the same orientation. Fig. 4.7 shows the conductance level of normalized inhibitory and excitatory neurons conductance strength after training from a 0 degree oriented bar swiping the circle with speed 10.0 mm/s when the influence is moved away from the circle and then the same bar comes back periodically. The initial conductances are random strength. Fig. 4.7 shows the emergence of clustering of similar conductance levels for both inhibitory and excitatory neurons, where inhibitory neurons' conductances are strong and excitatory neurons' conductance are weak. The average conductance level becomes stabilized over time as shown in Fig. 4.8. After the training, we ran the different oriented bars without changing conductance levels. We swiped with one direction and waited for the same distance to clear all influences in the input neurons firing by stimulus, then repeated this for several times depends on the speed of the bar. For testing we used the same stimulus from training and showed both orientation and direction selectivity in Fig. 4.9a with the same speed, and in Fig. 4.9b

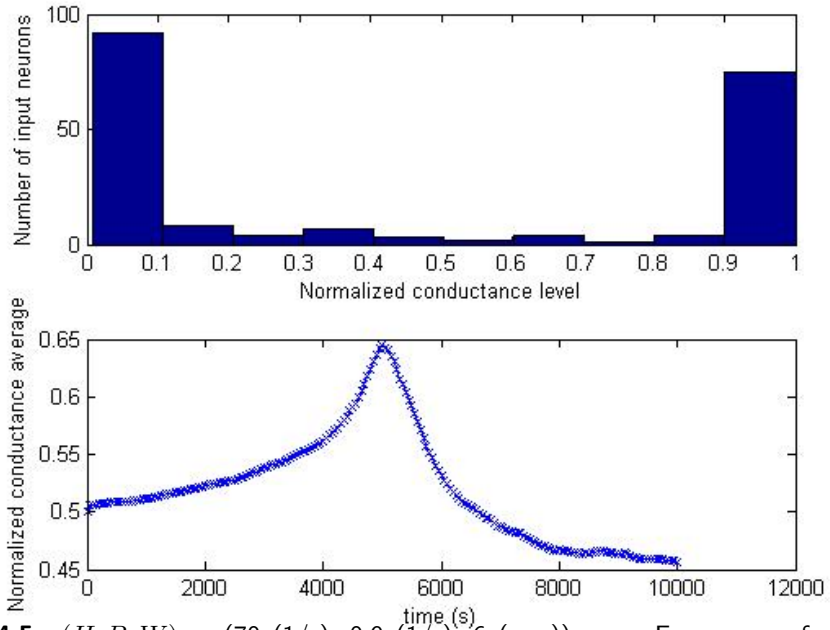

Figure 4.5: $(H, B, W) =$ (70 (1/s), 0.9 (1/s), 6 (mm)) case: Emergence of community formation of group of neurons for moving input stimulus from Rule 1b, 2b, 3a, 4a, and 5 with $L = 0$, $s = 1000$ (mm/s), and periodic boundary condition.

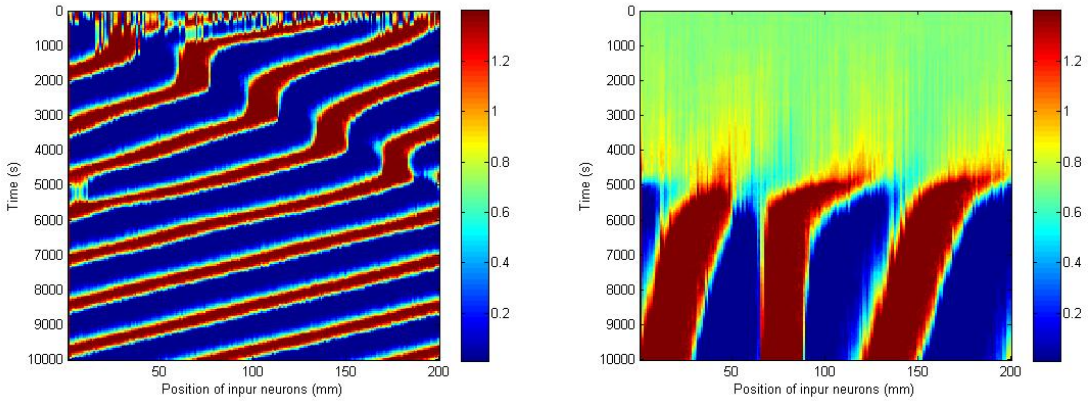

(a) conductance value **(b)** conductance value

Figure 4.6: Cluster of high conductance levels moving over time from Rule 1b, 2b, 3a, 4a, and 5 with $L = \infty$, $s = 1/\Delta t$ (1/ms), and periodic boundary condition. (a) $(H, B, W) =$ (70 (1/s), 1 (1/s), 10 (mm)) (b) $(H, B, W) =$ (70 (1/s), 0.9 (1/s), 6 (mm))

with 10 times slower speed. Both run for same amount of time and show similar result.

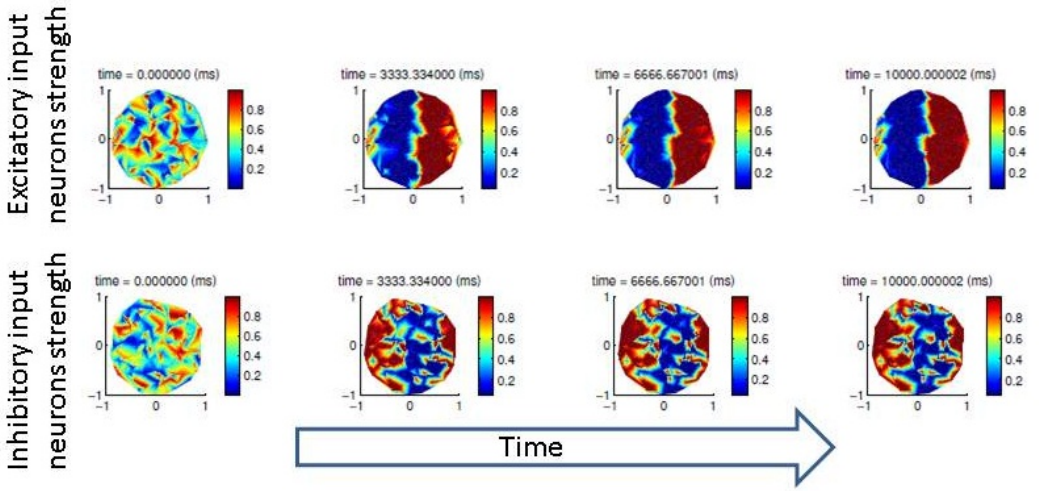

Figure 4.7: 200 inhibitory input neurons with conductance level -19 $(1/\Omega)$ to -1 $(1/\Omega)$ and 200 excitatory input neurons with conductance level 20 $(1/\Omega)$ to 1 $(1/\Omega)$ are randomly distributed in the unit circle and bar stimulus with degree 0 moves over the receptive field in $s = 10$ (mm/s) with $(H, B, W) =$ (30 (1/s), 1 (1/s), 0.2 (mm)). Use Rule 1b, 2b, 3a, 4a, and 5 with $L = \infty$, the parameters from Table 3.2, $C = 2.0$(s), $b = 0.001$(s), and $dt = 0.001(s)$. The figure shows the conductance levels of input neurons. The top row shows excitatory input neurons conductance levels. The lower row shows the negative of inhibitory input neurons conductance levels to show the strength.

Next, we ran simulations with a randomly oriented bar for training. After each sweep, we changed the orientation randomly so that it was closer to the real biological system. We chose the same parameters as previous simulations, and observed different oriented selectivity for the each simulation as in Fig. 4.10 and 6.17. This is caused by the STDP winner-take-all property. Note, this also test with two different speed of bars, but shows similar results.

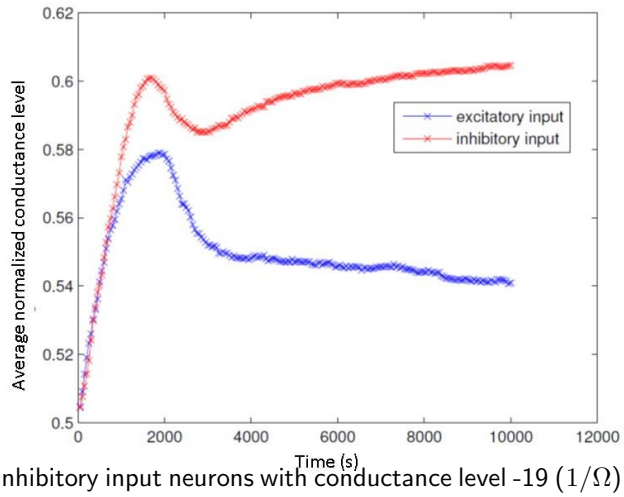

Figure 4.8: 200 inhibitory input neurons with conductance level -19 $(1/\Omega)$ to -1 $(1/\Omega)$ and 200 excitatory input neurons with conductance level 20 $(1/\Omega)$ to 1 $(1/\Omega)$ are randomly distributed in the unit circle and bar stimulus with degree 0 moves over the receptive field in $s = 10$ (mm/s) with $(H, B, W) =$ (30 (1/s), 1 (1/s), 0.2 (mm)). Use Rule 1b, 2b, 3a, 4a, and 5 with $L = \infty$, the parameters from Table 3.2, $C = 2.0$(s), $b = 0.001$(s), and $dt = 0.001(s)$. The figure shows the average normalized conductance level over time for both excitatory and inhibitory input neurons.

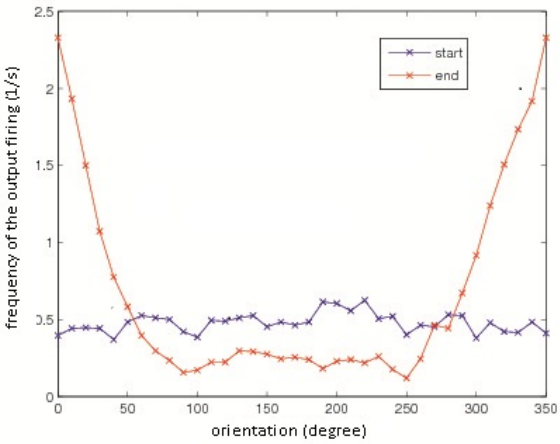

(a) number of firing with moving stimulus with speed 10

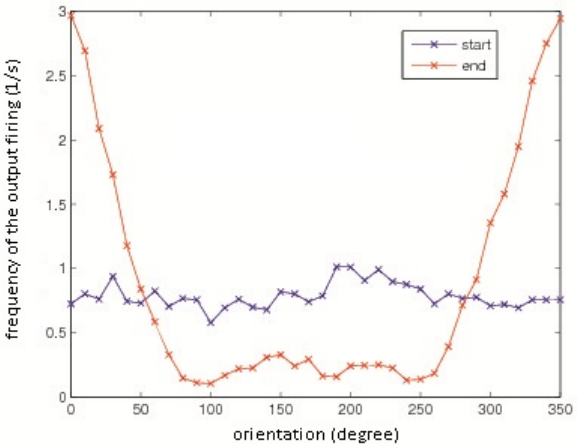

(b) number of firing with moving stimulus with speed 1

Figure 4.9: After the previous training. (a) Run 400 swipes for each degree to test with 10 (mm/s) speed of bar. (b) Run 40 swipes with different degree and the speed of bar is 1 (mm/s).

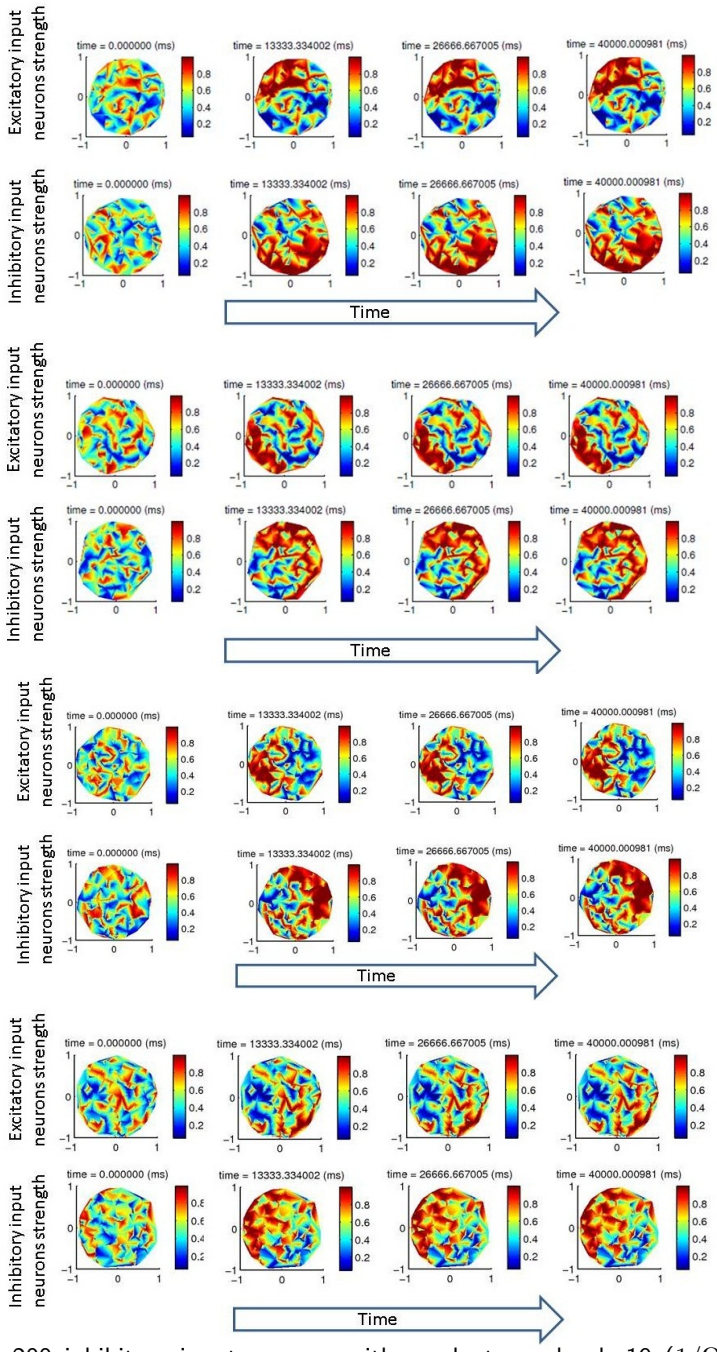

Figure 4.10: 200 inhibitory input neurons with conductance level -19 $(1/\Omega)$ to -1 $(1/\Omega)$ and 200 excitatory input neurons with conductance level 20 $(1/\Omega)$ to 1 $(1/\Omega)$ are randomly distributed in the unit circle and bar stimulus with random degree moves over the receptive field in $s = 10$ (mm/s) with $(H, B, W) =$ (30 (1/s), 1 (1/s), 0.2 (mm)). Use Rule 1b, 2b, 3a, 4a, and 5 with $L = \infty$ and the parameters from Table 3.2. Four different realization show different results from the randomness of the inputs.

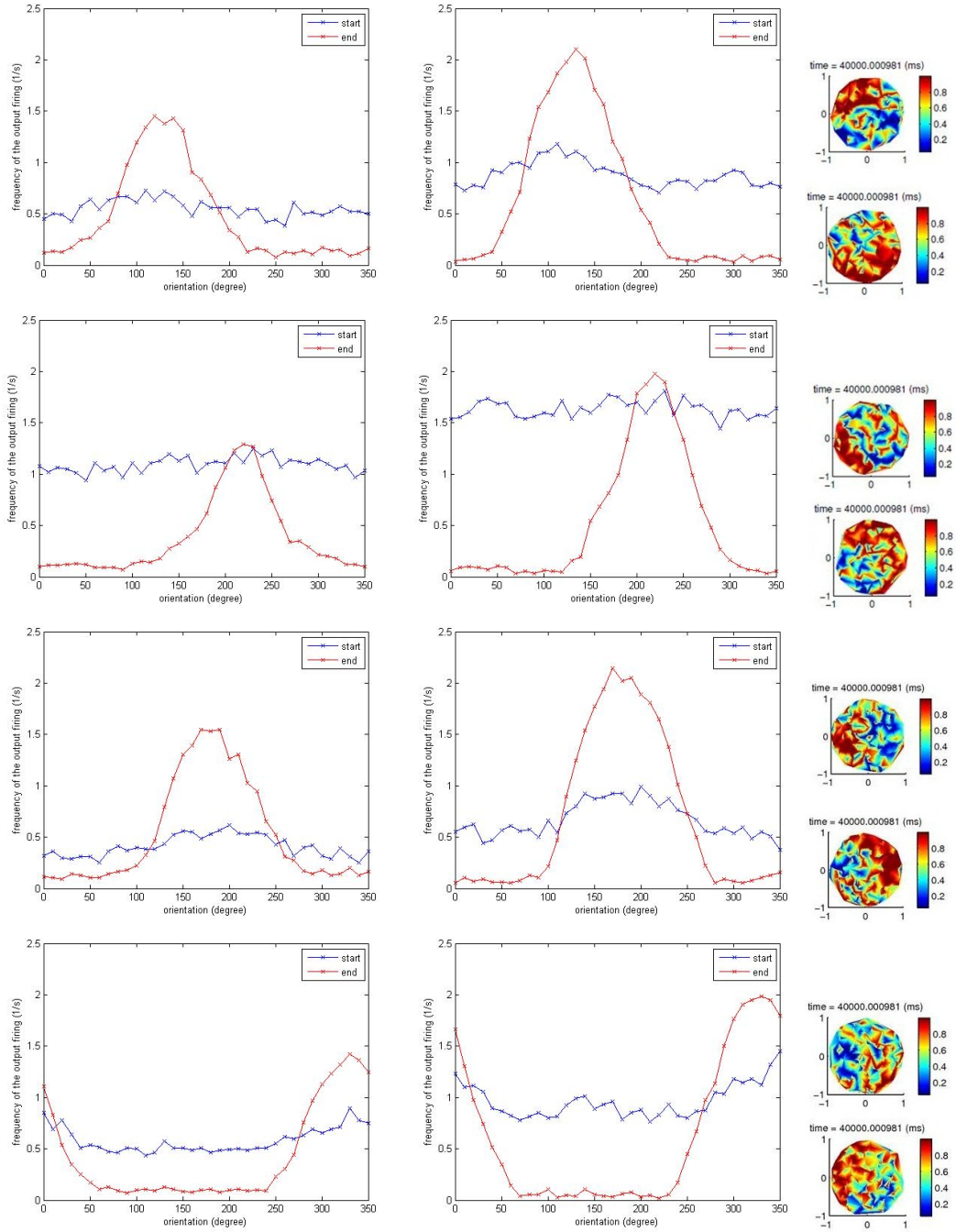

Figure 4.11: After the previous training. Run testing swipes with different degrees. Left column shows the results from speed of bar in 10 (mm/s) with 400 swipes, and middle column shows the results from ten times faster speed of bar from the training in 1 (mm/s) with 40 swipes. Right column shows the last configuration of both excitatory and inhibitory input neurons' conductance level.

Part III

Mathematical and Structural Study

Chapter 5

Markov Chain Analysis

5.1 Introduction

We would like to analyze why those interesting emergence properties happened in the last section. However, even with the discretized space in the case of Markov chain (3.3), the size of the state space is large. Consider the conductance G to be discretized with Δg then the number of conductance level M is $(g_{\max} - g_{\min})/\Delta g$ and the membrane potential V is discretized with Δv and the size of whole space is

$$2^{N(L+1)}\, 2\, M^{N(L+1)}\, ((V_{\max} - V_{\text{rest}})/\Delta v).$$

We make more assumptions to make the Markov chain smaller, and make it possible to analyze. What we would like to observe is the properties of selectivity, which explains the physiology of the system. If the model has the stable distribution then the system has selectivity, therefore we would like to study the distributions of the model. If the system is a Markov chain then we can find the stable distribution through the invariant distribution of the Markov matrix. In other words, the eigenvector corresponding to the eigenvalue 1 is the stable distribution of the system. Once we know the invariant distribution, then the next question is the convergence rate, which is represented by the second biggest eigenvalue. If the second biggest eigenvalue is close to one then the speed of convergence is very slow. The slow convergence is something to worry about, since many of the simulations are done by the Monte Carlo method, which shows the end results after running a long time and that time may in fact not be long enough.

5.2 Markov Chain Space Reduction

It is not feasible to study a large space, so we reduced the space by adding more assumptions. For these reduced models, we needed to show the system is still a Markov chain and therefore we

could extend the methods and analysis for the reduced system to the original system. We will show an example using the one time step history,

$L = 0$, case. The system with assumptions in Section 3.3 and assumption $L = 0$ is still a Markov chain. From (3.3), the original state is

$$S_k = \left\{ dY_k^k, dZ_k^k, G_k^k, V_k \right\}. \tag{5.1}$$

We can make the system smaller by using the condition $L = 0$.

First, we show the past input neuron's firing dY_{k-1} is depended on the current stimulus X_k. Using this, the other variables, which depended on all the past input neuron's firing, are now depended on the current stimulus.

Lemma 5.2.1. *If the stimulus X is deterministic then the point process $dY_{k-1,i}$ of the ith input neuron at time $k-1$ is conditionally independent from everything except the stimulus X_k at time k:*

$$\begin{aligned} & \mathbb{P}(dY_{k-1,i} = dy_{k-1,i} | E^{k-2} = e^{k-2}, E_k^K = e_k^K, X^K = x^k, G_{k-1} = g_{k-1}, V_{k-1} = v_{k-1}, dZ_{k-1} - dz_{k-1}) \\ = \quad & \mathbb{P}(dY_{k-1,i} = dy_{k-1,i} | X_k = x_k). \end{aligned}$$

Proof. Note that,

$$
\begin{aligned}
& \mathbb{P}(dY_{k-1,i} = dy_{k-1,i} | E^{k-2} = e^{k-2}, E_k^K = e_k^K, X^K = x^k, G_{k-1} = g_{k-1}, V_{k-1} = v_{k-1}, dZ_{k-1} - dz_{k-1}) \\
= \quad & \mathbb{P}(dY_{k-1,i} = dy_{k-1,i} | X_k = x_k, X_{k-1} = x_{k-1}) && (5.2) \\
= \quad & \frac{\mathbb{P}(dY_{k-1,i} = dy_{k-1,i} | X_k = x_k) \mathbb{P}(X_{k-1,i} = x_{k-1,i} | X_k = x_k, dY_{k-1,i} = dy_{k-1,i})}{\sum_{dy \in \mathtt{dY}} \mathbb{P}(dY_{k-1,i} = dy | X_k = x_k) \mathbb{P}(X_{k-1,i} = x_{k-1,i} | X_k = x_k, dY_{k-1,i} = dy)} && (5.3) \\
= \quad & \frac{\mathbb{P}(dY_{k-1,i} = dy_{k-1,i} | X_k = x_k) \mathbb{P}(X_{k-1,i} = x_{k-1,i} | X_k = x_k)}{\sum_{dy \in \mathtt{dY}} \mathbb{P}(dY_{k-1,i} = dy_{k-1,i} | X_k = x_k) \mathbb{P}(X_{k-1,i} = x_{k-1,i} | X_k = x_k)} && (5.4) \\
= \quad & \frac{\mathbb{P}(dY_{k-1,i} = dy_{k-1,i} | X_k = x_k)}{\sum_{\{dy \in \mathtt{dY}\}} \mathbb{P}(dY_{k-1,i} = dy | X_k = x_k)} \\
= \quad & \mathbb{P}(dY_{k-1,i} = dy_{k-1,i} | X_k = x_k)
\end{aligned}
$$

where (5.2) holds from Assumption 2; (5.3) holds from Bayes theorem; (5.4) holds because X is deterministic and also from Assumption 1 □

Using this, we show the conductance $G_{k,i}$ and the voltage V_k does not depend on the previous input neuron's firing $dY_{k-1,i}$.

Lemma 5.2.2. *The probability of the conductance level $G_{k,i}$ of the ith input neuron at time k is independent from $G^{k-2,i}$, X^{k-1}, and V^{k-2} given $G_{k-1,i}$, X_k, and V_{k-1}:*

$$
\begin{aligned}
\mathbb{P}\left(G_{k,i} = g_{k,i} | G^{k-1,i} = g^{k-1,i}, V^{k-1} = v^{k-1}, X^k = x^k, \bigcap_{j \neq i} G^{k,j} = g^{k,j} \right) \\
= \mathbb{P}(G_{k,i} = g_{k,i} | G_{k-1,i} = g_{k-1,i}, V_{k-1} = v_{k-1}, X_k = x_k).
\end{aligned}
$$

Proof. Note that

$$
\begin{aligned}
& \mathbb{P}\left(G_{k,i} = g_{k,i} | G^{k-1,i} = g^{k-1,i}, V^{k-1} = v^{k-1}, X^k = x^k, \bigcap_{j \neq i} G^{k,j} = g^{k,j}\right) \\
= & \sum_{dy_{k-1,i} \in (\mathsf{d}Y)^N, dz_{k-1} \in (\mathsf{d}Z)^N} \mathbb{P}(G_{k,i} = g_{k,i} | G^{k-1,i} = g^{k-1,i}, \\
& V^{k-1} = v^{k-1}, X^k = x^k, \bigcap_{j \neq i} G^{k,j} = g^{k,j}, dY_{k-1,i} = dy_{k-1,i}, dZ_{k-1} = dz_{k-1}) \\
& \mathbb{P}(dY_{k-1,i} = dy_{k-1,i} | X_k = x_k) \mathbb{P}(dZ_{k-1} = dz_{k-1} | V_{k-1} = v_{k-1}) \qquad (5.5) \\
= & \sum_{dy_{k-1,i} \in (\mathsf{d}Y)^N, dz_{k-1} \in (\mathsf{d}Z)^N} \mathbb{P}(G_{k,i} = g_{k,i} | G_{k-1,i} = g_{k-1,i}, \\
& V_{k-1} = v_{k-1}, X_k = x_k, dY_{k-1,i} = dy_{k-1,i}, dZ_{k-1} = dz_{k-1}) \qquad (5.6) \\
& \mathbb{P}(dY_{k-1,i} = dy_{k-1,i} | X_k = x_k) \mathbb{P}(dZ_{k-1} = dz_{k-1} | V_{k-1} = v_{k-1}) \\
= & \mathbb{P}(G_{k,i} = g_{k,i} | G_{k-1,i} = g_{k-1,i}, V_{k-1} = v_{k-1}, X_k = x_k) \qquad (5.7)
\end{aligned}
$$

where (5.7) follows from chain rule; (5.5) follows from chain rule, Lemma 5.2.1 and Assumption 5; (5.6) follows from Assumption 3. □

The probability of the membrane potential V_k is evaluated by X_k, V_{k-1} and $G_{k-1,i}$ for all $i = 1, 2, \cdots, N$.

Lemma 5.2.3. *The Probability of the membrane potential V_k at time k is independent from G^{k-2}, X^{k-1}, and V^{k-2} given X_k, V_{k-1} and G_{k-1}:*

$$
\begin{aligned}
& \mathbb{P}(V_k = v_k | G^k = g^k, V^{k-1} = v^{k-1}, X^k = x^k) \\
= & \mathbb{P}(V_k = v_k | G_{k-1} = g_{k-1}, V_{k-1} = v_{k-1}, X_k = x_k).
\end{aligned}
$$

Proof. Note that,

$$\begin{aligned}
& \mathbb{P}(V_k = v_k | G^k = g^k, V^{k-1} = v^{k-1}, X^k = x^k) \\
= & \sum_{dy_{k-1} \in (\mathrm{d}Y)^N} \mathbb{P}(V_k = v_k | G^k = g^k, V^{k-1} = v^{k-1}, X^k = x^k, dY_{k-1} = dy_{k-1}) \\
& \mathbb{P}(dY_{k-1} = dy_{k-1} | X_k = x_k) \qquad (5.8) \\
= & \sum_{dy_{k-1} \in (\mathrm{d}Y)^N} \mathbb{P}(V_k = v_k | G_{k-1} = g_{k-1}, V_{k-1} = v_{k-1}, X_k = x_k, dY_{k-1} = dy_{k-1}) \qquad (5.9) \\
& \mathbb{P}(dY_{k-1} = dy_{k-1} | X_k = x_k) \\
= & \mathbb{P}(V_k = v_k | G_{k-1} = g_{k-1}, V_{k-1} = v_{k-1}, X_k = x_k) \qquad (5.10)
\end{aligned}$$

where (5.8) follows from Lemma 5.2.1, and chain rule; (5.9) follows from Assumption 4; (5.10) follows from chain rule. □

We now denote a random process S pertaining to the state in this simpler model as:

$$S_k = \{G_k, V_k\}. \qquad (5.11)$$

This is smaller than the original (5.1).

Lemma 5.2.4. *The random process S as defined in* (5.11) *satisfies*

$$\mathbb{P}(S_k = s_k | S^{k-1} = s^{k-1}, X^k = x^k) = \mathbb{P}(S_k = s_k \, | S_{k-1} = s_{k-1}, X_k = x_k).$$

Proof. Note that,

$$\begin{aligned}
& \mathbb{P}(S_k = s_k | S^{k-1} = s^{k-1}, X^k = x^k) \\
= & \mathbb{P}(G_k = g_k | S^{k-1} = s^{k-1}, X^k = x^k) \mathbb{P}(V_k = v_k | S^{k-1} = s^{k-1}, X^k = x^k, G_k = g_k) \qquad (5.12) \\
= & \mathbb{P}(G_k = g_k | S_{k-1} = s_{k-1}, X_k = x_k) \mathbb{P}(V_k = v_k | S_{k-1} = s_{k-1}, X_k = x_k, G_k = g_k) \qquad (5.13) \\
= & \mathbb{P}(S_k = s_k \, | S_{k-1} = s_{k-1}, X_k = x_k) \qquad (5.14)
\end{aligned}$$

where (5.12) and (5.14) follows from chain rule; (5.13) follows from Lemma 5.2.2 and 5.2.3 □

Theorem 5.2.5. *The random process S as defined in* (5.11) *is a controlled Markov chain with respect to X.*

Proof. Analogous argument as proof of Th. 3.4.2 with Lemma . □

Adding $L = 0$ condition makes smaller state space. We only need G_k and V_k values to know the state in the next time step.

5.3 Markov Chain Space Reduction: Specific Rules

It this section, we assume following conditions.

1. The look back is the size of time step Δt, meaning $L = 0$.
2. Only one input neuron fires in one time step, meaning $\sum_i dY_i < 2$.
3. Constant input firing $\Delta t\rho$ independent from stimulus, so that the system becomes a time-independent Markov chain.

As mentioned in Rule 3c, we need new conductance modification rules. We consider the following two cases.

$dY_{k,i}$	dZ_k	modification of $G_{k+1,i}$ (case 1)	modification of $G_{k+1,i}$ (case 2)
1	1	going up Δg	
1	0	going down Δg	no difference
0	1	no difference	going down Δg with some probability Δ
0	0	no difference	

In Case 1, if an input neuron fires and the output neuron does not fire then we consider the output neuron to be fired before the close interval. On the other hand, in Case 2 if the output neuron fires and an input neuron does not fire then we consider the input neuron to have fired in the short interval. In this section, we show existence of the community formation of maximum and minimum conductance levels for these cases.

5.3.1 Case 1: no conductance modification without input firing with $V_{\max} = V_{\min}$

To study case 1, we need much stronger assumptions, so we add the following:

Assumption 6. *If the ith input neuron does not fire then the conductance level of the ith input neuron does not change,*

$$\begin{aligned} & \mathbb{P}\Big(G_{k,i} = g_{k,i} | E^{k-2} = e^{k-2}, E_{k-1}^{K} = e_{k-1}^{K}, \\ & \bigcap_{j \neq i} (G_{k-1,j} = g_{k-1,j}, dY_{k-1,j} = dy_{k-1,j}), X_k = x_k, dY_{k-1,i} = 0\Big) \\ = \quad & \mathbb{P}(G_{k,i} = g_{k,i} | G_{k-1,i} = g_{k-1,i}, dY_{k-1,i} = 0) = 1_{g_{k-1,i} = g_{k,i}}. \end{aligned}$$

Further assume conductance to be the same value $V_{\text{rest}} = V_{\max} = V_{\text{const}}$. Then the output neuron fires only if one of the input neurons fires in the same time interval.

Lemma 5.3.1. *If firing of the ith input neuron is given then firing of the output neuron is conditionally independent from the conductance levels of non-ith input neurons:*

$$\mathbb{P}(dZ_k = dz_k | dY_{k,i} = 1, G^{k,i} = g^{k,i}, X^k = x^k) = \mathbb{P}(dZ_k = dz_k | dY_{k,i} = 1, G_{k,i} = g_{k,i}).$$

Proof. Note that

$$\begin{aligned} & \mathbb{P}(dZ_k = dz_k | dY_{k,i} = 1, G^{k,i} = g^{k,i}, X^k = x^k) \\ = \quad & \mathbb{P}\left(dZ_k = dz_k | dY_{k,i} = 1, \bigcap_{j \neq i} dY_{k,j} = 0, G^k = g^k, X^k = x^k\right) \\ & \prod_{j \neq i} (\mathbb{P}(dY_{k,j} = 0 | X^k = x^k) \mathbb{P}(G_{k,j} = g_{k,j} | G_{k-1,i} = g_{k-1,i}, dY_{k,j} = 0)) \qquad (5.15) \\ = \quad & \mathbb{P}\left(dZ_k = dz_k | dY_{k,i} = 1, \bigcap_{j \neq i} dY_{k,j} = 0, G_k = g_k, X_k = x_k\right) \qquad (5.16) \\ & \prod_{j \neq i} (\mathbb{P}(dY_{k,j} = 0 | X^k = x^k) \mathbb{P}(G_{k,j} = g_{k,j} | dY_{k,j} = 0)) \\ = \quad & \mathbb{P}(dZ_k = dz_k | dY_{k,i} = 1, G_{k,i} = g_{k,i}) \qquad (5.17) \end{aligned}$$

where (5.15) holds from chain rule, Lemma 5.2.1 and Assumption 6; (5.16) holds from original Assumption 5; (5.17) holds from chain rule. □

Each input neuron is independent from each other, therefore we denote the smaller random process S_i representing the state of each neuron i:

$$S_{k,i} = \{G_{k,i}\}. \tag{5.18}$$

Lemma 5.3.2. *The random process S_i satisfies*

$$\mathbb{P}(S_{k,i} = s_{k,i} | S^{k-1,i} = s^{k-1,i}) = \mathbb{P}(S_{k,i} = s_{k,i} \ | S_{k-1,i} = s_{k-1,i}).$$

Proof. Note that,

$$\begin{aligned}
& \mathbb{P}(G_{k,i} = g_{k,i} | G^{k-1,i} = g^{k-1,i} X^k = x^k) \\
= \ & \mathbb{P}(G_{k,i} = g_{k,i} | G^{k-1,i} = g^{k-1,i}, X^k = x^k, dY_{k-1,i} = 0) \mathbb{P}(dY_{k-1,i} = 0 | X_k = x_k) \\
+ \ & \sum_{dz \in \mathtt{d}Z} \mathbb{P}(G_{k,i} = g_{k,i} | G^{k-1,i} = g^{k-1,i}, X^k = x^k, dY_{k-1,i} = 1, dZ_{k-1} = dz_{k-1}) \\
& \mathbb{P}(dZ_{k-1} = dz_{k-1} | G^{k-1,i} = g^{k-1,i}, X^k = x^k, dY_{k-1,i} = 1) && (5.19) \\
= \ & \mathbb{P}(G_{k,i} = g_{k,i} | G_{k-1,i} = g_{k-1,i}, X_k = x_k, dY_{k-1,i} = 0) \mathbb{P}(dY_{k-1,i} = 0 | X_k = x_k) && (5.20) \\
+ \ & \sum_{dz \in \mathtt{d}Z} \mathbb{P}(G_{k,i} = g_{k,i} | G_{k-1,i} = g_{k-1,i}, X_k = x_k, dY_{k-1,i} = 1, dZ_{k-1} = dz_{k-1}) && (5.21) \\
& \mathbb{P}(dZ_{k-1} = dz_{k-1} | G_{k-1,i} = g_{k-1,i}, X_k = x_k, dY_{k-1,i} = 1) && (5.22) \\
= \ & \mathbb{P}(G_{k,i} = g_{k,i} | G_{k-1,i} = g_{k-1,i}, X_k = x_k) && (5.23)
\end{aligned}$$

where (5.19) holds from chain rule and Lemma 5.2.1; (5.20) holds from Assumption 6; (5.21) holds from original Assumption 3; (5.22) holds from Lemma 5.3.1; (5.23) holds from chain rule. □

Lemma 5.3.3. *The random process S_i satisfies*

$$\mathbb{P}(S_{k,i} = s_{k,i} | S^{k-1,i} = s^{k-1,i}) = \mathbb{P}(S_{k,i} = s_{k,i} \ | S_{k-1,i} = s_{k-1,i}).$$

Proof. Analogous argument as proof of Th. 3.4.2. □

Because all of the input neurons are independent, each will individually be drawn according to the distribution of each neuron's conductance level. The invariant measure for the N neuron system is of the form

$$\mu_N(\mathbf{n}) = \prod_{i=1}^{N} \pi(n_i),$$

where we just mean the measure concentrated on the point $\mathbf{n} = (n_1, n_2, \cdots, n_N)$ is independent in each slot. When we look at the population as a whole, we expect it to look like a sample drawn from each distribution.

Each input neuron is independent from each other, so the Markov chain we need to consider is (5.18) and the size of the state space becomes only M.

We choose probability rules from Rule 4b, and 5:

$$\begin{aligned}
\mathbb{P}(dZ_k = 1 | dY_{k,i} = 1, G_{k,i} = g_{k,i}) &= (g_{k,i}V_{\text{ex}} + V_{\text{rest}}) \,/\, (g_{k,i}V_{\text{ex}} + V_{\text{rest}} + V_{\text{const}}(g_{k,i} + 1)) \\
\mathbb{P}(dZ_k = 0 | dY_{k,i} = 1, G_{k,i} = g_{k,i}) &= 1 - (g_{k,i}V_{\text{ex}} + V_{\text{rest}}) \,/\, (g_{k,i}V_{\text{ex}} + V_{\text{rest}} + V_{\text{const}}(g_{k,i} + 1)).
\end{aligned}$$

Apply these to the following equation to find the transition probability:

$$\begin{aligned}
\mathbb{P}(G_{k+1,i} = g_{k+1,i} | G_{k,i} = g_{k,i}) &= \mathbb{P}(G_{k+1,i} = g_{k+1,i} | G_{k,i} = g_{k,i}, dY_{k,i} = 1, dZ_{k,i} = dz_{k,i}) \\
&\quad \mathbb{P}(dY_{k,i} = 1)\mathbb{P}(dZ_k = dz_k | dY_{k,i} = 1, G_{k,i} = g_{k,i}) \\
&+ \mathbb{P}(G_{k+1,i} = g_{k+1,i} | G_{k,i} = g_{k,i}, dY_{k,i} = 0)\mathbb{P}(dY_{k,i} = 0).
\end{aligned}$$

For convenience, we introduce a function $f(j)$ for the probability of the output firing given an input neuron fire, which has conductance level j as:

$$f(j) = \frac{jV_{\text{ex}} + V_{\text{rest}}}{jV_{\text{ex}} + V_{\text{rest}} + V_{\text{const}}(j+1)}.$$

Choose $V_{\text{rest}} = 0$ (mV) and normalize this with $g_{\max}$. Then we discretize $f(j)$ with normalized

conductance step size $\Delta g_n = \Delta g / g_{\max}$:

$$f_k = \frac{(g_{min}/g_{max} + k\Delta g_n)V_{\text{ex}}}{(g_{min}/g_{max} + k\Delta g_n)V_{\text{ex}} + V_{\text{const}}((g_{min}/g_{max} + k\Delta g_n) + 1/g_{\max})}. \tag{5.24}$$

We choose the conductance value to be between Δg_n and 1, meaning $g_{\min} = \Delta g / g_{\max}$, and the rest of the relevant values are from Table 3.2. The numerical simulation with Rule 1a, 2a, 4a, and 5, with parameters $\rho_{k,i} = 1.0$ (1/s), $L = \infty$, and $V_{\text{const}} = 21$ (mV) shows community formation with tendency of maximum and minimum conductance levels as shown in Fig. 5.1 for $\Delta g_n = 1/10$ (Ω) and Fig.5.2 for $\Delta g_n = 1/90$ (Ω).

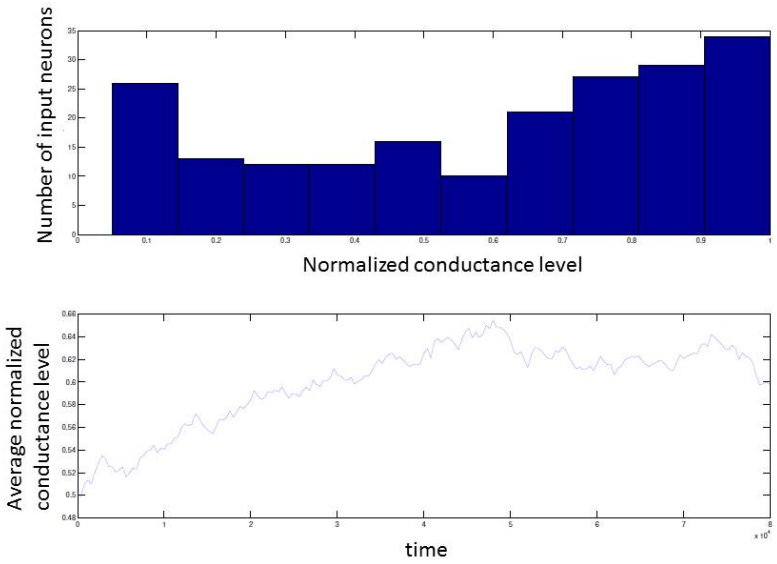

Figure 5.1: Emergence of community formation of group of neurons for Rule 1a, 2a, 3c of case 1, 4a, and 5 with $L = \infty$, $\rho_{k,i} = 1.0$ (1/s), $V_{\text{const}} = 21$ (mV) and $\Delta g_n = 1/10$ (Ω).

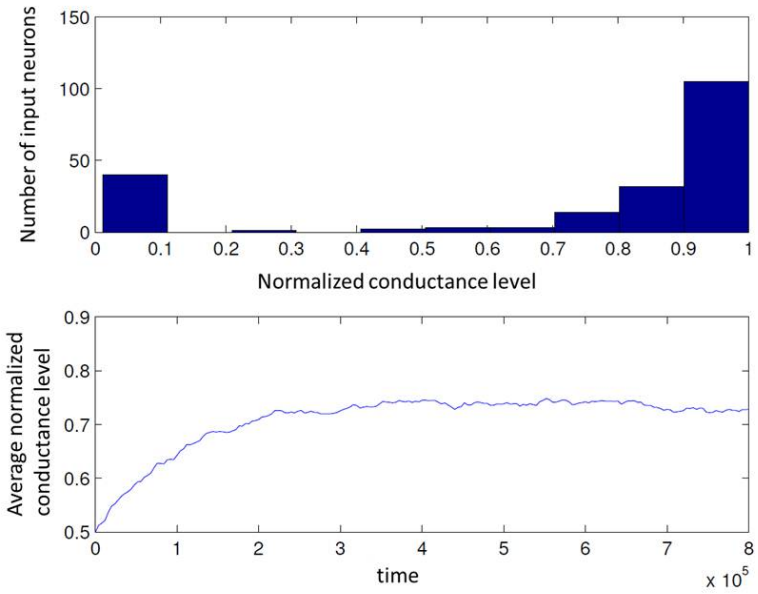

Figure 5.2: Emergence of community formation of group of neurons for Rule 1a, 2a, 3c of case 1, 4a, and 5 with $L = \infty$, $\rho_{k,i} = 1.0$ (1/s), $V_{\text{const}} = 21$ (mV) and $\Delta g_n = 1/90$ (Ω).

The transition matrix T becomes $T = \Delta t \rho P + (1 - \Delta t \rho) I$, where

$$P = \begin{bmatrix} 1-f_1 & f_1 & 0 & 0 & 0 & \cdots & 0 & 0 & 0 \\ 1-f_2 & 0 & f_2 & 0 & 0 & \cdots & 0 & 0 & 0 \\ 0 & 1-f_3 & 0 & f_3 & 0 & \cdots & 0 & 0 & 0 \\ 0 & 0 & 1-f_4 & 0 & f_4 & \cdots & 0 & 0 & 0 \\ \vdots & \vdots & \vdots & \vdots & \vdots & \cdots & \vdots & \vdots & \vdots \\ 0 & 0 & 0 & 0 & 0 & \cdots & 0 & f_{M-2} & 0 \\ 0 & 0 & 0 & 0 & 0 & \cdots & 1-f_{M-1} & 0 & f_{M-1} \\ 0 & 0 & 0 & 0 & 0 & \cdots & 0 & 1-f_M & f_M \end{bmatrix}. \tag{5.25}$$

The invariant measure satisfies $\pi^T T = \pi^T$, which means $(T - I)^T \pi = \mathbf{0}$. Multiply both sides by

lower triangle matrix L where all components are 1. This leads to the series of equations

$$\pi_{k+1} = \frac{f_k}{1 - f_{k+1}} \pi_k. \tag{5.26}$$

Lemma 5.3.4. *If g_{max}, V_{ex} and V_{const} are positive, then f is a an increasing function.*

Proof. Consider

$$\frac{df_k}{dk} = \frac{V_{\mathrm{ex}} V_{\mathrm{const}} / g_{\max}}{(k(V_{\mathrm{ex}} + V_{\mathrm{const}}) + V_{\mathrm{const}}/g_{\max}))^2},$$

so f_k is a increasing function except a point $k = -\dfrac{V_{\mathrm{const}}/g_{\max}}{V_{\mathrm{ex}} + V_{\mathrm{const}}}$. Since $k \in \{0, 1\}$ and all $g_{\max}, V_{\mathrm{ex}}, V_{\mathrm{const}}$ are positive, we can conclude f_k is increasing function. □

Lemma 5.3.5. *If f is an increasing function and*

$$\frac{\Delta g_n V_{ex}}{1/g_{max} + \Delta g_n} < V_{const} < \frac{V_{ex}}{1/g_{max} + 1}$$

then the invariant distribution has community formation.

Proof. If the following equation is always bigger than 0 then the invariant distribution is convex:

$$\begin{aligned} \pi_{k+1} + \pi_{k-1} - 2\pi_k &= \left(\frac{f_k}{1 - f_{k+1}} + \frac{1 - f_k}{f_{k-1}} - 2 \right) \pi_k \\ &= (f_k f_{k-1} + (1 - f_k)(1 - f_{k+1}) - 2f_{k-1}(1 - f_{k+1})) \frac{\pi_k}{f_{k-1}(1 - f_{k+1})}. \end{aligned}$$

Since f is an increasing function and the value is less than 1 from conditions of probability, then

$$\begin{aligned} \pi_{k+1} + \pi_{k-1} - 2\pi_k &\geq (f_{k-1} f_{k-1} + (1 - f_{k+1})(1 - f_{k+1}) - 2f_{k-1}(1 - f_{k+1})) \frac{\pi_k}{f_{k-1}(1 - f_{k+1})} \\ &= (f_{k-1} - (1 - f_{k+1}))^2 \frac{\pi_k}{f_{k-1}(1 - f_{k+1})} \\ &> 0, \end{aligned}$$

because distribution π and function f are in between 0 to 1.

If f is an increasing function, then $1 - f$ is a decreasing function. Consider Eq. (5.26), then if

$f_k < 0.5$ then $\pi_{k+1} < \pi_k$ and if $f_k > 0.5$ then $\pi_{k+1} > \pi_k$. Therefore, to have community formation, f must cross 0.5, which means $f_1 < 0.5$ and $f_N > 0.5$. Plug in the values from Eq. (5.24) to get,

$$\frac{\Delta g_n V_{\text{ex}}}{1/g_{\max} + \Delta g_n} < V_{\text{const}} < \frac{V_{\text{ex}}}{1/g_{\max} + 1}.$$

If this is satisfied then the invariant distribution has community formation. □

For Fig. 5.1 and 5.2, we chose $V_{\text{ex}} = 25$ (mV), $V_{\text{const}} = 21$ (mV) and $g_{\max} = 20$, so that $\frac{V_{\text{const}}/g_{\max}}{V_{\text{ex}} - V_{\text{const}}} = 0.2625$, which is in fact between 0 and 1. If we assume the invariant distribution has community formation, then f has to cross 0.5, which is shown in Fig. 5.3a for the case of $\Delta g_n = 1/10$. The output firing is smaller than 0.5 with a smaller conductance level, but becomes larger than 0.5 for larger conductance levels. Plug in the parameters we used to the condition in the lemma 5.3.5 for the strong community formation. We have approximately 16.7 (mV) $\leq V_{\text{const}} \leq$ 23.8 (mV) and that follows Fig. 5.3b, which represents several invariant distributions using the same parameters for different V_{const} values.

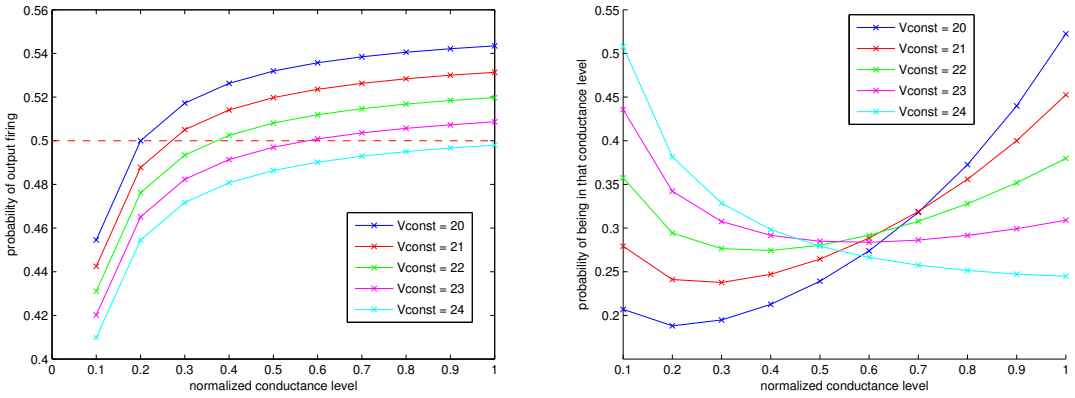

(a) Function f from (5.24) **(b)** Invariant distributions

Figure 5.3: (a) Function f_k from (5.24) with $\Delta g_n = 0.1$, showing the probability of the output neuron's firing given an input neuron has fired (b) Invariant distributions of a matrix 5.25 for different V_{const} (mV) values in $\Delta g_n = 0.1$.

Fig. 5.2 seems to have stronger community formation than Fig. 5.1. We have the following

lemma to explain the effect:

Lemma 5.3.6. *If f is an increasing function then smaller conductance step Δg_n cause stronger community formation.*

Proof. Consider Δg_n to be the conductance step of original distribution, and the smaller conductance step size to be Δg_s. Consider following sequences

$$\begin{aligned} d &= \{\Delta g_n, 2\Delta g_n, \cdots, \alpha\Delta g_n\} \text{ where } \alpha = \max\{f(g_{min}/g_{max} + j\Delta g_n) < 1/2\} \\ d^s &= \{\Delta g_s, 2\Delta g_s, \cdots, \beta\Delta g_s\} \text{ where } \beta = \max\{f(g_{min}/g_{max} + i\Delta g_s) < 1/2\}. \end{aligned}$$

Because f is an increasing function and smaller than $1/2$ for all d and d^s we have

$$\frac{f_{d_i}}{1 - f_{d_{i+1}}} > \frac{f_{d^s_k}}{1 - f_{d^s_l}} \prod_{i=k+1}^{l-1} \frac{d^s_i}{1 - d^s_i}, \tag{5.27}$$

where $k = \min_k \left\{ \begin{cases} d_i - d^s_k & \text{if } d_i - d^s_k > 0 \\ 1 & \text{else} \end{cases} \right\}$ and $l = \min_k \left\{ \begin{cases} d^s_k - d_i & \text{if } d^s_k - d_i > 0 \\ 1 & \text{else} \end{cases} \right\}$.
From the proof of Lemma 5.3.5, minimum distribution of original distribution π is

$$\pi_m = \prod_{i=1}^{\max_i\{f(g_{\min}/g_{\max} + i\Delta g_s) < 1/2\}} \frac{f(g_{\min}/g_{\max} + i\Delta g_n)}{1 - f(g_{\min}/g_{\max} + i\Delta g_n)} \pi_1.$$

Using Eq. (5.27), minimum distribution of the smaller conductance π^s_m has the larger ratio with π_1. We follow the same way to show the ratio of maximum distribution and minimum also become larger by the smaller conductance step. Consider following sequences

$$\begin{aligned} e = \{\alpha\Delta g_n, (\alpha+1)\Delta g_n, \cdots, \gamma\Delta g_n\} \quad & \text{where} \quad \alpha = \min\{f(g_{min}/g_{max} + j\Delta g_n) > 1/2\} \\ & \text{and} \quad \gamma = \max\{f(g_{min}/g_{max} + k\Delta g_n) < 1\} \\ e^s = \{\beta\Delta g_s, (\beta+1)\Delta g_s, \cdots, \delta\Delta g_s\} \quad & \text{where} \quad \beta = \min\{f(g_{min}/g_{max} + i\Delta g_s) > 1/2\} \\ & \text{and} \quad \delta = \max\{f(g_{min}/g_{max} + l\Delta g_n) < 1\}. \end{aligned}$$

Because f is an increasing function and larger than $1/2$ for all d and d^s we have

$$\frac{1-f_{e_{i+1}}}{f_{e_i}} > \frac{1-f_{e_l^s}}{f_{e_k^s}} \prod_{i=k+1}^{l-1} \frac{1-e_i^s}{e_i^s}, \tag{5.28}$$

where $k = \min_k \left\{ \begin{cases} e_k^s - e_i & \text{if } e_k^s - e_i > 0 \\ 1 & \text{else} \end{cases} \right\}$ and $l = \min_k \left\{ \begin{cases} e_i - e_k^s & \text{if } e_i - e_k^s > 0 \\ 1 & \text{else} \end{cases} \right\}$. From the proof of Lemma 5.3.5, minimum distribution of original distribution π is

$$\pi_m = \prod_{\min_i\{f(g_{\min}/g_{\max}+i\Delta g_s)>1/2\}}^{\max_i\{f(g_{\min}/g_{\max}+i\Delta g_s)<1\}} \frac{1-f(g_{\min}/g_{\max}+i\Delta g_n)}{f(g_{\min}/g_{\max}+i\Delta g_n)} \pi_M.$$

Using Eq. (5.28), a smaller conductance step causes the ratio of π_m and π_M to increase. The α from Def. 3.2.3 becomes smaller, and this causes the community formation to become stronger. □

Since $\Delta g \to 0$ for the continuous case, if the invariant distribution has community formation it has to be strong.

Here we show the invariant distribution with different Δg_n values in Fig. 5.4. As shown in the previous lemma, the invariant distribution becomes stronger as Δg_n becomes smaller. The invariant distribution of transition matrix T is in fact almost same as the results from Fig. 5.1 with $\Delta g_n = 1/10$ and Fig. 5.2 with $\Delta g_n = 1/90$.

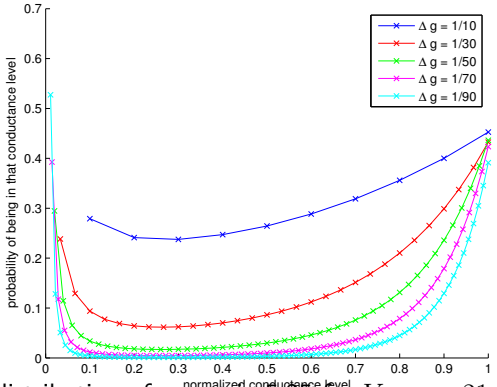

Figure 5.4: Invariant distribution of a matrix 5.25 for $V_{\text{const}} = 21$ (mV) case with different conductance levels.

5.3.2 Large network limit for Case 1

Consider the limiting case of $\Delta g_n \to 0$, from the proof of 5.3.6, when $f_m = 1/2$, π_m becomes minimum and

$$\pi_1 = \prod_{i=1}^{m} \frac{1-f_i}{f_{i-1}} \pi_m, \quad \pi_M = \prod_{i=m+1}^{M} \frac{f_{i-1}}{1-f_i} \pi_m. \tag{5.29}$$

Since we take the limiting case, consider $f(j) = 1/2$ instead of the discretized case. Here we normalize f with $g_{\max}$ and call it f_m. We use $g_{\max}$ to produce a normalized conductance that produces minimum π as

$$j_m = \frac{V_{\text{const}}/g_{\max}}{V_{\text{ex}} - V_{\text{const}}}.$$

Lemma 5.3.7. *If the following equation holds then the maximum and minimum of invariant distribution is the same:*

$$\log(V_{const}) = \log(V_{ex}) - (1/g_{max} + 1)\log(1/g_{max} + 1) - \log(g_{max})/g_{max}.$$

Proof. Since

$$\pi_M = \prod_{i=1}^{M} \frac{f_{i-1}}{1-f_i} \pi_1,$$

$\pi_M = \pi_1$ iff $\prod_{i=1}^{M} \frac{f_{i-1}}{1-f_i} = 1$. Take the log of both sides and multiply both sides with Δg_n then we get

$$0 = \sum_{i-1}^{M} log\left(\frac{f_{i-1}}{1-f_i}\right) \Delta g_n.$$

In the limit of $\Delta g_n \to 0$, this is a Riemann sum, so we have

$$0 = \int_0^1 \log\left(\frac{f_n(j)}{1-f_n(j)}\right) d\, j.$$

Plug in the parameters and we have

$$\log(V_{\text{const}}) = \log(V_{\text{ex}}) - (1/g_{\max} + 1)\log(1/g_{\max} + 1) - \log(g_{\max})/g_{\max}.$$

If this is satisfied then $\pi_1 = \pi_M$. □

Plug in the parameters we used, $V_{\text{ex}} = 25$ and $g_{\max} = 20$. If $V_{\text{const}} = \exp(\log(V_{\text{ex}}) - (1/g_{\max} + 1)\log(1/g_{\max} + 1) - \log(g_{\max})/g_{\max}) \approx 20.45$, then $\pi_1 = \pi_M$.

5.3.3 Convergence for Case 1

To study the convergence rate to the invariant distribution, we need to study the second biggest eigenvalue. If the second biggest eigenvalue is close to one then the convergence rate is slow, and the end time of the Monte Carlo simulation may not represent the invariant distribution. The eigenvalues of P are calculated and shown in Fig. 5.5a for different V_{const} values. Note, all eigenvalues are real.

Lemma 5.3.8. *All eigenvalues from Matrix 5.25 are real.*

Proof. Consider $P = D^{-1}P'D$, where D is a triangle matrix with diagonal entry $d_1 = 1$, $d_2 = \sqrt{(1-f_2)/(f_1)}d_1, \cdots, d_i = \sqrt{(1-f_i)/(f_{i-1})}d_{i-1}, \cdots$. Since f is a probability, it is between 0 and 1, and P' is a real symmetric tridiagonal matrix similar to P. P is similar to a real diagonal matrix, since P' is a real symmetric matrix. Therefore, P only has real eigenvalues. □

All eigenvalues look the same for all V_{const}, but actually they are only close and they have different spectrums. The second biggest eigenvalues become closer to 1 if V_{const} becomes closer to V_{ex} as shown in Fig. 5.5b, which uses all same parameters as before except V_{const}. Also with the case of $V_{\text{const}} = 21$ (mV), if the Δg_n becomes smaller, then the second biggest eigenvalue as well as the third, fourth, fifth, and sixth become closer to 1 as shown in Fig. 5.6a. The eigenvector related to the second biggest eigenvalue seems to have a monotonic components values as shown in Fig. 5.7.

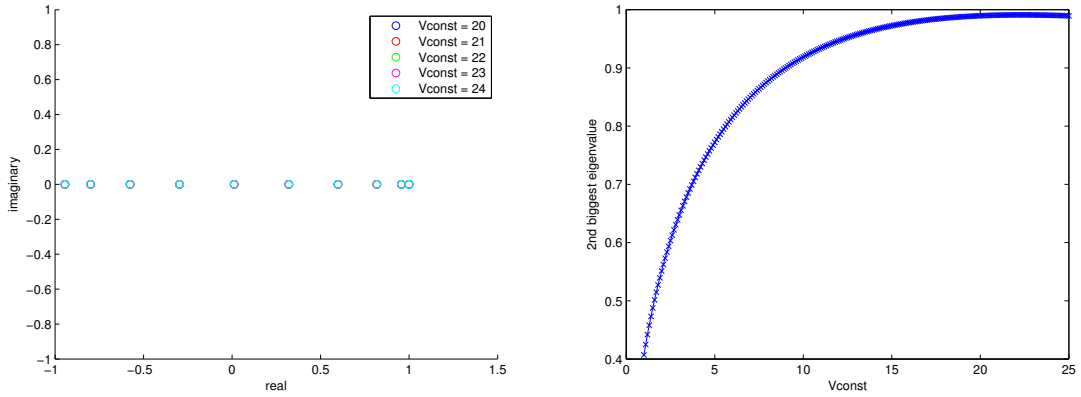

(a) Eigenvalues **(b)** 2nd biggest eigenvalues

Figure 5.5: (a) All eigenvalues of a matrix 5.25 for different V_{const} values in $\Delta g_n = 0.1$ (b) 2nd biggest eigenvalues of a matrix 5.25 over the different V_{const} value

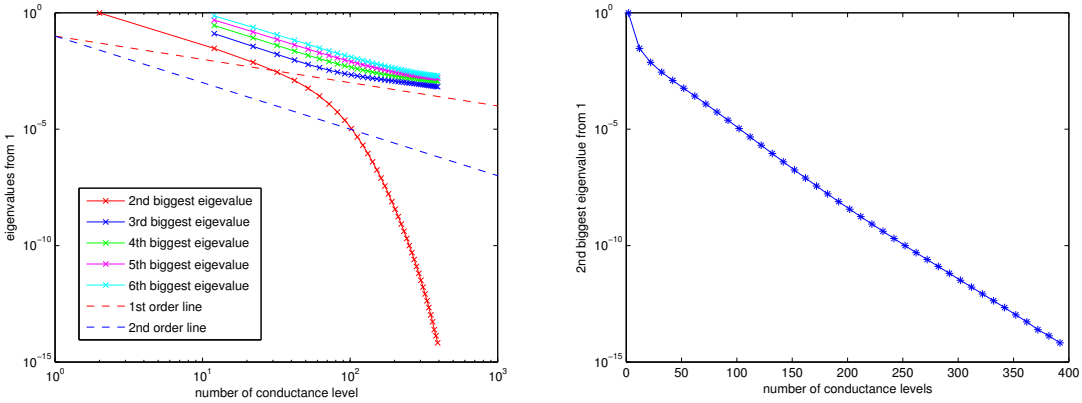

(a) 2nd biggest eigenvalues **(b)** 2nd biggest eigenvalues

Figure 5.6: (a) 2nd biggest eigenvalues of a matrix 5.25 over different Δg_n with $V_{\text{const}} = 21$ 9mV) (b) semi-logy plot of Fig. 5.6a. Invariant distribution of a matrix 5.25 for $V_{\text{const}} = 21$ (mV) case with different conductance levels.

5.3.4 Case 2: no conductance modification without output firing

To study Case 2 of Rule 3c, we need to add the following assumption to make the system tight:

Assumption 7. *If the ith input neuron does not fire then the conductance level of the ith input*

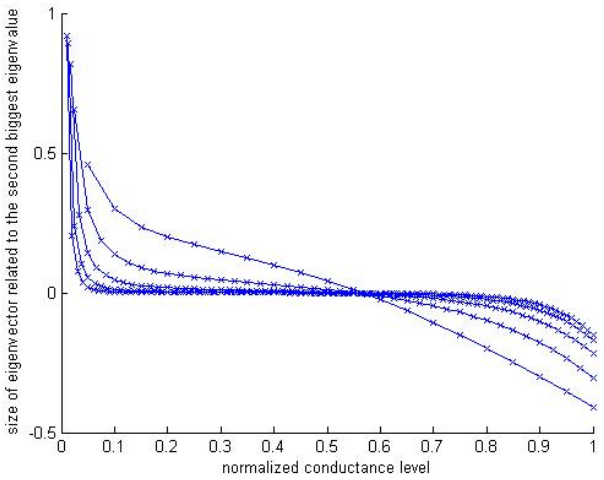

Figure 5.7: The eigenvector related to the second biggest eigenvalue of a matrix 5.25 over different Δg_n with $V_{\text{const}} = 21$. The size of the matrices are 20 by 20, 40 by 40, 60 by 60, 80 by 80, and 100 by 100. All have monotonic changing eigenvector components.

neuron does not change,

$$\begin{aligned} & \mathbb{P}\Big(G_{k,i} = g_{k,i} | E^{k-2} = e^{k-2}, E_{k-1}^{K} = e_{k-1}^{K}, \\ & \bigcap_{j \neq i} (G_{k-1,j} = g_{k-1,j}, dY_{k-1,j} = dy_{k-1,j}), X_k = x_k, dZ = 0\Big) \\ = \quad & \mathbb{P}(G_{k,i} = g_{k,i} | G_{k-1,i} = g_{k-1,i}, dZ = 0) = 1_{g_{k-1,i} = g_{k,i}}. \end{aligned}$$

With this assumption, the conductance levels are only modified when the voltage exceeds $V_{\max}$. We have a Markov chain $S_k = \{G_k, V_k\}$ from Eq. 5.11 and the constant input stimulus assumption, which shows

$$\mathbb{P}(G_k = g_k, V_k = v_k | G^{k-1} = g^{k-1}, V^{k-1} = v^{k-1}) = \mathbb{P}(G_k = g_k, V_k = v_k | G_{k-1} = g_{k-1}, V_{k-1} = v_{k-1}).$$

Consider the discrete voltage level. Since the conductance levels only change with the maximum

voltage level, we can only consider the Markov chain when the output neuron fires, so we define

$$\begin{aligned} T_0 &= 0 \\ T_k &= \inf_{k>T_{k-1}} (V_{k-1} = V_{\max}, V_k \neq V_{\max}). \end{aligned}$$

Lemma 5.3.9. *T_k are stopping times for the Markov chain (G_k, V_k).*

Proof. Since the conductance level G_K is only modified when $V_{k-1} = V_{\max}$, once the conductance levels are changed at time T_{k-1} then the next time the conductance levels change is when the time the voltage attains the maximum value. □

Then from the strong Markov property, we define a new stochastic process $\tilde{S}_\tau = G_{k_\tau}$.

$$\tilde{S}_\tau = \{G_{k_\tau}\}. \tag{5.30}$$

This is also a Markov chain and the size of the state is $g_{\max}^N$.

To make a state size smaller, we use the symmetry of input neurons firing, so it is convenient to consider

$$G'_k = (G'_{k,1}, G'_{k,2}, \cdots, G'_{k,M}),$$

where $G'_{k,i}$ is the number of input neurons with conductance level i at time k, and

$$dY'_k = (dY'_{k,1}, dY'_{k_2}, \cdots, dY'_{k,M}),$$

where $dY'_{k,i} = 1$ represents any input with conductance level $g_{\min}/g_{\max} + i\Delta g_n$ firing at time k. Since we assume only one input neuron fires in one time step, $\sum dY' < 2$ as well.

From the construction of dY', it is deduced that

$$\begin{aligned} & \mathbb{P}(dY'_k = dy'_k | E^{k-1} = e^{k-1}, dZ_k = dz_k, (G')_k = (g')_k) \\ = & \sum_{i=1}^{N} \mathbb{P}(dY'_k = dy'_k | G_{k-1,i} = g_{k-1,i}, dY_{k,i} = 1) + \mathbb{P}\left(dY'_k = dy'_k | \bigcap_{i=1}^{N} dY_{k,i} = 0 \right). \end{aligned}$$

Note that, there are only one input neuron to fire in each time step from assumption. We also assume there are more than two voltage levels in this case.

To use Rule 4b, we could constrain Assumption 4:

Assumption 8. *The output neuron's voltage V_k at time k only depends on the previous voltage level and accumulative conductance H_k:*

$$\begin{aligned} & \mathbb{P}(V_k = v_k | E^{k-1} = e^{k-1}, X^k = x^k, dY_k = dy_k, G_k = g_k) \\ = \; & \mathbb{P}(V_k = v_k | V_{k-1} = v_{k-1}, G_k = g_k, dY_k = dy_k) \\ = \; & \mathbb{P}(V_k = v_k | V_{k-1} = v_{k-1}, H_k = h_k), \end{aligned}$$

where

$$\begin{aligned} H_k(G_k, dY_k) &= \sum_{i=1}^{N} G_{k,i} dY_{k,i} \\ &= \sum_{g=1}^{gmax} g dY'_{k,g} = H_k(dY'_k). \end{aligned}$$

Further assume there are more than two voltage levels in this case.

From this assumption, we can conclude

$$\mathbb{P}(V_k = v_k | (G')^k = (g')^k, V^{k-1} = v^{k-1}, dY'_k = dy'_k) = \mathbb{P}(V_k = v_k | V_{k-1} = v_{k-1}, dY'_k = dy'_k). \quad (5.31)$$

Lemma 5.3.10. *The probability of $dY'_{k,i}$ only depends on $(G')_{K-1}$:*

$$\begin{aligned} & \mathbb{P}(dY'_{k,i} = dy'_{k,i} | (G')^{k-1} = (g')^{k-1}, dZ_{k-1} = dz_{k-1}, V^{k-1} = v^{k-1}) \\ = \; & \mathbb{P}(dY'_{k,i} = dy'_{k,i} | (G')_{k-1} = (g')_{k-1}) \end{aligned}$$

Proof. In this section, we assumed that the input neuron's firing only depends on the stimulus, so

$$\begin{aligned}
& \mathbb{P}(dY'_{k,i} = dy'_{k,i} | (G')^{k-1} = (g')^{k-1}, dZ_{k-1} = dz_{k-1}, V^{k-1} = v^{k-1}) \\
= \; & \mathbb{P}\left(dY'_{k,i} = dy'_{k,i} | (G')^{k-1} = (g')^{k-1}, dZ_{k-1} = dz_{k-1}, V^{k-1} = v^{k-1}, \bigcap_{i=1}^{N} dY_{k,i} = 0 \right) \\
& \mathbb{P}\left(\bigcap_{i=1}^{N} dY_{k,i} = 0 | (G')_{k-1} = (g')_{k-1} \right) \\
+ \; & \sum_{i=1}^{N} \mathbb{P}(dY'_{k,i} = dy'_{k,i} | (G')^{k-1} = (g')^{k-1}, dZ_{k-1} = dz_{k-1}, V^{k-1} = v^{k-1}, dY_{k,i} = 1) \\
& \mathbb{P}(dY_{k,i} = 1 | (G')_{k-1} = (g')_{k-1}).
\end{aligned}$$

If all the input neurons do not fire then $dY'_i = 0$ for all i, and we can continue on the chain rule with the conductance levels.

$$\begin{aligned}
& \mathbb{P}(dY'_{k,i} = dy'_{k,i} | (G')^{k-1} = (g')^{k-1}, dZ_{k-1} = dz_{k-1}, V^{k-1} = v^{k-1}) \\
= \; & \mathbb{P}\left(dY'_{k,i} = dy'_{k,i} | (G')_{k-1} = (g')_{k-1}, \bigcap_{i=1}^{N} dY_{k,i} = 0 \right) \mathbb{P}\left(\bigcap_{i=1}^{N} dY_{k,i} = 0 | (G')_{k-1} = (g')_{k-1} \right) \\
+ \; & \sum_{i=1}^{N} \mathbb{P}(dY'_{k,i} = dy'_{k,i} | (G')^{k-1} = (g')^{k-1}, dZ_{k-1} = dz_{k-1}, V^{k-1} = v^{k-1}, dY_{k,i} = 1, G_{k-1,i} = g_{k-1,i}) \\
& \mathbb{P}(dY_{k,i} = 1 | (G')_{k-1} = (g')_{k-1}) \\
& \mathbb{P}(G_{k-1,i} = g_{k-1,i} | (G')^{k-1} = (g')^{k-1}, dZ_{k-1} = dz_{k-1}, V^{k-1} = v^{k-1}, dY_{k,i} = 1).
\end{aligned}$$

Since $(G')_{k,g}$ is the number of the conductance level g and if we know the conductance level of the

input neurons that fire at time k then we know the update rule of dY', so

$$\begin{aligned}
& \mathbb{P}(dY'_{k,i} = dy'_{k,i} | (G')^{k-1} = (g')^{k-1}, dZ_{k-1} = dz_{k-1}, V^{k-1} = v^{k-1}) \\
= \; & \mathbb{P}\left(dY'_{k,i} = dy'_{k,i} | (G')_{k-1} = (g')_{k-1}, \bigcap_{i=1}^{N} dY_{k,i} = 0 \right) \mathbb{P}\left(\bigcap_{i=1}^{N} dY_{k,i} = 0 | (G')_{k-1} = (g')_{k-1} \right) \\
+ \; & \sum_{i=1}^{N} \mathbb{P}(dY'_{k,i} = dy'_{k,i} | (G')_{k-1} = (g')_{k-1}, dY_{k,i} = 1, G_{k-1,i} = g_{k-1,i}) \\
& \mathbb{P}(dY_{k,i} = 1 | (G')_{k-1} = (g')_{k-1}) \mathbb{P}(G_{k-1,i} = g_{k-1,i} | (G')_{k-1} = (g')_{k-1}, dY_{k,i} = 1) \\
= \; & \mathbb{P}(dY'_{k,i} = dy'_{k,i} | (G')^{k-1} = (g')^{k-1}).
\end{aligned}$$

From the chain rule, we conclude the proof. □

Lemma 5.3.11. *Voltage at time k depends on G'_k and G'_{k-1} and the previous voltage level:*

$$\mathbb{P}(V_k = v_k | (G')^k = (g')^k, V^{k-1} = v^{k-1}) = \mathbb{P}(V_k = v_k | G'_k = g'_k, G'_{k-1} = g'_{k-1}, V_{k-1} = v_{k-1}).$$

Proof. Note that

$$\begin{aligned}
& \mathbb{P}(V_k = v_k | (G')^k = (g')^k, V^{k-1} = v^{k-1}) \\
= \; & \mathbb{P}(V_k = v_k | (G')^k = (g')^k, V^{k-1} = v^{k-1}, dY'_k = dy'_k) \mathbb{P}(dY'_k = dy'_k | (G')_{k-1} = (g')_{k-1}) && (5.32) \\
= \; & \mathbb{P}(V_k = v_k | (G')_k = (g')_k, (G')_{k-1} = (g')_{k-1}, V_{k-1} = v_{k-1}, dY'_k = dy'_k) \\
& \mathbb{P}(dY'_k = dy'_k | (G')_{k-1} = (g')_{k-1}) && (5.33) \\
= \; & \mathbb{P}(V_k = v_k | (G')_k = (g')_k, (G')_{k-1} = (g')_{k-1}, V_{k-1} = v_{k-1}). && (5.34)
\end{aligned}$$

where (5.32) holds from chain rule and 5.3.10; (5.33) holds from 5.31; (5.34) holds from chain rule. □

Lemma 5.3.12. *G'_k only depends on previous value and the previous voltage level:*

$$\mathbb{P}(G'_k = g'_k | (G')^{k-1} = (g')^{k-1}, V^{k-1} = v^{k-1}) = \mathbb{P}(G'_k = g'_k | G'_{k-1} = g'_{k-1}, V_{k-1} = v_{k-1}).$$

Proof. Note that,

$$
\begin{aligned}
& \mathbb{P}((G')_k = (g')_k | (G')^{k-1} = (g')^{k-1}, V^{k-1} = v^{k-1}) \\
= \; & \mathbb{P}((G')_k = (g')_k | (G')^{k-1} = (g')^{k-1}, V^{k-1} = v^{k-1}, dZ_{k-1} = 0) \\
& \mathbb{P}(dZ_{k-1} = 0 | V_{k-1} = v_{k-1}) && (5.35) \\
+ \; & \mathbb{P}((G')_k = (g')_k | (G')^{k-1} = (g')^{k-1}, V^{k-1} = v^{k-1}, dZ_{k-1} = 1, dY'_{k-1} = dy'_{k-1}) \\
& \mathbb{P}(dZ_{k-1} = 1 | V_{k-1} = v_{k-1}) \\
& \mathbb{P}(dY'_{k-1} = dy'_{k-1} | (G')_{k-2} = (g')_{k-2}, dZ_{k-1} = 1, V_{k-1} = v_{k-1}) && (5.36) \\
= \; & \mathbb{P}((G')_k = (g')_k | (G')_{k-1} = (g')_{k-1}, V_{k-1} = v_{k-1}, dZ_{k-1} = 0) \\
& \mathbb{P}(dZ_{k-1} = 0 | V_{k-1} = v_{k-1}) && (5.37) \\
+ \; & \mathbb{P}((G')_k = (g')_k | (G')_{k-1} = (g')_{k-1}, V_{k-1} = v_{k-1}, dZ_{k-1} = 1, dY'_{k-1} = dy'_{k-1}) && (5.38) \\
& \mathbb{P}(dZ_{k-1} = 1 | V_{k-1} = v_{k-1}) \\
& \mathbb{P}(dY'_{k-1} = dy'_{k-1} | (G')_{k-1} = (g')_{k-1}, dZ_{k-1} = 1, V_{k-1} = v_{k-1}) && (5.39) \\
= \; & \mathbb{P}((G')_k = (g')_k | (G')_{k-1} = (g')_{k-1}, V_{k-1} = v_{k-1}), && (5.40)
\end{aligned}
$$

where (5.47) holds from chain rule and the original Assumption 5; (5.48) holds from chain rule, the original Assumption 5 and Lemma 5.3.10; (5.49) holds since the conductance does not change without the output neuron's firing and from 7. This non-modification is independent from the previous conductance levels and the voltage levels. (5.50) holds from the original Assumption 3 and Assumption 7 that the conductance levels modification is dependent only on the previous conductance levels and firing of the neurons; 5.51 holds since there are more than two voltage levels and $dZ_{k-1} = 1$, which concludes $dZ_{k-2} = 0$ and $(G')_{k-1} = (G')_{k-2}$; (5.52) holds from chain rule. □

We denote a random process S pertaining to the state in this model

$$S_k = \{G'_k, V_k\}. \tag{5.41}$$

Lemma 5.3.13. *The random process S as defined* (5.41) *satisfies*

$$\mathbb{P}(S_k = s_k | S^{k-1} = s^{k-1}) = \mathbb{P}(S_k = s_k | S_{k-1} = s_{k-1}).$$

Proof. Note that,

$$\begin{aligned}
& \mathbb{P}((G')_k = (g')_k, V_k = v_k | (G')^{k-1} = (g')^{k-1}, V^{k-1} = v^{k-1}) \\
= \quad & \mathbb{P}((G')_k = (g')_k | (G')^{k-1} = (g')^{k-1}, V^{k-1} = v^{k-1}) \\
& \mathbb{P}(V_k = v_k | (G')^k = (g')^k, V^{k-1} = v^{k-1}) && (5.42) \\
= \quad & \mathbb{P}((G')_k = (g')_k | (G')_{k-1} = (g')_{k-1}, V_{k-1} = v_{k-1}) && (5.43) \\
& \mathbb{P}(V_k = v_k | (G')_k = (g')_k, (G')_{k-1} = (g')_{k-1}, V_{k-1} = v_{k-1}) && (5.44) \\
= \quad & \mathbb{P}(S_k = s_k | S_{k-1} = s_{k-1}), && (5.45)
\end{aligned}$$

where (5.42) and (5.45) hold from chain rule; (5.43) holds from 5.3.12; (5.44) holds from 5.3.11. □

Theorem 5.3.14. *The random process S as defined in* (5.41) *is a Markov chain.*

Proof. Analogous argument as proof of Th. 3.4.2 with constant X and previous Lemma. □

Again the conductance only changes with maximum voltage level, we only need to pay attention to the Markov chain when the output neuron fires.

Lemma 5.3.15. *T_k are stopping times for the Markov chain (G'_k, V_k).*

Proof. Same argument as proof of Lemma 5.3.9. □

Define a new stochastic process $\tilde{S}_\tau = G'_{k_\tau}$. Then from the strong Markov property

$$\tilde{S}_\tau = \{G'_{k_\tau}\} \tag{5.46}$$

is a Markov chain.

The size of the state becomes smaller than (3.3). Since $\sum_{i=1}^{M} G'_i = N$, we only need to consider N neurons into $g_{\max}$ different conductance levels, which is

$$\binom{N+M-1}{M-1} = \frac{(N+M-1)!}{N!(M-1)!}.$$

From the constant firing rate assumption, we have

$$\mathbb{P}(dY'_{k,i} = 1 | G'_{k-1} = g'_{k-1}) = g'_{k-1,i}\Delta t\rho.$$

Consider f_j to be the probability of the output neuron fire when the input neuron with conductance level j fires. From rule 4b with normalization with $g_{\max}$ and assuming $V_{\text{rest}} = 0$ as in case 1, we have

$$f_j = \mathbb{P}(dZ_k = 1 | dY'_{k,j} = 1) = \frac{(g_{min}/g_{max} + j\Delta g_n)V_{\text{ex}}}{(g_{min}/g_{max} + j\Delta g_n)V_{\text{ex}} + V_{\max}((g_{min}/g_{max} + j\Delta g_n) + 1/g_{\max})}.$$

Only one input neuron fires in one time step and the output neuron does not fire unless one input neuron fires. Using these assumptions with the chain rule,

$$\begin{aligned}
\mathbb{P}(dZ_k = 1 | G'_{k-1} = g'_{k-1}) &= \sum_{j=1}^{M} \mathbb{P}(dZ_k = 1 | dY'_{k,j} = 1, G'_{k-1} = g'_{k-1}) \mathbb{P}(dY'_{k,g} = 1 | G'_{k-1} = g'_{k-1}) \\
&= \sum_{j=1}^{M} f_j g'_{k-1,j} \Delta t\rho.
\end{aligned}$$

Consider β_j to be the probability of any of the input neurons with conductance j firing given the output neuron firing:

$$\beta_j = \mathbb{P}(dY'_{k,j} = 1 | dZ_k = 1, G'_{k-1} = g'_{k-1}).$$

Use Bayes' Theorem and previous remarks

$$\begin{aligned}\beta_j &= \frac{\mathbb{P}(dZ_k = 1 | dY'_{k,j} = 1, G'_{k-1} = g'_{k-1})\mathbb{P}(dY'_{k,j} = 1 | G'_{k-1} = g'_{k-1})}{\mathbb{P}(dZ_k = 1 | G'_{k-1} = g'_{k-1})} \\ &= \frac{g'_{k-1,j} f_j}{\sum_{i=1}^{M} g'_{k-1,i} f_i}\end{aligned}$$

Note that β depends on the values of all the conductances, unlike in the previous section.

Set the probability of decrementing conductance given the output neuron is fired to be,

$$\mathbb{P}(G_{k,i} = g/g_{\max} - \Delta g_n | G_{k-1,i} = g/g_{\max}, dZ_{k-1} = 1) = \Delta.$$

Consider Markov chain (5.41), where conductances change every time step:

$$\begin{aligned}&\mathbb{P}(G'_{k+1} = g'_{k+1} | G'_k = g'_k, dZ_k = 1) \\ = &\sum_{i=1}^{M} \mathbb{P}(G'_{k+1} = g'_{k+1} | G'_k = g'_k, dZ_k = 1, dY'_{k,i} = 1)\mathbb{P}(dY'_{k,i} = 1 | dZ_k = 1, G'_k = g'_k) \\ = &\sum_{i=1}^{M} \mathbb{P}(G'_{k+1} = g'_{k+1} | G'_k = g'_k, dZ_k = 1, dY'_{k,i} = 1)\mathbb{P}(dY'_{k,i} = 1 | dZ_k = 1, G'_{k-1} = g'_k)\end{aligned}$$

since the voltage has more than two levels. Using this, we can calculate the modification of conductances. This leads to the community formation we observed in Fig. 5.8, which is a realization of simulation with parameters in Table 3.2 except $V_{\text{rest}} = 10$ (mV), and choose $\Delta v = 0.01$ (mV), $\Delta g = 0.1$ (Ω), $\rho_{k,i} = 2.0$ (1/s) and $\Delta = \Delta t \rho$. As we showed, the voltage movement does not affect the result, so even $V_{\text{rest}} = 20$ (mV) gives the same result.

Instead of taking probability, we could use an actual input neuron's firing at the current time to update conductance. To do that, we need to change the original Assumption 3:

Assumption 9. *The conductance levels G'_k at time k are conditionally independent on E^k given the conductance level and both the input and the output neuron's firing at the previous time step*

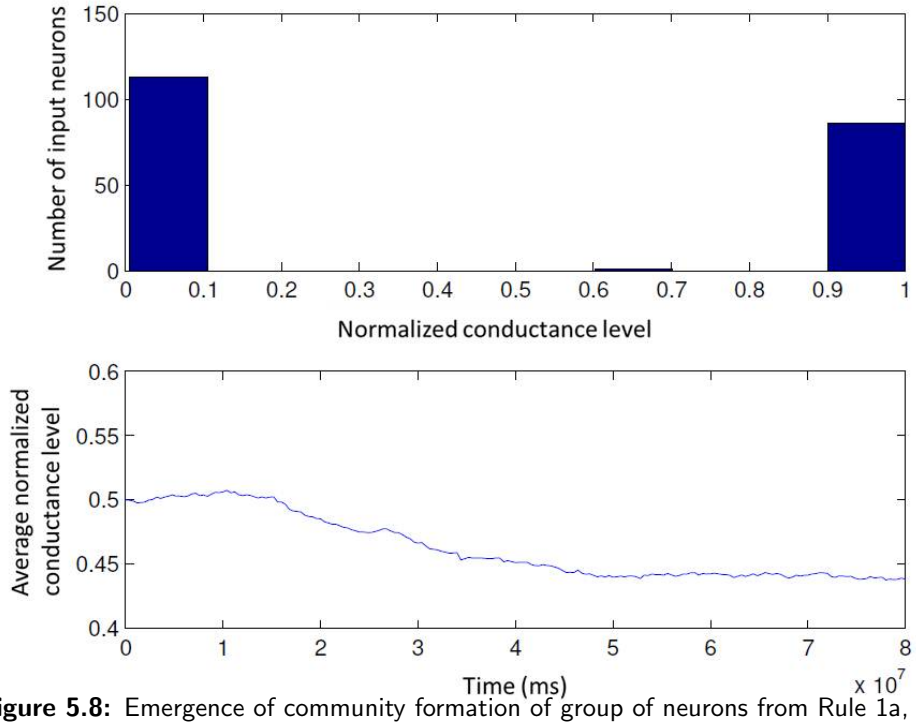

Figure 5.8: Emergence of community formation of group of neurons from Rule 1a, 2a, 3c of Case 2 $L = 0$, 4a, and 5 with parameters from Table 3.2 except $V_{\text{rest}} = 10$ (mV), and choose $\Delta v = 0.01$ (mV), $\Delta g = 0.1$ (Ω), $V_{\text{rest}} = 10$ (mV), $\rho_{k,i} = 5.0$ (1/s), and $\Delta = \Delta t \rho$.

and the current input neuron's firing:

$$\begin{aligned} & \mathbb{P}((G'_k = g'_k | E^{k-1} = e^{k-1}, dY'_k = dy'_k) \\ = \quad & \mathbb{P}(G'_k = g'_k | G'_{k-1} = g'_{k-1}, dZ_{k-1} = dz_{k-1}, dY'_{k-1} = dy'_{k-1}, dY'_k = dy'_k). \end{aligned}$$

This does not affect Eq. (5.31), Lemma 5.3.10 and 5.3.11, however the proof of Lemma 5.3.12 needs to be modified.

Lemma 5.3.16. *$(G')_k$ depends only on the previous value and the previous voltage level:*

$$\mathbb{P}((G')_k = (g')_k | (G')^{k-1} = (g')^{k-1}, V^{k-1} = v^{k-1}) = \mathbb{P}((G')_k = (g')_k | (G')_{k-1} = (g')_{k-1}, V_{k-1} = v_{k-1}).$$

Proof. Note that,

$$
\begin{aligned}
& \mathbb{P}((G')_k = (g')_k | (G')^{k-1} = (g')^{k-1}, V^{k-1} = v^{k-1}) \\
= \; & \mathbb{P}((G')_k = (g')_k | (G')^{k-1} = (g')^{k-1}, V^{k-1} = v^{k-1}, dZ_{k-1} = 0) \\
& \mathbb{P}(dZ_{k-1} = 0 | V_{k-1} = v_{k-1}) \qquad (5.47) \\
+ \; & \mathbb{P}((G')_k = (g')_k | (G')^{k-1} = (g')^{k-1}, V^{k-1} = v^{k-1}, dZ_{k-1} = 1, dY'_{k-1} = dy'_{k-1}, dY'_k = dy'_k) \\
& \mathbb{P}(dZ_{k-1} = 1 | V_{k-1} = v_{k-1}) \\
& \mathbb{P}(dY'_{k-1} = dy'_{k-1} | (G')_{k-2} = (g')_{k-2}, dZ_{k-1} = 1, V_{k-1} = v_{k-1}) \\
& \mathbb{P}(dY'_k = dy'_k | (G')_{k-1} = (g')_{k-1}, dZ_{k-1} = 1, V_{k-1} = v_{k-1}, dY'_{k-1} = dy'_{k-1}) \qquad (5.48) \\
= \; & \mathbb{P}((G')_k = (g')_k | (G')_{k-1} = (g')_{k-1}, V_{k-1} = v_{k-1}, dZ_{k-1} = 0) \\
& \mathbb{P}(dZ_{k-1} = 0 | V_{k-1} = v_{k-1}) \qquad (5.49) \\
+ \; & \mathbb{P}((G')_k = (g')_k | (G')_{k-1} = (g')_{k-1}, V_{k-1} = v_{k-1}, dZ_{k-1} = 1, dY'_{k-1} = dy'_{k-1}, dY'_k = dy'_k) \qquad (5.50) \\
& \mathbb{P}(dZ_{k-1} = 1 | V_{k-1} = v_{k-1}) \\
& \mathbb{P}(dY'_{k-1} = dy'_{k-1} | (G')_{k-1} = (g')_{k-1}, dZ_{k-1} = 1, V_{k-1} = v_{k-1}) \qquad (5.51) \\
& \mathbb{P}(dY'_k = dy'_k | (G')_{k-1} = (g')_{k-1}, dZ_{k-1} = 1, V_{k-1} = v_{k-1}, dY'_{k-1} = dy'_{k-1}) \\
= \; & \mathbb{P}((G')_k = (g')_k | (G')_{k-1} = (g')_{k-1}, V_{k-1} = v_{k-1}), \qquad (5.52)
\end{aligned}
$$

where (5.47) holds from chain rule and the original Assumption 5; (5.48) holds from chain rule, the original Assumption 5 and Lemma 5.3.10; (5.49) holds from Assumption 7 and since the conductance does not change without output neuron's firing. This non-modification is independent from the previous conductance levels and the voltage levels. (5.50) holds from Assumption 9 and Assumption 7. Modification of the conductance level is dependent only on the previous conductance levels and firing of neurons. 5.51 holds since there are more than two voltage levels and $dZ_{k-1} = 1$, which concludes $dZ_{k-2} = 0$ and $(G')_{k-1} = (G')_{k-2}$; (5.52) holds from chain rule. □

If $\Delta = \Delta t\rho$, then this is the same probability without this assumption. Fig. 5.9 shows one realization of the result from the simulation that has all parameters set the same as in the previous

case, which is almost the same as Fig. 5.8.

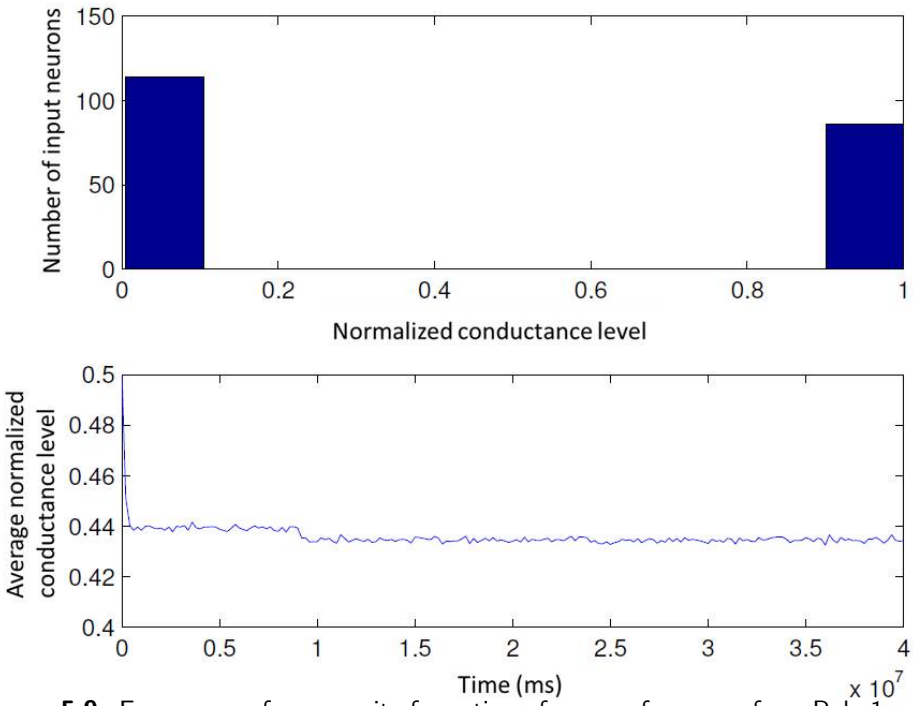

Figure 5.9: Emergence of community formation of group of neurons from Rule 1a, 2a, 3c of Case 2 $L = 0$ without probability Δ, 4a, and 5with parameters from Table 3.2 except $V_{\text{rest}} = 10$ (mV), and choose $\Delta v = 0.01$ (mV), $\Delta g = 0.1$ (Ω), $V_{\text{rest}} = 10$ (mV), and $\rho_{k,i} = 5.0$ (1/s).

5.3.5 Large network limit for Case 2

Let $\theta_i = G_i'/N$, and define $\theta = (\theta_1, \theta_2, \cdots \theta_M)$ where $\sum \theta_i = 1$ and again define

$$\gamma_g(\theta) = \frac{\theta_g f_g}{\sum_{i=1}^{M} \theta_i f_i},$$

for the probability of promotion. Each promotion of a neuron is infinitesimal, so we can write it as the ordinal differential equations,

$$\frac{d}{dt}\theta_k = \gamma_{k-1} - \gamma_k + \Delta\theta_{k+1} - \Delta\theta_k, k = 2, 3, \cdots M - 1,$$

and boundary terms are

$$\begin{aligned}\frac{d}{dt}\theta_1 &= \Delta\theta_2 - \gamma_1 \\ \frac{d}{dt}\theta_M &= \gamma_{M-1} - \Delta\theta_M.\end{aligned}$$

If θ is going into an invariant distribution π then

$$\frac{d}{dt}\pi_k = 0 \text{ for all } k \text{ and } F = \sum_{i=1}^{M} \pi_i f_i \text{ is a constant.}$$

This concludes

$$\begin{bmatrix} -\frac{f_1}{F} & \Delta & 0 & 0 & 0 & \cdots & 0 & 0 & 0 \\ \frac{f_1}{F} & -(\Delta + \frac{f_2}{F}) & \Delta & 0 & 0 & \cdots & 0 & 0 & 0 \\ 0 & \frac{f_2}{F} & -(\Delta + \frac{f_3}{F}) & \Delta & 0 & \cdots & 0 & 0 & 0 \\ \vdots & \vdots & \vdots & \vdots & \vdots & \cdots & \vdots & \vdots & \vdots \\ 0 & 0 & 0 & 0 & 0 & \cdots & -(\Delta + \frac{f_{M-2}}{F}) & \Delta & 0 \\ 0 & 0 & 0 & 0 & 0 & \cdots & \frac{f_{M-2}}{F} & -(\Delta + \frac{f_{M-1}}{F}) & \Delta \\ 0 & 0 & 0 & 0 & 0 & \cdots & 0 & \frac{f_{M-1}}{F} & -\Delta \end{bmatrix} \pi = \mathbf{0}.$$

Multiply both sides with a lower triangle matrix with all components 1. This leads to the series of equations

$$\pi_{j+1} = \frac{f_j}{\Delta F}\pi_j. \tag{5.53}$$

Lemma 5.3.17. *If we assume f is a increasing function and $\Delta < 1$ then the invariant distribution has community formation.*

Proof. Since f is a probability, the value is in between 0 and 1. Using this with the assumption of

increasing function, we have

$$(\Delta F - f_{j-1})^2 + f_{j-1}(f_j - f_{j-1}) \geq 0.$$

This leads to

$$f_j f_{j-1} + (\Delta F)^2 \geq 2\Delta F f_{j-1}.$$

Δ is also a probability and bigger than 0. π shows the distribution and each π_j is bigger than 0. Also, from the construction of F, it is bigger than 0. So, divide the equation with $\Delta F f_{j-1}$ and multiply with π_j leading to

$$\frac{f_j}{\Delta F}\pi_j + \frac{\Delta F}{f_{j-1}}\pi_j \geq 2\pi_j.$$

From Eq. (5.53), this becomes

$$\frac{\pi_{j+1} + \pi_{j-1}}{2} \geq \pi_j.$$

This is the definition of convex function.

If there exists a j between 1 and M that satisfies

$$\frac{\pi_{j+1} - \pi_j}{\Delta g_n} = 0$$

then the invariant distribution has community formation with j as the minimum. Since

$$\frac{\pi_{j+1} - \pi_j}{\Delta g_n} = \left(\frac{f_j}{\Delta F} - 1\right)\frac{\pi_j}{\Delta g_n},$$

if there exists an f_j which is the same as ΔF then the condition is satisfied.

We can bound F using convexity of f as

$$f_1 < F = \sum_{i=1}^{M} \pi_i f_i < f_M.$$

Also note that Δ is smaller than 1, therefore

$$f_1 < F = \sum_{i=1}^{M} \pi_i f_i < f_M < \frac{f_M}{\Delta}.$$

Consider $f_1 = \dfrac{\Delta g_n V_{\mathrm{ex}}}{\Delta g_n V_{\mathrm{ex}} + V_{\max}(\Delta g_n + 1/g_{\max})}$, this becomes 0 as the limit of Δg_n goes to 0. In the limit, $f_1/\Delta \to 0$, and

$$\frac{f_1}{\Delta} < F < \frac{f_N}{\Delta},$$

which concludes the existence of the minimum point between the borders. Therefore it is community formation. □

These Lemma explain the community formation observed in Fig. 5.8 and 5.9. Also, in the continuous conductance simulation, if we choose small enough time steps then the invariant distribution always becomes a strong community formation.

Chapter 6

Emergence of selectivity

6.1 One Dimensional Place Selectivity

The property of place selectivity emerges from our model with input neurons organized in a one dimensional receptive field. The place selectivity is an important feature, since it is the key to the place cells in the hippocampus and the grid cells in enthorhinal cortex (EC). The difference in the conductance creates this property, however the initial condition is not important. The initial condition can be half of the conductance as shown in Fig. 4.6a or could start from a random conductance level as shown in Fig. 6.3and both cases will show place selectivity. There are a lot of parameters in our model, which could change the structure of the network. We are interested in the difference in the stimulus, so unless otherwise noted we use parameters from Table 3.2.

The interesting phenomenon that we observe is the preferable place moving over time. This movement is important, since this shows the convergence of the structure. Fig. 6.1 shows the strength of the conductance level over time for each input neuron with $(H, B, W) = (70(1/\text{s}), 1(1/\text{s}), 10(\text{mm}))$, $s = 1000(\text{mm/s})$, periodic boundary condition, $C = 0.05(\text{s})$, $b = 0.005(\text{s})$, $dt = 0.0001(\text{s})$, $g_{\max} = 1.4(1/\Omega)$, $g_{\min} = 0.01(1/\Omega)$, and the initial condition is set to average of the conductance level. This shows three different types within $10^4(\text{s})$ running time: the band which has jumps, the band which does not have jumps, and the band which starts with jumps and moves to a no jump state. Since the system is a Markov chain, it should converge to a stable state. As we showed for the smaller state case in Chap. 4, we assume this system should have a long live state which is not the convergent state. As shown in the right most panel of Fig. 6.1, the band with jumps can change to the band without jump. So, we believe that the system should converge to the non-jump

band in the longer run. As with the longer run of 30000(s), 10 out of 10 cases showed the band without jumps in the end. If we chose initial condition at random then 7 out of 10 cases showed the band without jumps as shown in the middle panel of Fig. 6.1 and 3 out of 10 cases shows non selective position from small tendency in the initial condition.

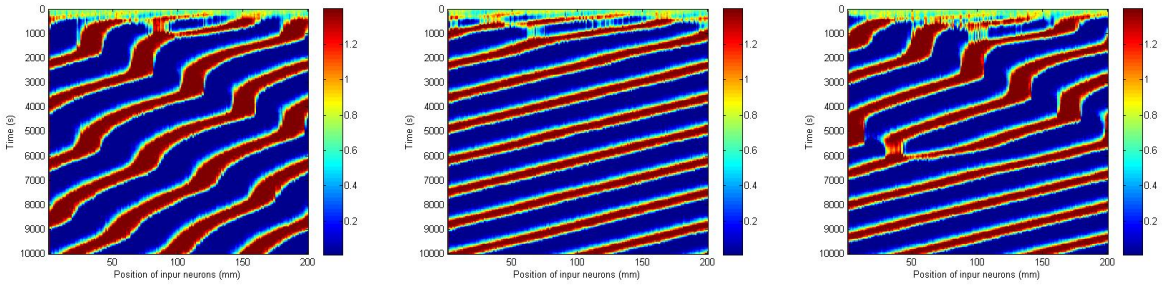

Figure 6.1: We set (H, B, W) = (70(1/s), 1(1/s), 10(mm)), s = 1000(mm/s), periodic boundary condition, C = 0.05(s), b = 0.005(s), dt = 0.0001(s), $g_{\max}$ = 1.4(1/Ω), $g_{\min}$ = 0.01(1/Ω), and periodic boundary condition. The initial condition is set to the average of the conductance level. The y-axis shows time between 0 to 10000(s) and the x-axis is the position of the input neurons. There are three different realizations from the same conditions in the figure.

6.1.1 Changing speed of stimulus

In this section, we used stimuli with (H, B, W) = (70(1/s), 1(1/s), 10(mm)), and different stimulus speed s. The other parameters are C = 0.05(s), b = 0.005(s), dt = 0.0001(s), $g_{\max}$ = 1.4(1/Ω), $g_{\min}$ = 0.01(1/Ω) and periodic boundary condition. The speed of the stimulus change between 200(mm/s) to 1600(mm/s) as shown in Fig. 6.2. The speed needs to be in some specific range to have place selectivity. Faster stimulus also cause non selective cases as well as selective case as shown in Fig. 6.2.

We were interested in the speed v of the band. If more than 10 neighboring input neurons had a conductance level greater than half of the maximum conductance level, then we considered this a band. We will use Fig. 6.3 which shows a conductance level between 57,000(s) and 60,000(s) with initial condition set to the average of the conductance as an example. The top panel shows

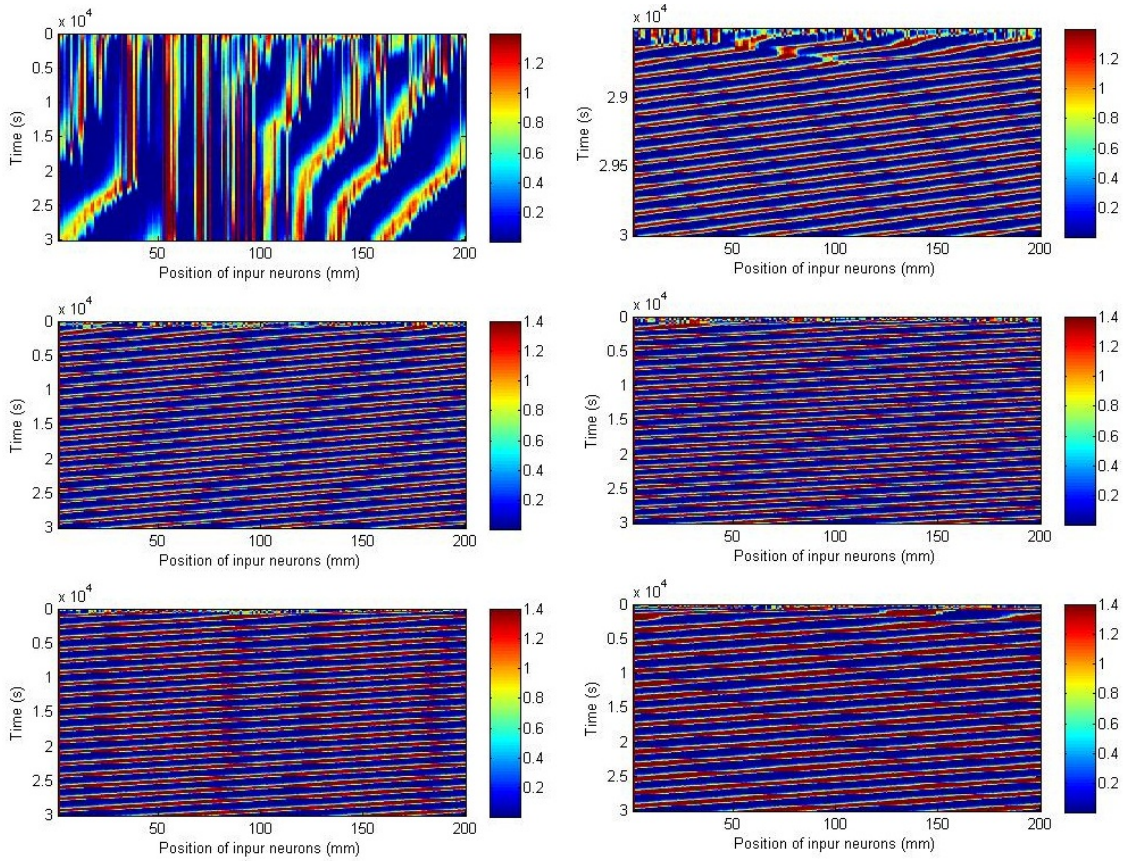

Figure 6.2: We set (H, B, W) = (70(1/s), 1(1/s), 10(mm)), and a periodic boundary condition. The initial condition is chosen randomly. From top left to bottom right S = 200, 400, 600, 1200, 1400, 1600(mm/s)

the bands by the boundary and the middle positions. Then using these values, we chose one band as shown in the top panel and fitted this data to a linear curve $p_1 x + p_2 = y$, where y is the position of the input and x is the time. As discussed in the last section, 7 out of 10 runs had this structure without jumps and the band's speed v was -4.2×10^{-2} (mm/s) with a standard deviation of 2.0×10^{-2} (mm/s) and the average width of the band at the specific time was 26.17 (mm) with a standard deviation of 2.7 (mm). When the initial condition was set to half of the conductance level, then 10 out of 10 runs showed the same structure. In this case the average of 10 runs was -4.7×10^{-2} (mm/s) with a standard deviation of 2.3×10^{-2} (mm/s) and the average width of the band at the specific time was 27.47 (mm) with a standard deviation of 3.53 (mm).

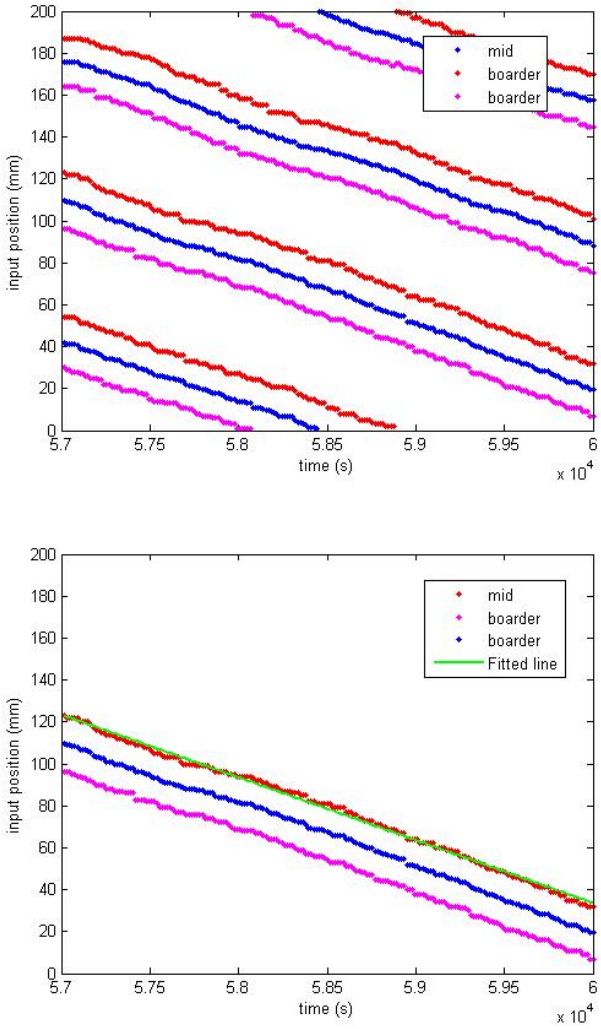

Figure 6.3: We set $(H, B, W) = (70(1/s), 1(1/s), 10(mm))$, $s = 1000(mm/s)$, periodic boundary condition, and the initial condition is set to the average of the conductance. If more than 10 neighboring input neurons have a conductance bigger than half of the maximum conductance, then it is considered as a band and shown in the top panel. The data in the top panel is fit to the $p_1 x + p_2 = y$ linear curve, where y is the position of the input and x is the time. The bottom panel shows one specific band and the fitted linear line in green.

Using this linear fit, we show the speed of the band v with respect to the speed of the stimulus s in the top panel of Fig. 6.4. The bottom panel shows the width of the band over the stimulus speed s. Because of the random initial condition and stochastic input firing, some of them has no preference.

Namely, 3 out of 10 cases for the $s = 1000$(mm/s), 8 out of 10 cases for the $s = 1400$(mm/s), and 7 out of 10 cases for the $s = 1600$(mm/s) became non-selective. That is why there are less standard deviation in these cases. The top and the bottom panels look to have a correlation. Considering the STDP window function, if the output neuron fires before the input neurons, then those input neurons lose conductance level. However, when the input neurons fire before the output neuron, those input neurons increase conductance level. Thus, the output neuron is more likely to fire when the stimulus is within the band, since the stimulus creates a larger influence by the input neurons firing. Consider the band from w_1 (mm) to w_2 (mm) and some floating number ϵ (mm) which is relatively small compared to the width $w = w_2 - w_1$. Our stimulus moves from left to right, so if the output neuron fires when the stimulus is on the left side of the band at x (mm), where $x - w_1 < \epsilon$, then the conductance level of the input neurons that are on the left side of x (mm) is likely to increase, and if the output neuron fires when the stimulus is on the right side of the band at y (mm) and does not fire until the stimulus is in the next band, then the conductance level of the input neurons between y (mm) and w_2 (mm) is likely to decrease. Therefore, the band is more likely to move in the opposite direction of the stimulus. This is what we observed in our experiments as shown in Fig. 6.5.

In this argument, it is important to know where the output neuron fires relative to the position of the stimulus within the band. To study this, we constructed artificial bands by setting the conductance levels of input neurons. Then we gave the stimulus to this system without changing the conductance level, i.e. stopping STDP. This showed where the output neuron fired within the bands, which is represented in Figures 6.6 6.7 6.8 6.9 for different speeds of the stimulus and the width of the band. The average of the firing position corresponding to the width of the band for a different speed of the stimulus is shown in Fig. 6.10. The average is around the midpoint of the bands and not related to the speed of the band. Maybe this causes the correlation between the width and the speed of the band. Though the width is also correlated to the stimulus speed as shown in 6.11, where STDP of the system is turned on for the artificial bands. All panels in Fig. 6.11 clearly show non-stable band movement. The speed of stimulus has a correlation with both the width of the band and the speed of the stimulus.

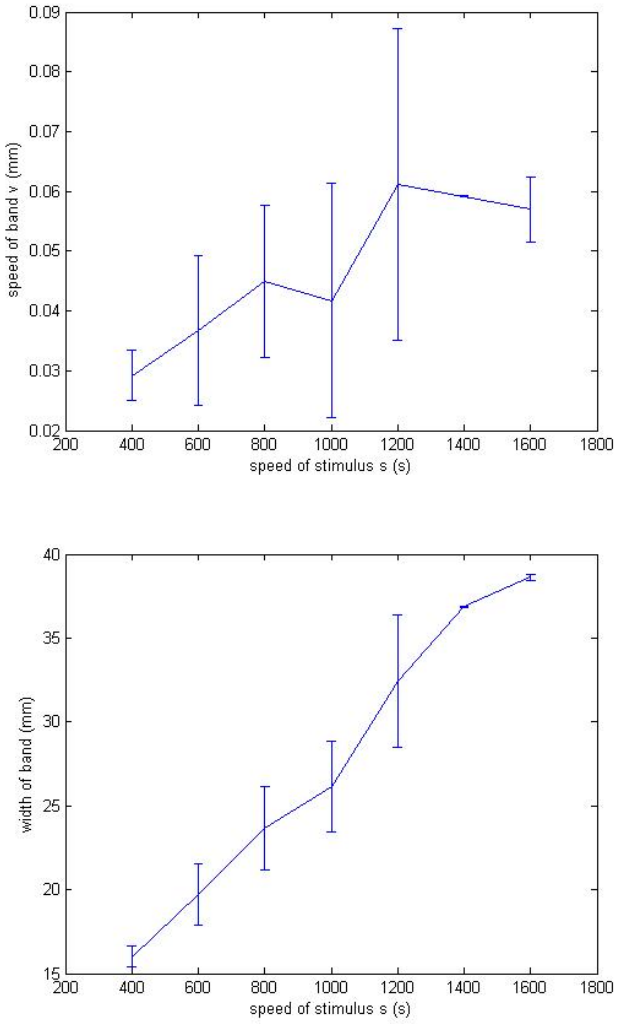

Figure 6.4: We set $(H, B, W) = (70(1/s), 1(1/s), 10(mm))$, and a periodic boundary condition. The initial condition is chosen randomly. Selective cases of 10 runs are used in this experiments, so 3 out of 10 cases for the $s = 1000$(mm/s), 8 out of 10 cases for the $s = 1400$(mm/s), and 7 out of 10 cases for the $s = 1600$(mm/s) are not used. If more than 10 neighboring input neurons have a conductance greater than half of the maximum conductance, then it is considered as a band and shown in the middle panel. The data in the top panel is fit to the $p_1 x + p_2 = y$ linear curve, where y is the position of the input and x is the time. The data is taken from 10 experiments between times 3.6×10^5 and 4×10^5 (s). The x-axis shows the speed of stimulus for both of the panels. The y-axis of the top panel shows the speed v of the band movement. The y-axis of the bottom panel shows the width of the band at the specific time.

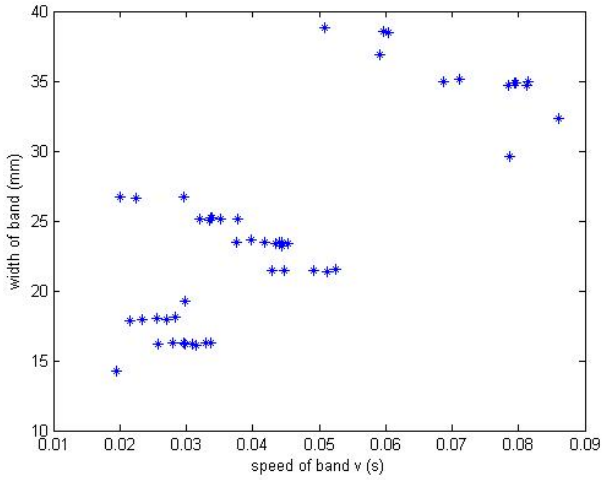

Figure 6.5: We set (H, B, W) = (70(1/s), 1(1/s), 10(mm)), and a periodic boundary condition. The initial condition is chosen randomly. Relation between speed of the band and the width of the band are shown.

6.1.2 Changing maximum strength of stimulus

In this section, we will change the maximum strength of the stimulus and fix everything else. We set the speed of the stimulus to be 1000(mm/ms), (B, W) = (1(1/s), 10(mm)), and the maximum strength of the stimulus to change between 50(1/s) and 110(1/s) as shown in Fig. 6.12. If the maximum strength is too small or too large, then the place selectivity does not emerge. Too small causes all conductance levels to go up, and too large causes all conductance levels to go down. There are some parameters that cause stable place selectivity. With the smaller maximum strength, the movement of the band does not seem to move quickly, though the systems do not go into the stable state. There could be some stimulus of the right amount of strength to the neurons such that the band does not change position.

6.1.3 Changing width of stimulus

In this section, we will change the width of the stimulus and fix everything else. We set the speed of the stimulus to be 1000(mm/s), (H, B) = (70(1/s), 1(1/s)) and the width of the stimulus to change between 6(mm) and 14(mm) as shown in Fig. 6.13. Again, the width needs to be in some

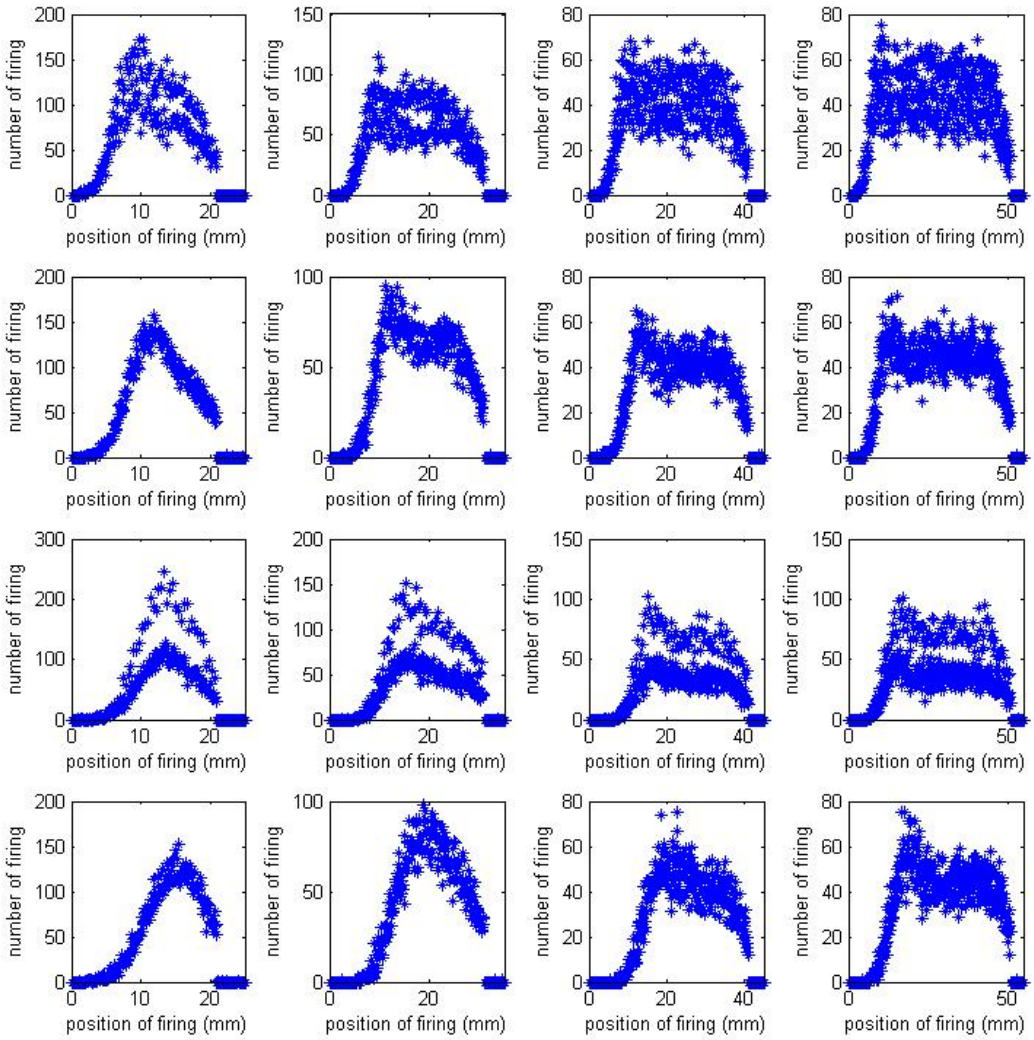

Figure 6.6: We set $(H, B, W) =$ (70(1/s), 1(1/s), 10(mm)), a periodic boundary condition, and the initial condition to be the width of the band. The x-axis shows the position of the output firing. The y-axis shows the number of neurons firing at the specific position in the band without STDP. Each column has a different band width: 20(mm), 30(mm), 40(mm), 50(mm). Each row has a different stimulus speed: 400(mm/s), 600(mm/s), 800(mm/s), 1000(mm/s).

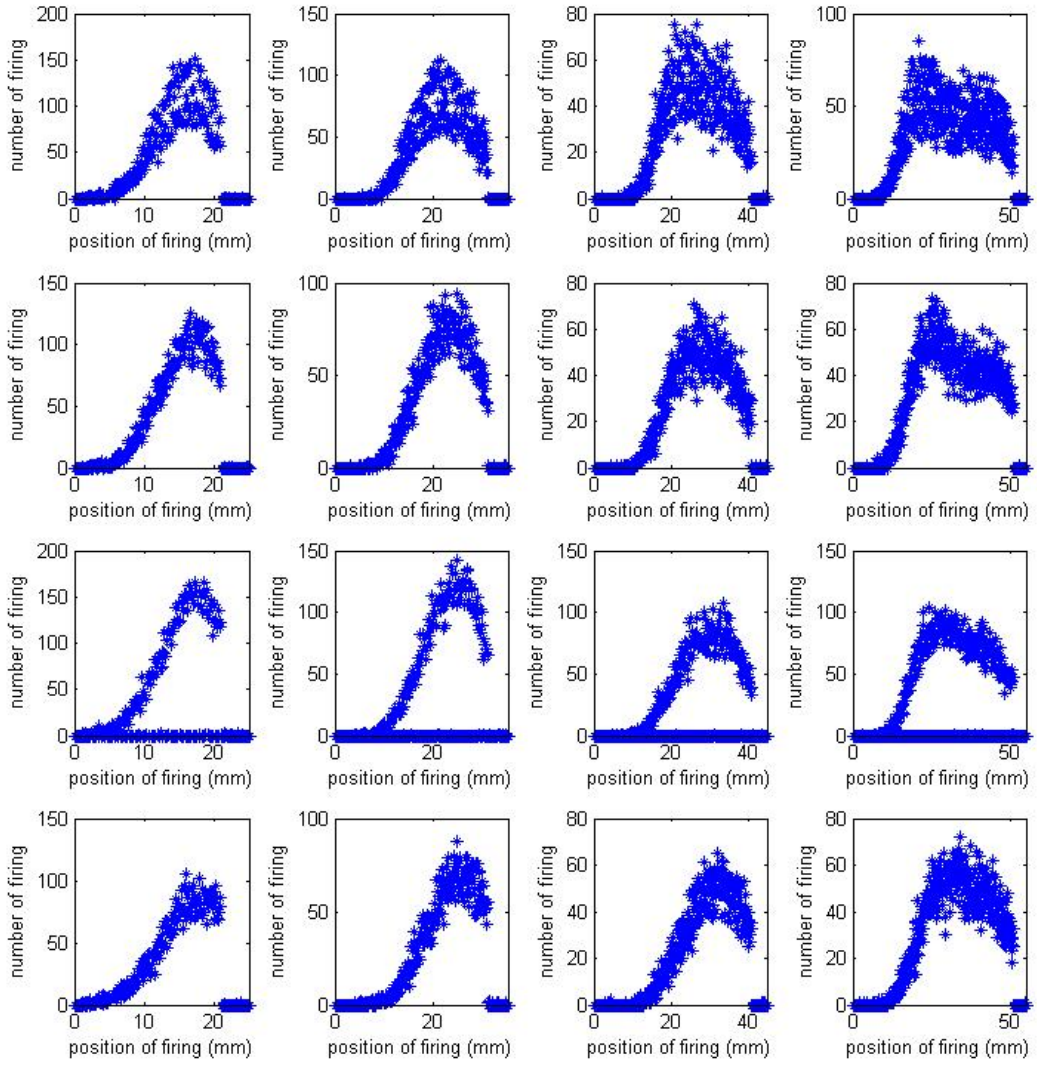

Figure 6.7: We set $(H, B, W) = (70(1/s), 1(1/s), 10(mm))$, a periodic boundary condition, and the initial condition to be the width of the band. The x-axis shows the position of the output firing. The y-axis shows the number of neurons firing at the specific position in the band without STDP. Each column has a different band width: 20(mm), 30(mm), 40(mm), 50(mm). Each row has a different stimulus speed: 1200(mm/s), 1400(mm/s), 1600(mm/s), 1800(mm/s).

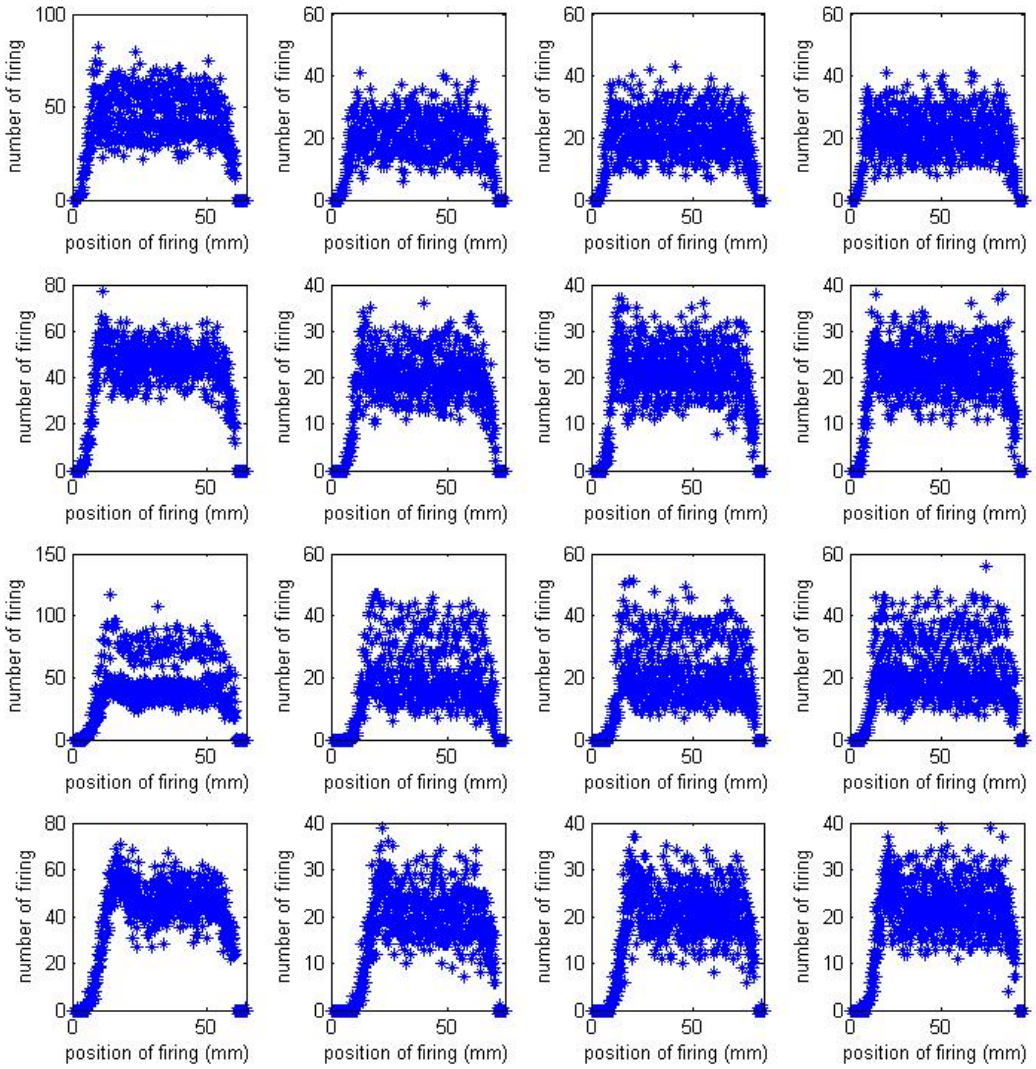

Figure 6.8: We set $(H, B, W) =$ (70(1/s), 1(1/s), 10(mm)), a periodic boundary condition, and the initial condition to be the width of the band. The x-axis shows the position of the output firing. The y-axis shows the number of neurons firing at the specific position in the band without STDP. Each column has a different band width: 60(mm), 70(mm), 80(mm), 90(mm). Each row has a different stimulus speed: 400(mm/s), 600(mm/s), 800(mm/s), 1000(mm/s).

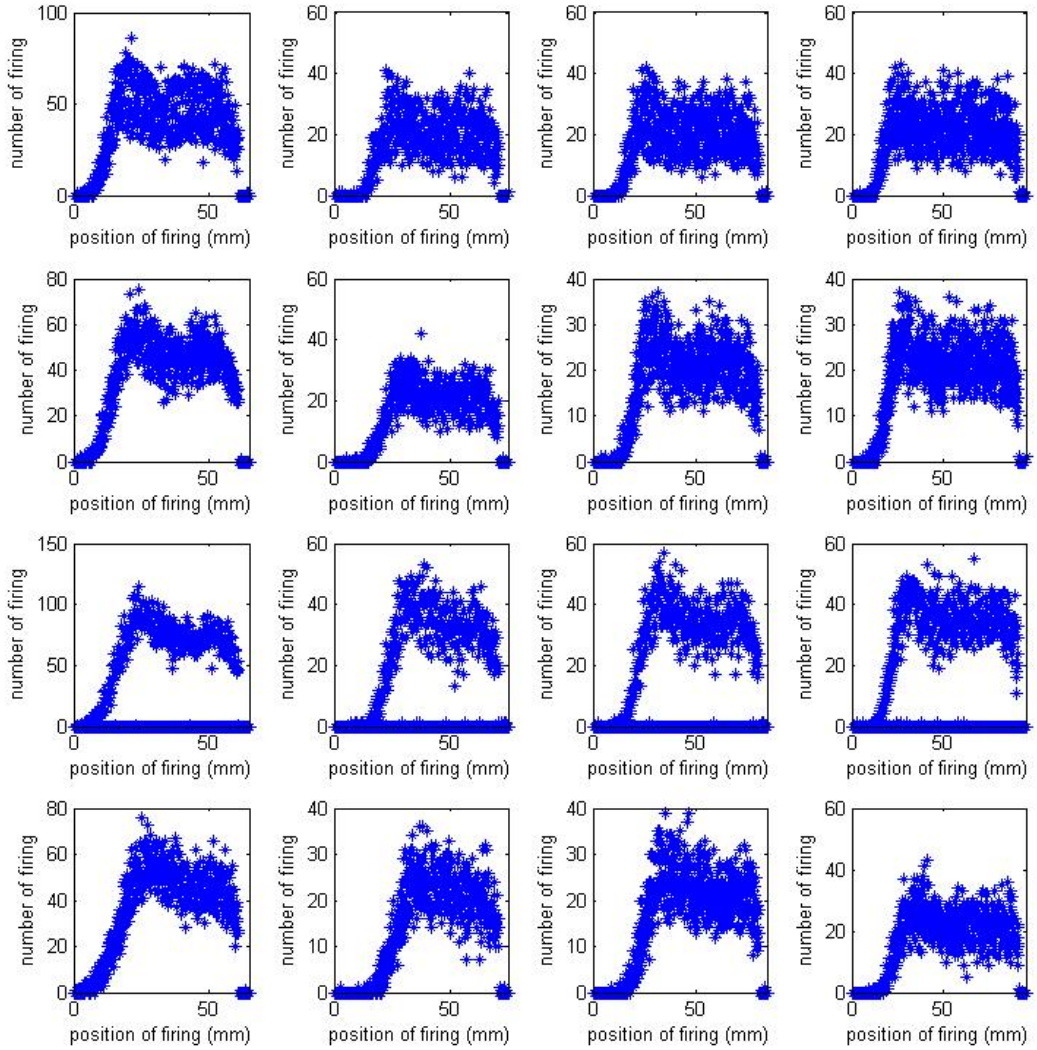

Figure 6.9: We set $(H, B, W) =$ (70(1/s), 1(1/s), 10(mm)), a periodic boundary condition, and the initial condition to be the width of the band. The x-axis shows the position of the output firing. The y-axis shows the number of neurons firing at the specific position in the band without STDP. Each column has a different band width: 60(mm), 70(mm), 80(mm), 90(mm). Each row has a different stimulus speed: 1200(mm/s), 1400(mm/s), 1600(mm/s), 1800(mm/s).

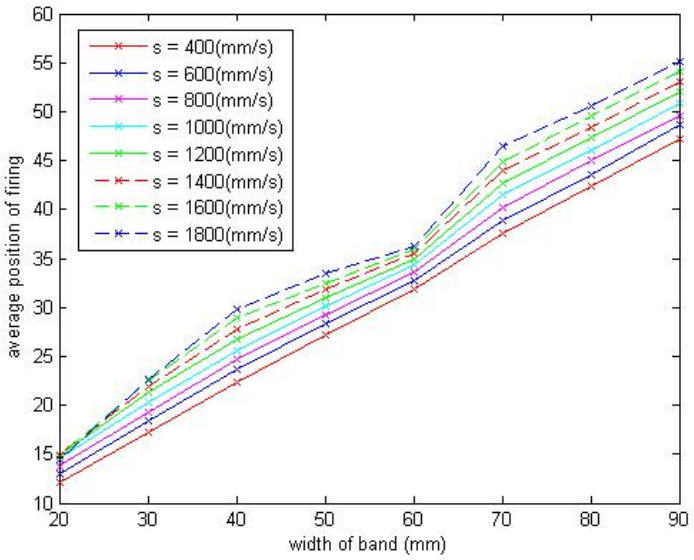

Figure 6.10: We set $(H, B, W) = (70(1/s), 1(1/s), 10(mm))$, a periodic boundary condition, and the initial condition to be the width of the band in the x-axis. The y-axis shows the average firing position inside the band in increments of 1000(s) without STDP.

specific range to make sure the system has place selectivity. Too small a width causes all values of conductance to go up and too large a width causes all values of conductance to go down. However, those extreme cases have bands that tend to stay in the same place.

6.1.4 Changing minimum strength of stimulus

In this section, we will change the base of the stimulus strength and fix everything else. We set the speed of the stimulus to be 1000(mm/s), (H, W) = (70(1/s), 10(mm)), and the base of stimulus strength to change between 0.4(1/s) and 1.6(1/s) as shown in Fig. 6.14. The base means the noise of the system. The neurons could fire without any stimulus, which we represent with the base. So, if the base is small, then the stimulus influence become larger. If the base becomes larger, then the stimulus influence become larger and lose the place selectivity.

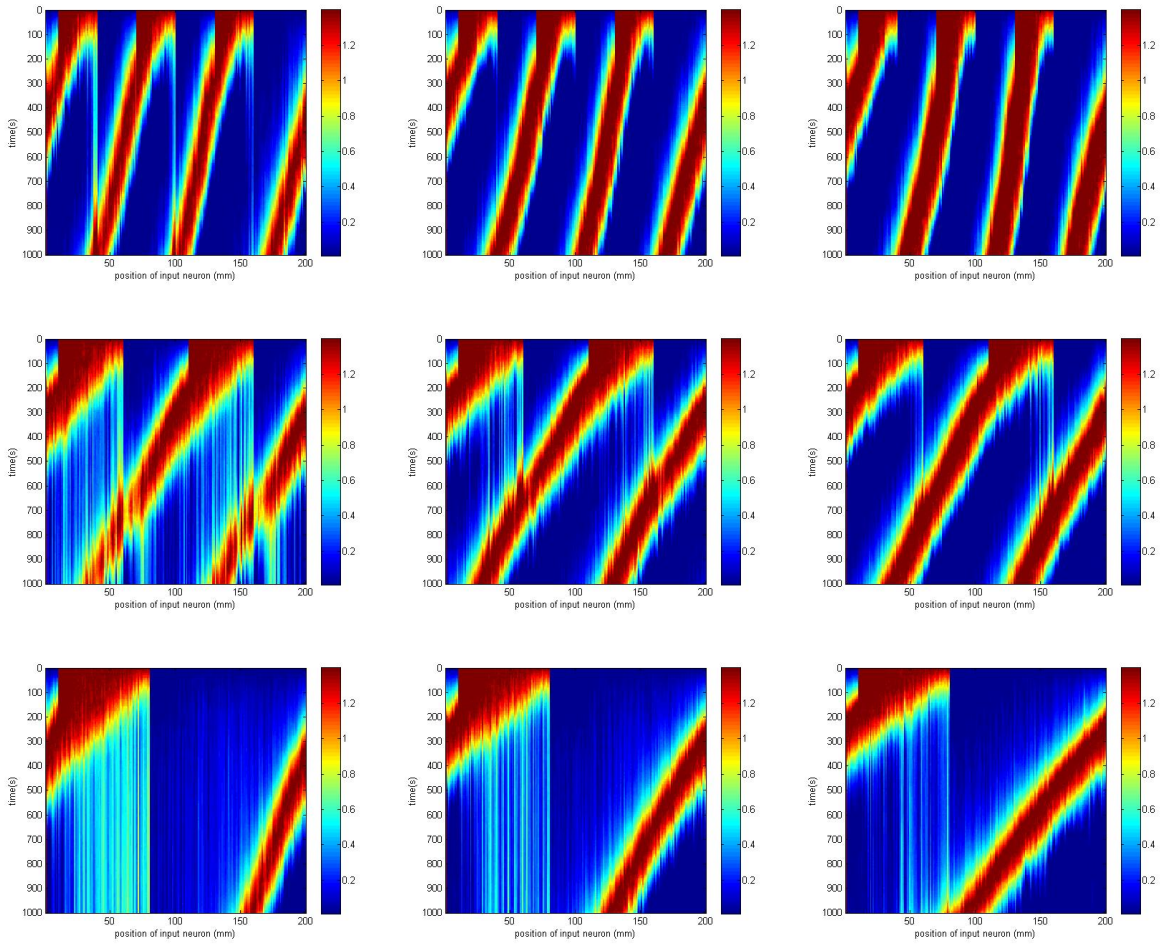

Figure 6.11: We set $(H, B, W) = (70(1/s), 1(1/s), 10(mm))$, a periodic boundary condition, and the initial condition to be the width of the band. Use STDP training for 1000(ms). The first row has a band width of 30(mm), and next of 50(mm), then next of 70(mm). The first column has a stimulus speed of 400(mm/s), the second of 600(mm/s) and the third of 800(mm/s).

6.1.5 Discussion

In previous works [25, 144, 151], the emergence of a preferable place was also shown computationally. However, the movement of place position over time was not studied. It was assumed that the preferable positions do not move over time. We have shown the movement of the place selectivity in the long time scale. The speed of the stimulus is around 1000 (mm/s), and the speed of the

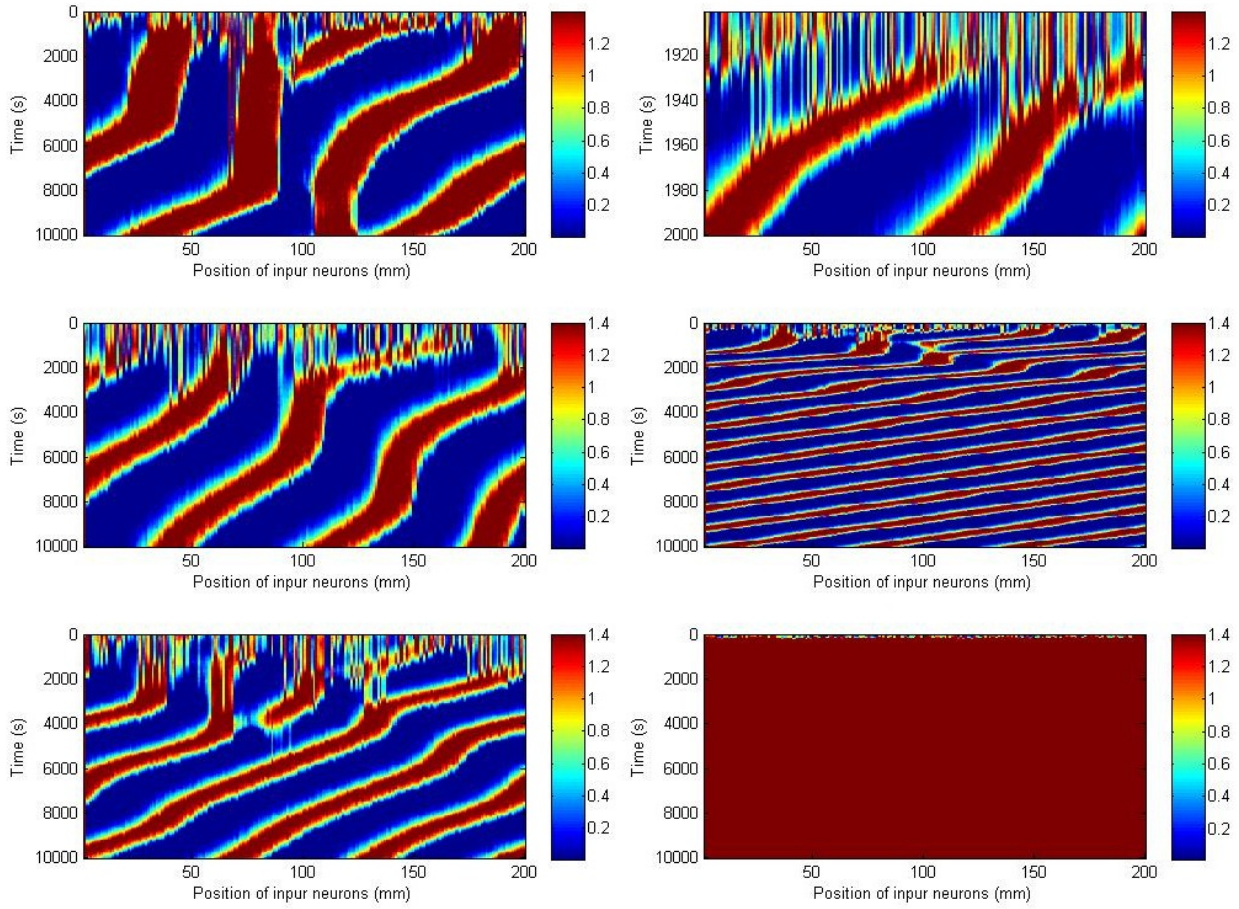

Figure 6.12: We set $(B,\ W) = (1(1/\text{s}),\ 10(\text{mm}))$, $s = 1000(\text{mm/s})$, a periodic boundary condition, and the initial condition to be random. From top left to bottom right $H = 50$, 60, 80, 90, 100, 110$(1/\text{s})$

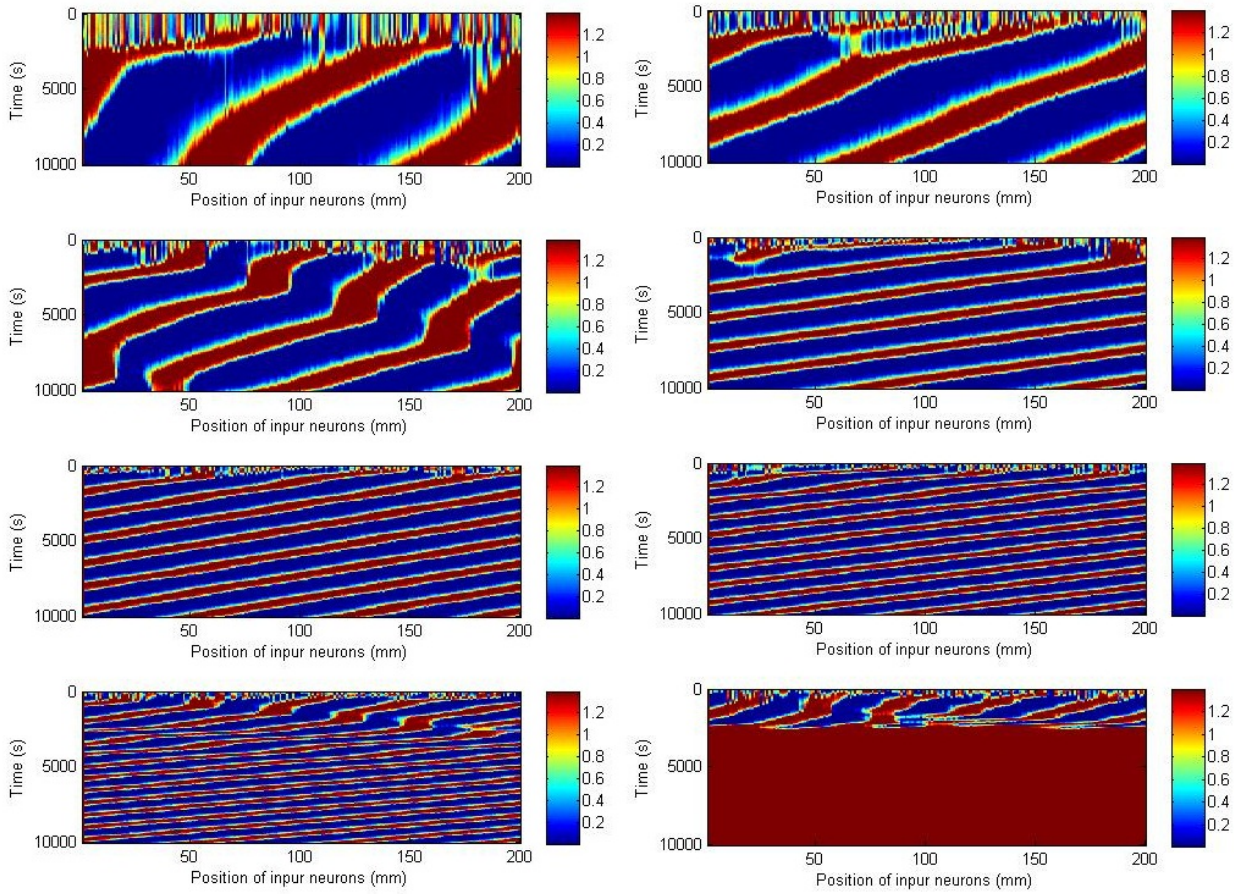

Figure 6.13: We set $(H,\ B)$ = (70(1/s), 1(1/s)), $s = 1000$(mm/s), a periodic boundary condition, and the initial condition to be random. From top left to bottom right W = 6, 7, 8, 9, 11, 12, 13, 14(mm)

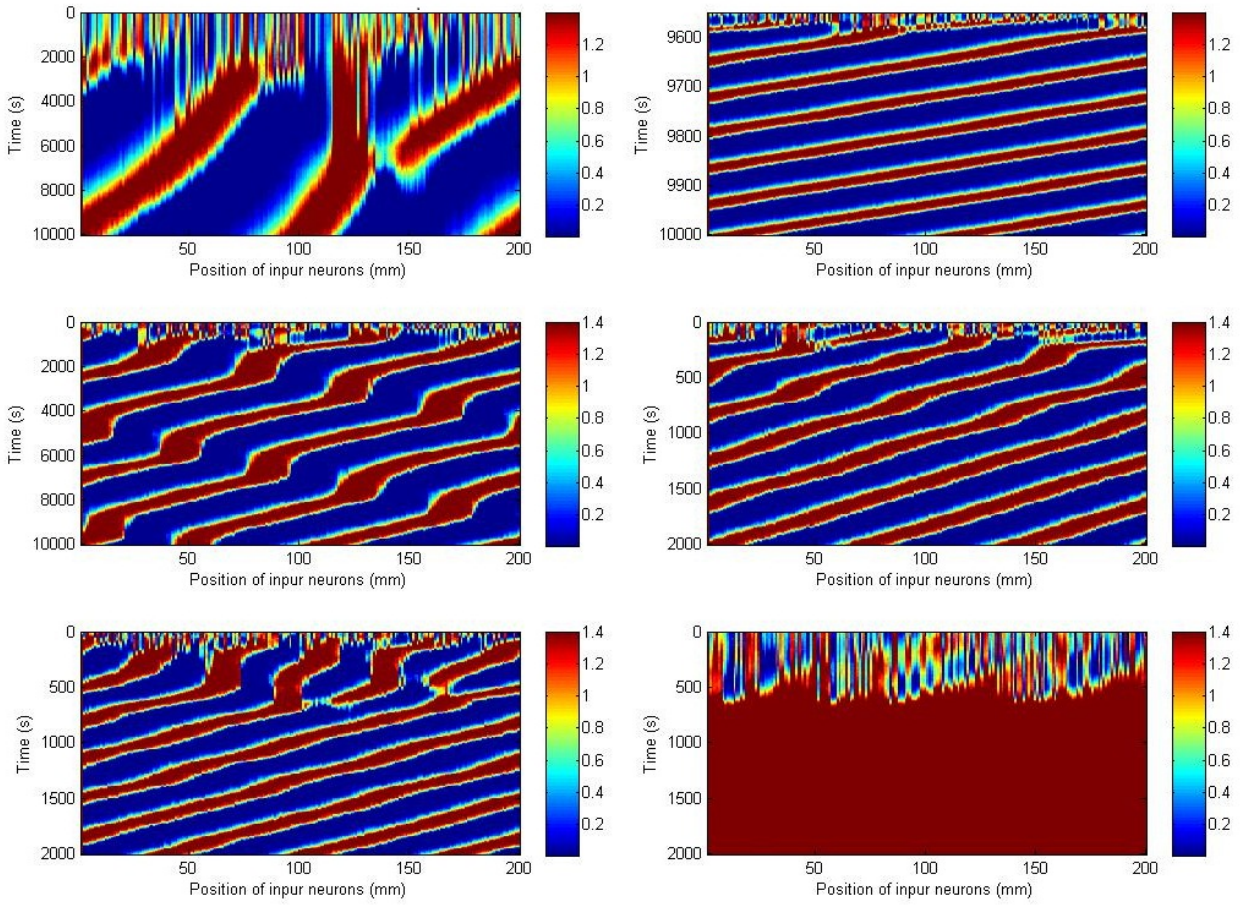

Figure 6.14: We set $(H,\ W)$ = (70(1/s), 10(mm)), $s = 1000(mm/s)$, a periodic boundary condition, and the initial condition to be random. From top left to bottom right B = 0.4, 0.6, 0.8, 1.2, 1.4, 1.6(1/s)

parameter	description	value
C (s)	parameter for integrate-and-fire model	2.0
b (s)	damping ratio of influence from an input neuron's firing	0.001
H (1/s)	maximum firing rate	30
B (1/s)	base firing rate	1
W (mm)	maximum distance of input neuron's receptive field	0.2
L	number of look back	∞
	number of inhibitory neurons	200
	number of excitatory neurons	200
	maximum inhibitory neurons	-1 (1/Ω)
	minimum inhibitory neurons	-19 (1/Ω)
	maximum excitatory neurons	20 (1/Ω)
	minimum excitatory neurons	1 (1/Ω)

Table 6.1: Values

band is around 8 $\times 10^{-3}$ (mm/s). There is an order of 6 difference in magnitude. This may be the reason why we do not see the change of preferable place positions in the hippocampus place cells and EC grid cells. It is interesting to see the development of place cells and grid cells. The place selectivity is not stable, since the preferable location change depends on the environment [56, 115, 118, 118, 122]. However, there is no specific change over time to fit to the different environment. Some place selectivity could be emerged in the 'critical period' over the long time scale compared to the speed of the stimulus.

6.2 Orientation and Direction Selectivity

As we have shown in Chapter 4, we have an orientation and direction selective system for specific parameters. We use values from Table 6.1 for this section. In this section, our goal is to model the visual systems in two dimensional receptive fields. All input neurons were scattered according to a uniformly distributed random variable in a unit circle with radius 1mm. We considered inhibitory lateral connections to also be input neurons for the simplicity of the arguments.

6.2.1 Convergence of Random Initial Conditions and Random Training

We tested the results of selectivity at every 400 s interval to understand the convergence. For measuring the selectivity, we fitted the curve of selectivity to the Gaussian curve

$$A \sum_{k=-1}^{1} \exp\left(\frac{(x - x^* + 2\pi k)^2}{2\sigma^2}\right) + B$$

using the Gauss-Newton method with an error of 0.01 (1/s). The ratio of the maximum and the minimum selectivity shows the convergence for two different cases as shown in Fig. 6.15. The average relative error was 0.031 (1/s) for the top panels and 0.0046 (1/s) for the bottom panels, so the Gaussian fit is reasonable. To show the rate of convergence, we fitted B/A, except with the initial time = 0, to the curve $x_1 t^{-x_2} + m$, where t is the time (s) and y is the value of B/A, using the Gauss-Newton method with linear least error of 0.001. We chose the average of the last 15 data to be the initial guess for m and chose $x_2 = 1$ and fitted x_1 using the first data point. The left panel of Fig. 6.16 corresponds with the top panels of Fig. 6.15, and the right panel of Fig. 6.15 corresponds with the bottom panels Fig. 6.15. The selectivity converged with an order of 0.99 for the top panel and 1.30 for the bottom panel with regards to the time of random training.

6.2.2 Random Initial Condition and Same Sequence of Random Training

If we choose a random initial condition, but set the sequence of random training, then we do not have the same preferred orientation as shown in Fig. 6.17. In these cases, we trained with the same training for 4000 s. This shows less of a tendency toward sequence of training for selectivity.

6.2.3 Same Initial Condition and Random Training

If we choose the same initial condition, but have randomly ordered training, then we have the same preferred orientation as shown in Fig. 6.18. In these cases, we trained with different training for 4000 s. Both panels start from different initial conditions, but both show specific preferable

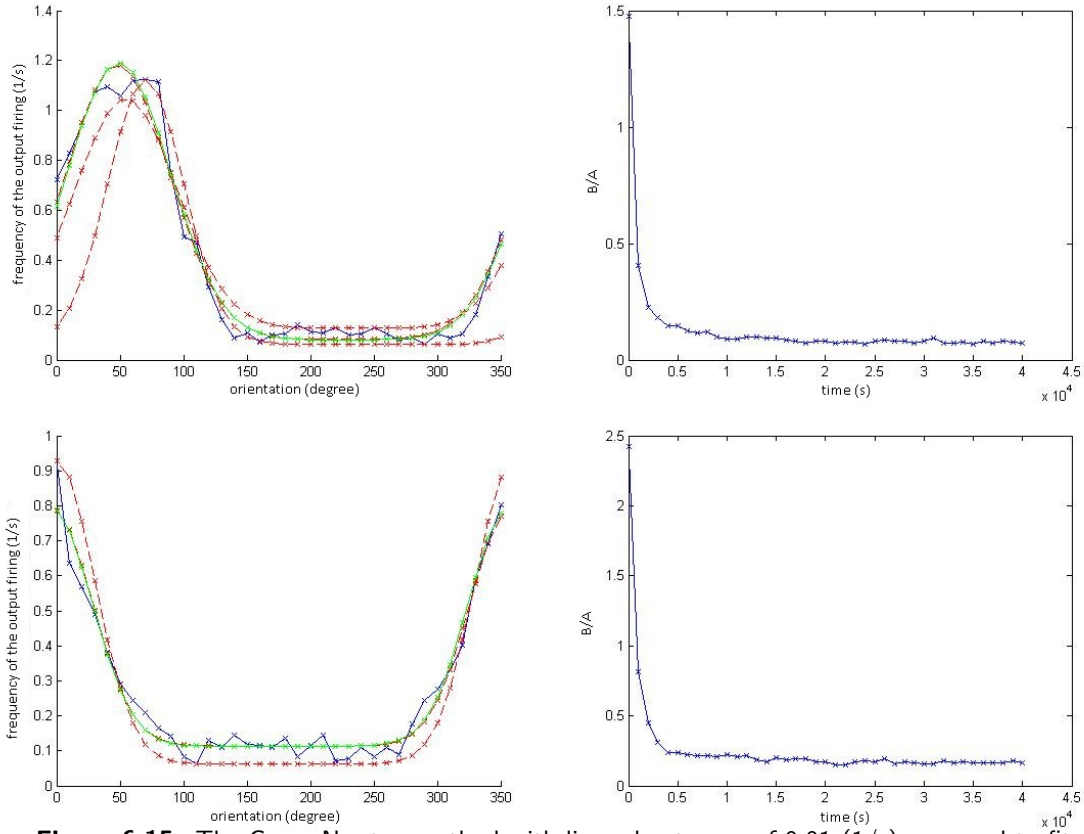

Figure 6.15: The Gauss-Newton method with linear least error of 0.01 (1/s) was used to fit data to the Gaussian curve $A\sum_{k=-1}^{1}\exp\left(\frac{(x-x^*+2\pi\,k)^2}{2\sigma^2}\right)+B$. The blue curves are the actual data and the green curves are the fitted data. The red curves are between the fitting. It shows two realizations from both random initial conditions and random sequence of training. Both show properties of direction- and orientation-selectivity. The top panels have 0.031 (1/s) average relative error and the bottom panels have 0.0046 (1/s).

orientation and direction.

6.2.4 Same Initial Condition and Limited Oriented Training

Next, we chose a limited degree of random training positions to see which orientation and direction the system prefers after 4000 (s). The training was randomly chosen within $(x\pm\alpha)$ mod 360 (degree), where α is the limiting orientation and x is the preferable orientation. To find a preferable location,

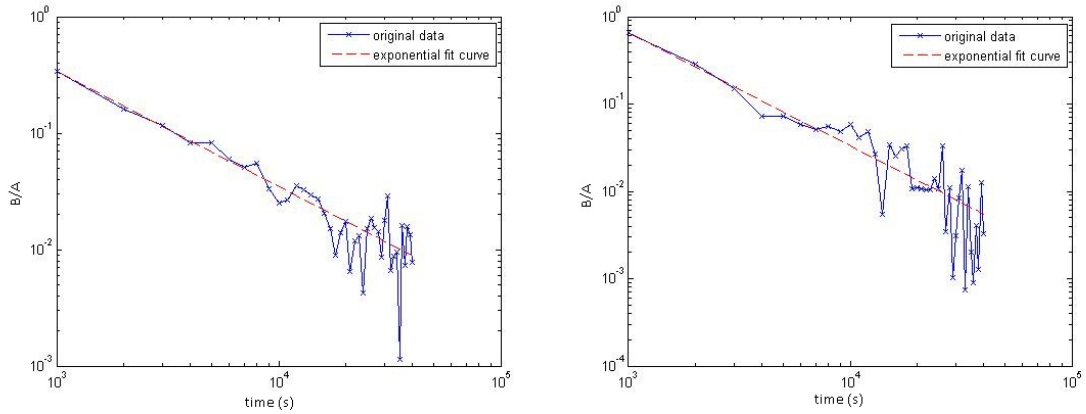

Figure 6.16: The Gauss-Newton method with linear least error of 0.001 was used to fit data to an exponent curve $x_1 t^{-x_2} + m$, where t is the time (s) and y is the value of B/A. The left panel is fit to $(x_1, x_2, m) \approx (312.69, 0.99, 0.065)$ and the right panel is fit to $(x_1, x_2, m) \approx (5127.4, 1.30, 0.1636)$. Both of them have an approximately exponential convergence rate relative to the running time.

we fitted the selection curve to a Gaussian curve $A \sum_{k=-1}^{1} \exp\left(\frac{(x - x^* + 2\pi\, k)^2}{2\sigma^2}\right) + B$ using the Gauss-Newton method with an error of 0.01 (1/s). x^* is the maximum preferable location and we considered this as the preferable location for this section. These computational experiments were to model noise from biological experiments. The animals eyes do not set in one place and always have some fluctuations.

We chose the initial condition of the top panel of Fig. 6.18 for the top panels of Fig. 6.19, Fig. 6.20 and Fig. 6.21 and the bottom panel of Fig. 6.18 for the bottom panels of Fig. 6.19, Fig. 6.20 and Fig. 6.21. We used 10 different random trainings for this initial condition and produced preferable curves and fitted them to the Gaussian curves, then took the average of its maximum preference. We chose $x = 0$ (degree) for both cases and chose limiting orientation from 0 (degree) to 180 (degree) in 15 degree increments. Fig. 6.19 shows the preference curve for all the experiments. The top panel shows more regular shapes than the bottom panel. Fig. 6.20 shows the average of the frequency of the output firing for each limiting orientation. The bottom panel has a gap, because the 105 (degree) and 120 (degree) limiting orientations cause non-selective cases. Two out of ten cases for the 150 (degree) limiting orientation also showed no selectivity and the panel does

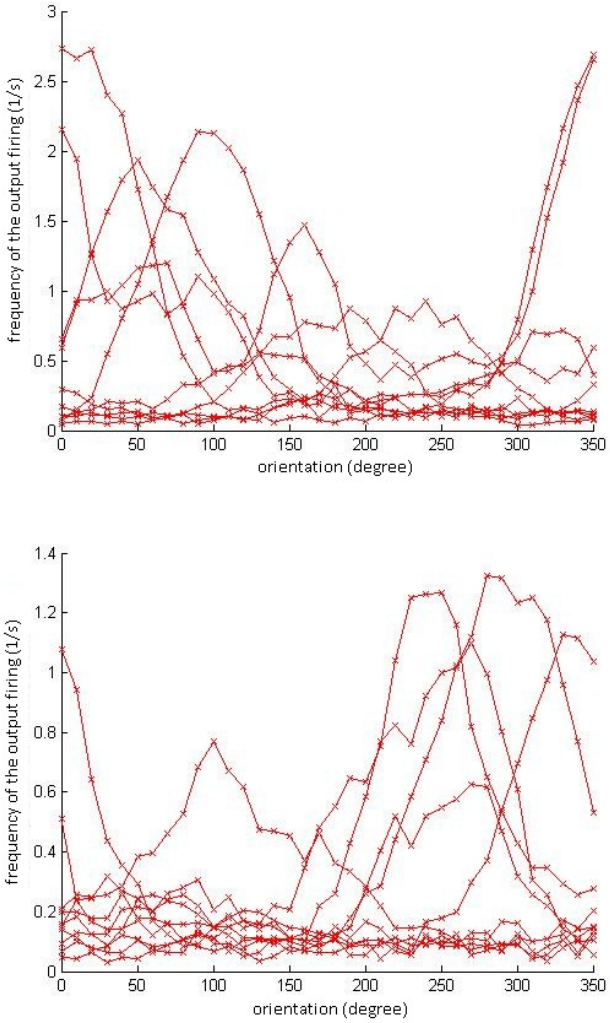

Figure 6.17: Both panels have a specific sequence of training, but a different initial condition for each run. The two panels use different sequences and each red curve represents experiments with a different initial condition.

not show those cases. Fig. 6.21 shows the mean preferable location for each limiting orientation α. Again, the bottom panel has gaps for the same reasons. Also, the bottom panel has a larger standard deviation for the preferable locations.

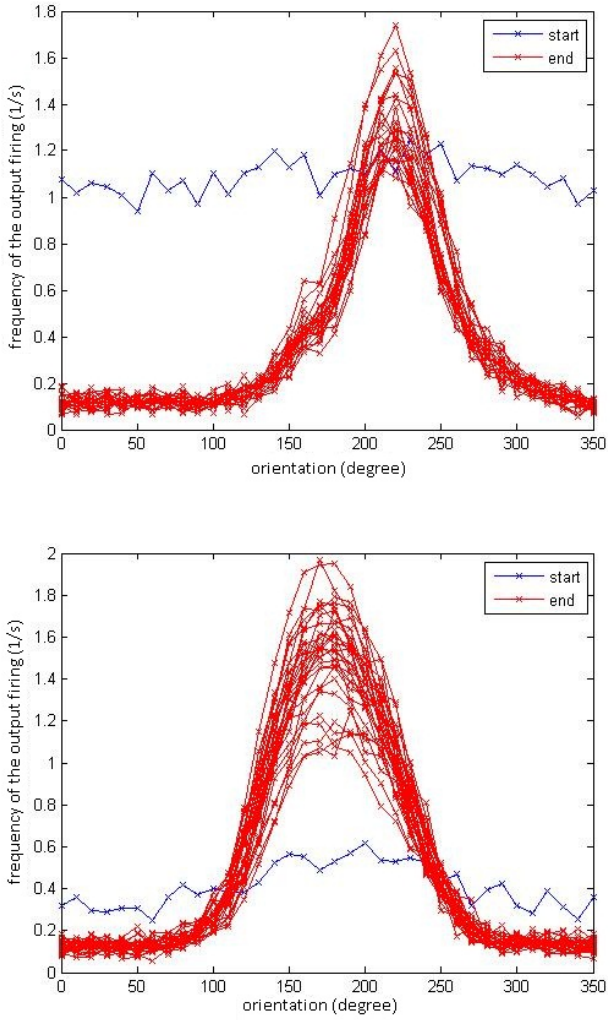

Figure 6.18: Both panels start from specific initial conditions and train with a different random sequence of stimulus orientation. The top and the bottom panel start from different orientations shown in the blue curves. The red curves represent trained orientation after each random training.

6.2.5 Same Initial Condition and Oriented Training in Beginning of Training

For the random training of 4000 (s) for the same initial condition, we could enforce x (degree) in the beginning of the training. Enforcing x (degree) by training at x (degree) for a long time causes preferable location at x (degree). Also, we know from the previous simulations, that strongly

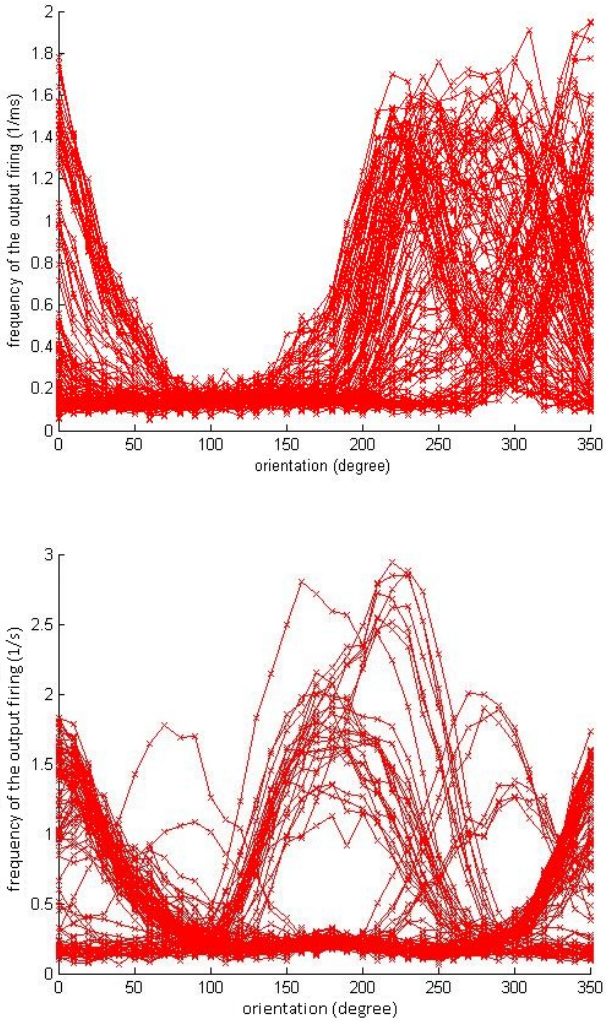

Figure 6.19: The top panel uses the same initial condition as the top panel of Fig. 6.18 and $x = 0.0$ (degree). The bottom panel uses the same initial condition as the bottom panel of Fig. 6.18 and $x = 0.0$ (degree). Different values of α produce different preferable curves, which are shown with red curves.

preferred selectivity does not break from a random sequence of training. Then the next question is how long do we need to train the system to make sure it learned the trained preference.

We chose the initial condition of the bottom panel of Fig. 6.18 and chose x to be 90 degree. The preferable orientation change over time as shown in the top panel of Fig. 6.22. The average and the standard deviation is shown in the bottom panel of Fig. 6.22.

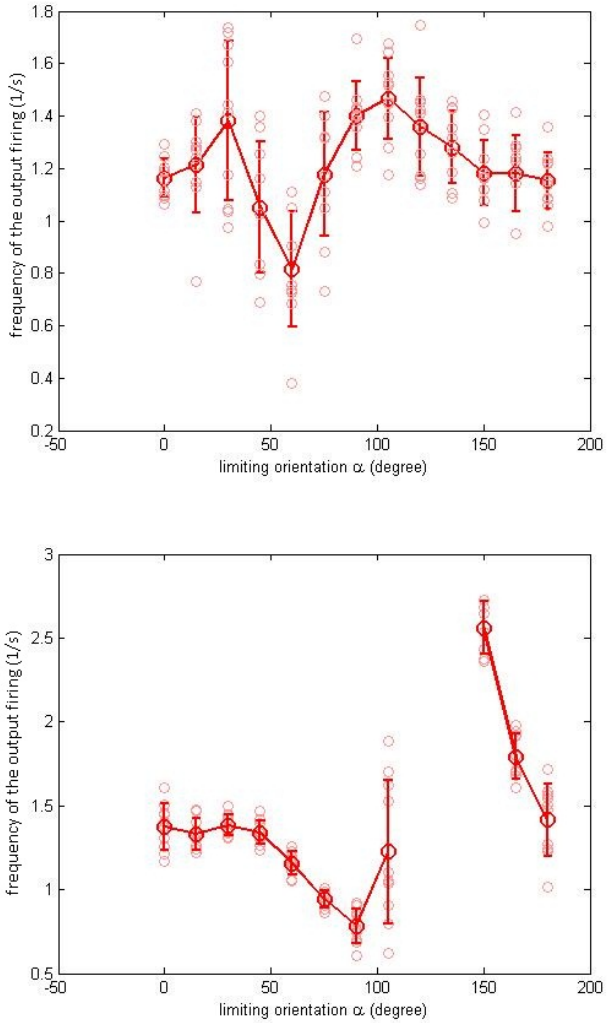

Figure 6.20: The top panel uses the same initial condition as the top panel of Fig. 6.18 and $x = 0.0$ (degree). The bottom panel uses the same initial condition of the bottom panel of Fig. 6.18 and $x = 0.0$ (degree). Both show the maximum frequency of each limiting orientation α (degree). The bottom panel has no selective cases for 105 (degree) and 120 (degree) for all 10 runs. Also, two cases of 150 (degree) became non-selective, and these cases are not used in the figure.

When we chose x to be 0 degree, then for 2400 swipes, it did not show the difference as seen in the left panel of Fig. 6.23 for 10 different runs, but it started to become non-selective as the number of swipes got larger. For 2800 swipes, 5 out of 10 did not show selectivity as shown in Fig. 6.24 but 5 out of 10 still preferred the original degree as shown in the upper right panel of Fig. 6.23.

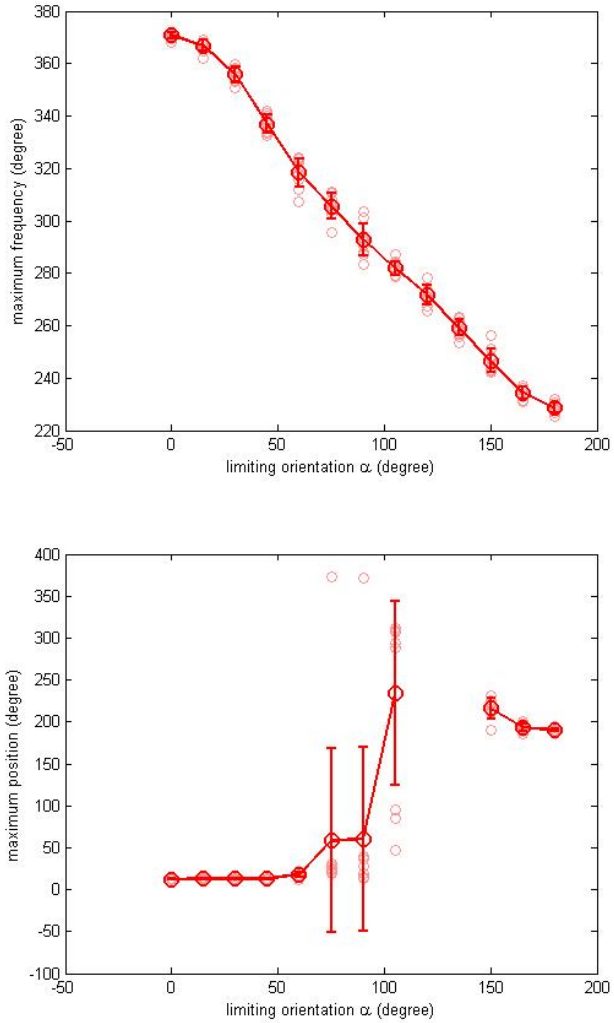

Figure 6.21: The top panel uses the same initial condition of the top panel of Fig. 6.18 and $x = 0.0$ (degree). The bottom uses the same initial condition of the bottom panel of Fig. 6.18 and $x = 0.0$ (degree). Both show the maximum position from the Gaussian linear least fit to the preferable curve of each limiting orientation α (degree). The bottom panel has no selective cases for 105 (degree) and 120 (degree) for all 10 runs. Also, two cases of 150 (degree) become non-selective, and these cases are not used in the figure.

As number of swipes became larger, then the system became more unstable and we did not see any of the preference. It started to prefer both the original and 0 degree preference or no preference. For 4417 swipes, we saw preferable locations in both original and 0 degrees in 5 out of 10 cases as shown in the lower left panel of Fig. 6.23. After that, it started to tend more to 0 degrees. With

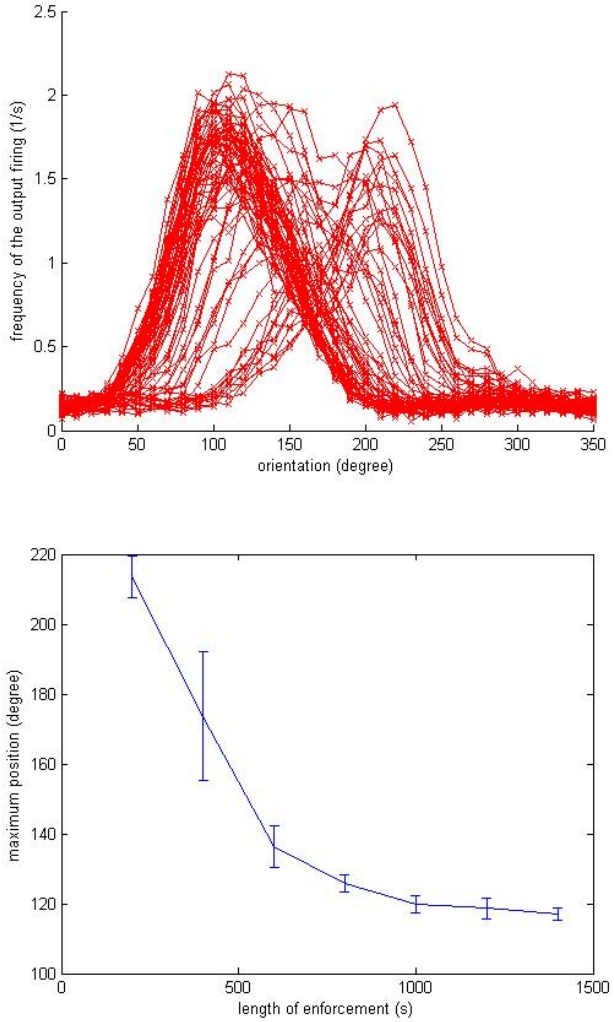

Figure 6.22: Chose same initial condition as the right panel of Fig. 6.18 and $x = 90.0$ (degree). The top panel shows all simulations using different length of training. The bottom panel shows maximum position over the length of enforcement.

4667 swipes, 9 out of 10 had a preference as shown in the lower right panel of Fig. 6.23.

To show the non-selective and selective cases, we ran 10 simulations for different lengths of training. If the simulation showed selectivity then we fitted the curve to two Gaussian curves

$$A \sum_{k=-1}^{1} \exp\left(\frac{(x - 189.17 + 2\pi k)^2}{2\sigma^2}\right) + C \sum_{k=-1}^{1} \exp\left(\frac{(x + 2\pi k)^2}{2\sigma^2}\right) + B. \tag{6.1}$$

We used this curve because we trained the system with 0(degree) and the initial condition had an average of 189.17(degree) preference from 30 runs. The Gauss-Newton method was used to fit with an error of 0.01(1/s). The non-selective cases were considered with $A = C = 0$. A/C and C/A showed a preference ratio, which should change according to the length of the training as shown in Fig. 6.25. Fig. 6.26 shows the average size of preferences A and C out of 10 runs over the length of the training time. The left panel shows the average with non-selective cases and the right panel shows the average without non-selective cases. Fig. 6.27 shows the number of non-selective cases out of 10 runs over the time of initial training. In between the two preferable cases, there are training lengths that did not show the property of selectivity.

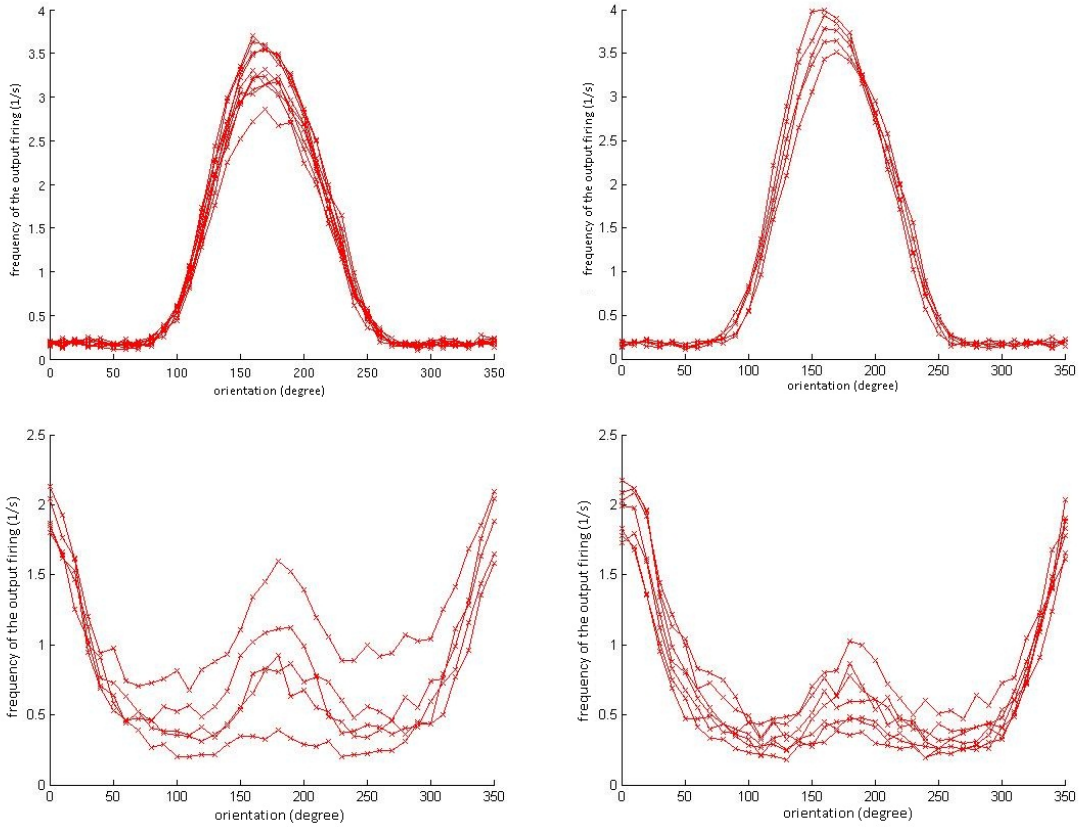

Figure 6.23: 4000 (s) training, but enforced in the beginning and then trained with a random sequence. The left panel of the first row shows 0 degree enforcement for 576 (s) and the right has 0 degree enforcement for 672 (s). The left panel of the second row shows 0 degree enforcement for 1060 (s) and the right has 0 degree enforcement for 1120 (s).

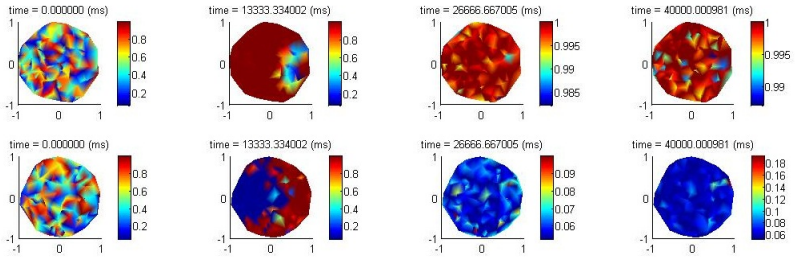

Figure 6.24: 4000 (s) training, but enforced in the beginning for 672 (s) and then a random sequence of trai

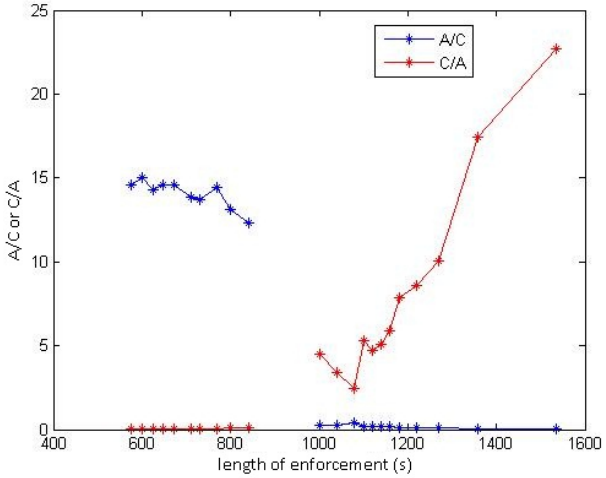

Figure 6.25: The x-axis shows the length of enforced training and the y-axis shows A/C and C/A from (6.1).

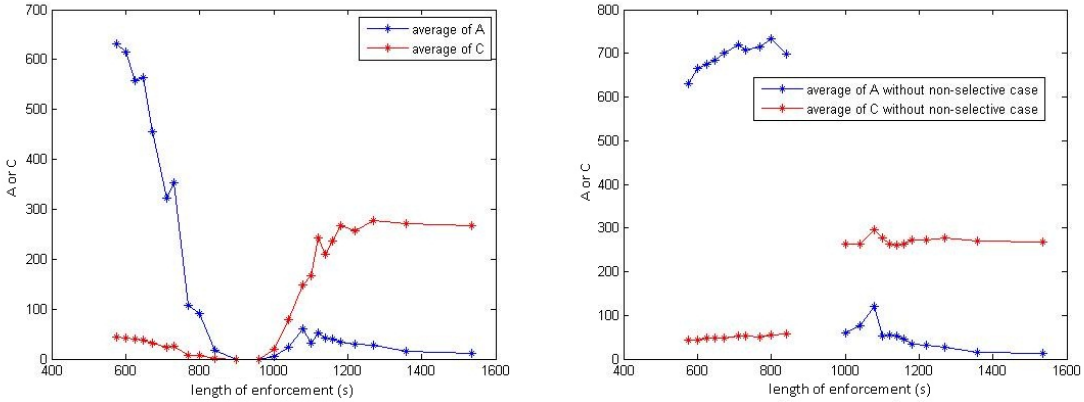

Figure 6.26: The x-axis shows the length of enforced training and the y-axis shows the average of A and C from (6.1). The left panel includes non-selective cases in the averages and the right panel does not include non-selective cases.

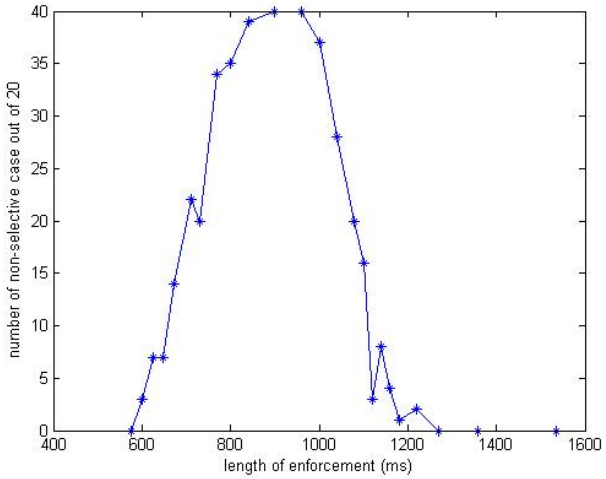

Figure 6.27: Number of non-selective cases out of 10 runs over the initial enforcement time.

6.2.6 Discussion

In our simple model, we showed the emergence of the properties of orientation- and direction-selectivity as we expect from visual system. So our system has a good insight on basic development and learning. In the early stages of the development of the visual cortex, orientation and direction selectivity is present without the experience of stimuli [142, 168, 169]. However, it requires normal visual experience for full development [19, 34, 36, 167]. In our system, the initial condition showed a small tendency toward some orientation and direction and this expanded to full selectivity by random oriented and directed training as shown in Fig. 6.15. This coincides with actual visual stimuli that do not a have single preferable stimulus for training. The visual cortex can also be taught by training with simple stimuli. For example, if only one oriented stimulus is given during the first few weeks of a cats development, then the preferable orientation is set to that specific orientation [15, 65], and if the one direction is shown to the cats, then the cats become preferential to that direction [38]. We can teach our system with preferable selectivity as well. In Fig. 6.23, we showed the sensitivity of the enforced training. If the training is too short, then nothing happens and if the training is not too short, but not long enough, then the system becomes non-selective. The slight tendency to one orientation is broken by relatively short training. Which may be the reason that a short training period of 4-7 weeks, causes more non-oriented selective simple cells in cats [126]. The longer training of 5 months does not seem to have many non-oriented cases [15].

Our simple model seems to capture the rich phenomenon of the visual system, so we could study this model to understand the basic components of the network of neurons. We could expand the model with several output neurons with lateral connections. Thus the inhibitory neurons could come from the cortex layer and be more closely related to the actual biology.

Chapter 7

Summary and Future Directions

We have developed a concise, biophysically plausible, quantitative probabilistic model of coupled networks of neurons exhibiting spike-timing dependent synaptic plasticity. We have also introduced quantitative notion of a neuron's selectivity as the community formation. The model demonstrates rich properties, such as selectivity of input structures and competition between input neurons previously demonstrated by qualitative simulations. Our general purpose stochastic model can be analyzed by the formulation of Markov chains, so that the existence of the community formation can be shown for different types of mathematically rigorous assumptions. Therefore, this method provides a well-positioned balance between neuro-biological relevance and theoretical tractability.

By extending our model to a large scale, we have shown the development of the visual system's physiological properties, namely direction- and orientation-selectivity, which is know through biological experimentation. Hence, this selectivity could be an epiphenomenon of the assumptions chosen for the computational models. The key insight here is that the model shows a robust phenomenon with respect to the initial condition, but not to the input stimulus, which implies the importance of the initial condition and the noisy inputs. These dynamics may explain learning and reinforcement of the visual neurons and could predict results in future experiments.

We could extend our model to make it more realistic to the visual system. The inhibitory and the excitatory lateral neuronal connections are key to the visual networks, which we did not include in our model. It might give more precise predictions of the visual connections and could add biological data to the model. Since we have a precise single output neuron model, extension to any neuronal system is easier. Our model can be used as a foundation for complicated neuronal systems.

References

[1] L. Abbott. Theoretical neuroscience rising. *Neuron*, 60(3):489–495, 2008. ISSN 0896-6273.

[2] D. Adams and J. Horton. Capricious expression of cortical columns in the primate brain. *Nature neuroscience*, 6(2):113–114, 2003.

[3] D. Adams and J. Horton. Monocular cells without ocular dominance columns. *Journal of neurophysiology*, 96(5):2253, 2006. ISSN 0022-3077.

[4] E. Adelson and J. Bergen. Spatiotemporal energy models for the perception of motion. *J. Opt. Soc. Am. A*, 2(2):284–299, 1985.

[5] B. Ahmed, J. Anderson, R. Douglas, K. Martin, and J. Nelson. Polyneuronal innervation of spiny stellate neurons in cat visual cortex. *The Journal of Comparative Neurology*, 341(1): 39–49, 1994. ISSN 1096-9861.

[6] J. Alonso, W. Usrey, and R. Reid. Rules of connectivity between geniculate cells and simple cells in cat primary visual cortex. *The Journal of Neuroscience*, 21(11):4002, 2001. ISSN 0270-6474.

[7] J. Anderson, M. Carandini, and D. Ferster. Orientation tuning of input conductance, excitation, and inhibition in cat primary visual cortex. *Journal of Neurophysiology*, 84(2):909, 2000. ISSN 0022-3077.

[8] H. Barlow and R. Hill. Selective sensitivity to direction of movement in ganglion cells of the rabbit retina. *Science*, 139(3553):412, 1963. ISSN 0036-8075.

[9] H. Barlow and W. Levick. The mechanism of directionally selective units in rabbit's retina. *The Journal of physiology*, 178(3):477, 1965.

[10] J. Barlow. Inertial navigation as a basis for animal navigation. *Journal of Theoretical Biology*, 6(1):76, 1964. ISSN 0022-5193.

[11] C. Barry, R. Hayman, N. Burgess, and K. Jeffery. Experience-dependent rescaling of entorhinal grids. *Nature Neuroscience*, 10(6):682–684, 2007. ISSN 1097-6256.

[12] A. Bartsch and J. Van Hemmen. Combined Hebbian development of geniculocortical and lateral connectivity in a model of primary visual cortex. *Biological Cybernetics*, 84(1):41–55, 2001. ISSN 0340-1200.

[13] C. Bell, V. Han, Y. Sugawara, and K. Grant. Synaptic plasticity in a cerebellum-like structure depends on temporal order. 1997.

[14] G. Bi and M. Poo. Synaptic modifications in cultured hippocampal neurons: dependence on spike timing, synaptic strength, and postsynaptic cell type. *Journal of Neuroscience*, 18(24): 10464, 1998.

[15] C. Blakemore and G. Cooper. Development of the brain depends on the visual environment. 1970.

[16] T. Bonhoeffer and A. Grinvald. Iso-orientation domains in cat visual cortex are arranged in pinwheel-like patterns. *Nature*, 353(6343):429–431, 1991. ISSN 0028-0836.

[17] L. Borg-Graham, C. Monier, and Y. Fregnac. Visual input evokes transient and strong shunting inhibition in visual cortical neurons. *Nature*, 393(6683):369–372, 1998. ISSN 0028-0836.

[18] E. Bostock, R. Muller, and J. Kubie. Experience-dependent modifications of hippocampal place cell firing. *Hippocampus*, 1(2):193–205, 1991. ISSN 1098-1063.

[19] B. Braastad and P. Heggelund. Development of spatial receptive-field organization and orientation selectivity in kitten striate cortex. *Journal of neurophysiology*, 53(5):1158–1178, 1985.

[20] P. Brémaud. *Point processes and queues, martingale dynamics*. Springer, 1981.

[21] E. Brown. Theory of point processes for neural systems, 2005.

[22] V. Brun, M. Otnæss, S. Molden, H. Steffenach, M. Witter, M. Moser, and E. Moser. Place cells and place recognition maintained by direct entorhinal-hippocampal circuitry. *Science*, 296(5576):2243, 2002. ISSN 0036-8075.

[23] V. Brun, T. Solstad, K. Kjelstrup, M. Fyhn, M. Witter, E. Moser, and M. Moser. Progressive increase in grid scale from dorsal to ventral medial entorhinal cortex. *Hippocampus*, 18(12): 1200–1212, 2008. ISSN 1098-1063.

[24] N. Brunel and O. Trullier. Plasticity of directional place fields in a model of rodent CA3. *Hippocampus*, 8(6):651–65, 1998.

[25] N. Buchs and W. Senn. Spike-based synaptic plasticity and the emergence of direction selective simple cells: Simulation results. *Journal of Computational Neuroscience*, 13(3):167–186, 2002. ISSN 0929-5313.

[26] N. Burgess. Grid cells and theta as oscillatory interference: Theory and predictions. *Hippocampus*, 18(12):1157–1174, 2008. ISSN 1098-1063.

[27] N. Burgess, C. Barry, and J. O'Keefe. An oscillatory interference model of grid cell firing. *Hippocampus*, 17(9):801–812, 2007. ISSN 1098-1063.

[28] R. Burwell and D. Hafeman. Positional firing properties of postrhinal cortex neurons. *Neuroscience*, 119(2):577–588, 2003. ISSN 0306-4522.

[29] R. Burwell, M. Shapiro, M. O'Malley, and H. Eichenbaum. Positional firing properties of perirhinal cortex neurons. *Neuroreport*, 9(13):3013, 1998. ISSN 0959-4965.

[30] J. Caldwell, N. Daw, and H. Wyatt. Effects of picrotoxin and strychnine on rabbit retinal ganglion cells: lateral interactions for cells with more complex receptive fields. *The Journal of Physiology*, 276(1):277, 1978. ISSN 0022-3751.

[31] M. Carandini and D. Ferster. Membrane potential and firing rate in cat primary visual cortex. *The Journal of Neuroscience*, 20(1):470, 2000. ISSN 0270-6474.

[32] Y. Chan and C. Chiao. Effect of visual experience on the maturation of ON-OFF direction selective ganglion cells in the rabbit retina. *Vision research*, 48(23-24):2466–2475, 2008. ISSN 0042-6989.

[33] F. Chance, S. Nelson, and L. Abbott. Synaptic depression and the temporal response characteristics of V1 cells. *The Journal of neuroscience*, 18(12):4785, 1998. ISSN 0270-6474.

[34] B. Chapman, M. Stryker, and T. Bonhoeffer. Development of orientation preference maps in ferret primary visual cortex. *The Journal of Neuroscience*, 16(20):6443–6453, 1996.

[35] M. Chen, S. Weng, Q. Deng, Z. Xu, and S. He. Physiological properties of direction-selective ganglion cells in early postnatal and adult mouse retina. *The Journal of Physiology*, 587(4): 819–828, 2009. ISSN 1469-7793.

[36] M. Crair, D. Gillespie, and M. Stryker. The role of visual experience in the development of columns in cat visual cortex. *Science*, 279(5350):566, 1998.

[37] O. Creutzfeldt. Generality of the functional structure of the neocortex. *Naturwissenschaften*, 64(10):507–517, 1977. ISSN 0028-1042.

[38] N. Daw and H. Wyatt. Kittens reared in a unidirectional environment: evidence for a critical period. *The Journal of physiology*, 257(1):155, 1976.

[39] D. Debanne, B. Gahwiler, and S. Thompson. Asynchronous pre-and postsynaptic activity induces associative long-term depression in area CA1 of the rat hippocampus in vitro. *Proceedings of the National Academy of Sciences of the United States of America*, 91(3):1148, 1994.

[40] D. Debanne, B. Gahwiler, and S. Thompson. Long-term synaptic plasticity between pairs of individual CA3 pyramidal cells in rat hippocampal slice cultures. *The Journal of Physiology*, 507(1):237–247, 1998. ISSN 1469-7793.

[41] A. Ekstrom, M. Kahana, J. Caplan, T. Fields, E. Isham, E. Newman, and I. Fried. Cellular networks underlying human spatial navigation. *Nature*, 425(6954):184–188, 2003. ISSN 0028-0836.

[42] J. Elstrott and M. Feller. Direction-Selective Ganglion Cells Show Symmetric Participation in Retinal Waves During Development. *The Journal of Neuroscience*, 30(33):11197, 2010. ISSN 0270-6474.

[43] J. Elstrott, A. Anishchenko, M. Greschner, A. Sher, A. Litke, E. Chichilnisky, and M. Feller. Direction selectivity in the retina is established independent of visual experience and cholinergic retinal waves. *Neuron*, 58(4):499–506, 2008. ISSN 0896-6273.

[44] F. Engert, H. Tao, L. Zhang, and M. Poo. Moving visual stimuli rapidly induce direction sensitivity of developing tectal neurons. *Nature*, 419(6906):470–475, 2002. ISSN 0028-0836.

[45] D. Feldman. Timing-based LTP and LTD at vertical inputs to layer II/III pyramidal cells in rat barrel cortex. *Neuron*, 27(1):45–56, 2000. ISSN 0896-6273.

[46] D. Ferster. Spatially opponent excitation and inhibition in simple cells of the cat visual cortex. *The Journal of neuroscience*, 8(4):1172, 1988. ISSN 0270-6474.

[47] D. Ferster and C. Koch. Neuronal connections underlying orientation selectivity in cat visual cortex. *Trends in Neurosciences*, 10(12):487–492, 1987. ISSN 0166-2236.

[48] D. Ferster and S. Lindstr
"om. An intracellular analysis of geniculo-cortical connectivity in area 17 of the cat. *The Journal of Physiology*, 342(1):181, 1983. ISSN 0022-3751.

[49] D. Ferster and K. Miller. Neural mechanisms of orientation selectivity in the visual cortex. *Annual review of neuroscience*, 23(1):441–471, 2000. ISSN 0147-006X.

[50] S. Fried, T. M
"unch, and F. Werblin. Mechanisms and circuitry underlying directional selectivity in the retina. *Nature*, 420(6914):411–414, 2002. ISSN 0028-0836.

[51] M. Fyhn, T. Hafting, A. Treves, M. Moser, and E. Moser. Hippocampal remapping and grid realignment in entorhinal cortex. *Nature*, 446(7132):190–194, 2007. ISSN 0028-0836.

[52] M. Glasier, R. Sutton, and D. Stein. Effects of unilateral entorhinal cortex lesion and ganglioside GM1 treatment on performance in a novel water maze task. *Neurobiology of learning and memory*, 64(3):203–214, 1995. ISSN 1074-7427.

[53] J. Gordon and M. Stryker. Experience-dependent plasticity of binocular responses in the primary visual cortex of the mouse. *The Journal of neuroscience*, 16(10):3274, 1996. ISSN 0270-6474.

[54] K. Gothard, W. Skaggs, and B. McNaughton. Dynamics of mismatch correction in the hippocampal ensemble code for space: interaction between path integration and environmental cues. *The Journal of neuroscience*, 16(24):8027, 1996. ISSN 0270-6474.

[55] B. Gustafsson, H. Wigstrom, W. Abraham, and Y. Huang. Long-term potentiation in the hippocampus using depolarizing current pulses as the conditioning stimulus to single volley synaptic potentials. *Journal of Neuroscience*, 7(3):774, 1987.

[56] T. Hafting, M. Fyhn, S. Molden, M. Moser, and E. Moser. Microstructure of a spatial map in the entorhinal cortex. *Nature*, 436(7052):801–806, 2005. ISSN 0028-0836.

[57] T. Hafting, M. Fyhn, T. Bonnevie, M. Moser, and E. Moser. Hippocampus-independent phase precession in entorhinal grid cells. *Nature*, 453(7199):1248–1252, 2008. ISSN 0028-0836.

[58] K. Harris, D. Henze, H. Hirase, X. Leinekugel, G. Dragoi, A. Czurkó, and G. Buzsáki. Spike train dynamics predicts theta-related phase precession in hippocampal pyramidal cells. *Nature*, 417(6890):738–741, 2002. ISSN 0028-0836.

[59] S. He and R. Masland. Retinal direction selectivity after targeted laser ablation of starburst amacrine cells. *Nature*, 389(6649):378–381, 1997. ISSN 0028-0836.

[60] D. Hebb. The Organization of Behavior: A Neuropsychological Theory. 1949.

[61] P. Heggelund. Receptive field organization of simple cells in cat striate cortex. *Experimental Brain Research*, 42(1):89–98, 1981. ISSN 0014-4819.

[62] T. Hensch. Critical period regulation. *Annu. Rev. Neurosci.*, 27:549–579, 2004. ISSN 0147-006X.

[63] A. Herz, T. Gollisch, C. Machens, and D. Jaeger. Modeling single-neuron dynamics and computations: a balance of detail and abstraction. *science*, 314(5796):80, 2006.

[64] A. Hill. First occurrence of hippocampal spatial firing in a new environment. *Experimental Neurology*, 62(2):282–297, 1978. ISSN 0014-4886.

[65] H. Hirsch and D. Spinelli. Visual experience modifies distribution of horizontally and vertically oriented receptive fields in cats. *Science*, 168(3933):869, 1970.

[66] J. Hirsch, J. Alonso, R. Reid, and L. Martinez. Synaptic integration in striate cortical simple cells. *Journal of neuroscience*, 18(22):9517, 1998.

[67] P. Hitchcock and T. Hickey. Ocular dominance columns: evidence for their presence in humans. *Brain research*, 182(1):176, 1980. ISSN 0006-8993.

[68] M. Honda, H. Urakubo, K. Tanaka, and S. Kuroda. Analysis of Development of Direction Selectivity in Retinotectum by a Neural Circuit Model with Spike Timing-Dependent Plasticity. *The Journal of Neuroscience*, 31(4):1516, 2011. ISSN 0270-6474.

[69] D. Hubel and T. Wiesel. Receptive fields of single neurones in the cat's striate cortex. *The Journal of physiology*, 148(3):574, 1959. ISSN 0022-3751.

[70] D. Hubel and T. Wiesel. Receptive fields, binocular interaction and functional architecture in the cat's visual cortex. *The Journal of Physiology*, 160(1):106, 1962. ISSN 0022-3751.

[71] D. Hubel and T. Wiesel. Receptive fields and functional architecture of monkey striate cortex. *The Journal of Physiology*, 195(1):215, 1968. ISSN 0022-3751.

[72] D. Hubel and T. Wiesel. Anatomical demonstration of columns in the monkey striate cortex. *Nature*, 221(182):747–50, 1969.

[73] J. Huxter, N. Burgess, and J. O'Keefe. Independent rate and temporal coding in hippocampal pyramidal cells. *Nature*, 425(6960):828–832, 2003. ISSN 0028-0836.

[74] A. Jeewajee, C. Barry, J. O'Keefe, and N. Burgess. Grid cells and theta as oscillatory interference: Electrophysiological data from freely moving rats. *Hippocampus*, 18(12):1175–1185, 2008. ISSN 1098-1063.

[75] M. Jung, S. Wiener, and B. McNaughton. Comparison of spatial firing characteristics of units in dorsal and ventral hippocampus of the rat. *The Journal of neuroscience*, 14(12):7347, 1994. ISSN 0270-6474.

[76] J. Kaas, L. Krubitzer, Y. Chino, A. Langston, E. Polley, and N. Blair. Reorganization of retinotopic cortical maps in adult mammals after lesions of the retina. *Science*, 248(4952): 229, 1990. ISSN 0036-8075.

[77] A. Kamondi, L. Acsády, X. Wang, and G. Buzsáki. Theta oscillations in somata and dendrites of hippocampal pyramidal cells in vivo: Activity-dependent phase-precession of action potentials. *Hippocampus*, 8(3):244–261, 1998. ISSN 1098-1063.

[78] A. Kepecs, M. van Rossum, S. Song, and J. Tegner. Spike-timing-dependent plasticity: common themes and divergent vistas. *Biological cybernetics*, 87(5):446–458, 2002.

[79] C. Kittila and S. Massey. Pharmacology of directionally selective ganglion cells in the rabbit retina. *Journal of neurophysiology*, 77(2):675, 1997. ISSN 0022-3077.

[80] J. Knierim, H. Kudrimoti, and B. McNaughton. Place cells, head direction cells, and the learning of landmark stability. *Journal of Neuroscience*, 15(3):1648, 1995.

[81] S. Kuffler. Discharge patterns and functional organization of mammalian retina. *J Neurophysiol*, 16(1):37–68, 1953.

[82] L. Lapicque. Recherches quantitatives sur lexcitation électrique des nerfs traitée comme une polarisation. *J. Physiol. Pathol. Gen*, 9:620–635, 1907.

[83] J. Lettvin, H. Maturana, W. McCulloch, and W. Pitts. What the frog's eye tells the frog's brain. *Proceedings of the IRE*, 47(11):1940–1951, 1959. ISSN 0096-8390.

[84] J. Leutgeb, S. Leutgeb, A. Treves, R. Meyer, C. Barnes, B. McNaughton, M. Moser, and E. Moser. Progressive Transformation of Hippocampal Neuronal Representations in. *Neuron*, 48(2):345–358, 2005. ISSN 0896-6273.

[85] S. LeVay and C. Gilbert. Laminar patterns of geniculocortical projection in the cat. *Brain Research*, 113(1):1–19, 1976. ISSN 0006-8993.

[86] S. Levay, M. Stryker, and C. Shatz. Ocular dominance columns and their development in layer IV of the cat's visual cortex: a quantitative study. *The Journal of comparative neurology*, 179(1):223–244, 1978. ISSN 1096-9861.

[87] W. Levy and O. Steward. Synapses as associative memory elements in the hippocampal formation. *Brain Research*, 175(2):233–245, 1979. ISSN 0006-8993.

[88] W. Levy and O. Steward. Temporal contiguity requirements for long-term associative potentiation/depression in the hippocampus. *Neuroscience*, 8(4):791–797, 1983. ISSN 0306-4522.

[89] Y. Li, D. Fitzpatrick, and L. White. The development of direction selectivity in ferret visual cortex requires early visual experience. *Nature neuroscience*, 9(5):676–681, 2006. ISSN 1097-6256.

[90] M. Livingstone and D. Hubel. Thalamic inputs to cytochrome oxidase-rich regions in monkey visual cortex. *Proceedings of the National Academy of Sciences of the United States of America*, 79(19):6098, 1982.

[91] T. Lømo. Frequency potentiation of excitatory synaptic activity in the dentate area of the hippocampal formation. *Acta physiol scand*, 68(Suppl 277):128, 1966.

[92] H. Markram, J. Lubke, M. Frotscher, and B. Sakmann. Regulation of synaptic efficacy by coincidence of postsynaptic APs and EPSPs. *Science*, 275(5297):213, 1997.

[93] E. Markus, C. Barnes, B. McNaughton, V. Gladden, and W. Skaggs. Spatial information content and reliability of hippocampal CA1 neurons: effects of visual input. *Hippocampus*, 4 (4):410–421, 1994. ISSN 1098-1063.

[94] E. Markus, Y. Qin, B. Leonard, W. Skaggs, B. McNaughton, and C. Barnes. Interactions between location and task affect the spatial and directional firing of hippocampal neurons. *The Journal of neuroscience*, 15(11):7079, 1995. ISSN 0270-6474.

[95] K. Martin. THE WELLCOME PRIZE LECTURE FROM SINGLE CELLS TO SIMPLE CIRCUITS IN THE CEREBRAL CORTEX. *Experimental Physiology*, 73(5):637, 1988. ISSN 0958-0670.

[96] K. Martin and D. Whitteridge. Form, function and intracortical projections of spiny neurones in the striate visual cortex of the cat. *The Journal of Physiology*, 353(1):463, 1984. ISSN 0022-3751.

[97] L. Martinez, J. Alonso, R. Reid, and J. Hirsch. Laminar processing of stimulus orientation in cat visual cortex. *The Journal of Physiology*, 540(1):321, 2002. ISSN 0022-3751.

[98] T. Masquelier, R. Guyonneau, and S. Thorpe. Spike timing dependent plasticity finds the start of repeating patterns in continuous spike trains. *PloS one*, 3(1):e1377, 2008.

[99] T. Masquelier, R. Guyonneau, and S. Thorpe. Competitive stdp-based spike pattern learning. *Neural computation*, 21(5):1259–1276, 2009.

[100] H. Maturana and S. Frenk. Directional movement and horizontal edge detectors in the pigeon retina. *Science*, 142(3594):977, 1963. ISSN 0036-8075.

[101] B. McNaughton, C. Barnes, and J. O'keefe. The contributions of position, direction, and velocity to single unit activity in the hippocampus of freely-moving rats. *Experimental Brain Research*, 52(1):41–49, 1983. ISSN 0014-4819.

[102] B. McNaughton, B. Leonard, and L. Chen. Cortical-hippocampal interactions and cognitive mapping: A hypothesis based on reintegration of the parietal and inferotemporal pathways for visual processing. *Psychobiology*, 1989. ISSN 0889-6313.

[103] B. McNaughton, C. Barnes, J. Gerrard, K. Gothard, M. Jung, J. Knierim, H. Kudrimoti, Y. Qin, W. Skaggs, W. Suster, et al. Deciphering the hippocampal polyglot: the hippocampus as a path integration system. *Journal of Experimental Biology*, 199:173–185, 1996. ISSN 0022-0949.

[104] M. Mehta and M. Wilson. From hippocampus to V1: Effect of LTP on spatio-temporal dynamics of receptive fields. *Neurocomputing*, 32:905–911, 2000. ISSN 0925-2312.

[105] M. Mehta, C. Barnes, and B. McNaughton. Experience-dependent, asymmetric expansion of hippocampal place fields. *Proceedings of the National Academy of Sciences of the United States of America*, 94(16):8918, 1997.

[106] M. Mehta, M. Quirk, and M. Wilson. Experience-dependent asymmetric shape of hippocampal receptive fields. *Neuron*, 25(3):707–715, 2000. ISSN 0896-6273.

[107] M. Mehta, A. Lee, and M. Wilson. Role of experience and oscillations in transforming a rate code into a temporal code. *Nature*, 417(6890):741–746, 2002. ISSN 0028-0836.

[108] C. Meliza and Y. Dan. Receptive-field modification in rat visual cortex induced by paired visual stimulation and single-cell spiking. *Neuron*, 49(2):183–189, 2006. ISSN 0896-6273.

[109] K. Miller and D. MacKay. The role of constraints in Hebbian learning. *Neural Computation*, 6(1):100–126, 1994. ISSN 0899-7667.

[110] M. Mittelstaedt and H. Mittelstaedt. Homing by path integration in a mammal. *Naturwissenschaften*, 67(11):566–567, 1980. ISSN 0028-1042.

[111] C. Monier, F. Chavane, P. Baudot, L. Graham, and Y. Frégnac. Orientation and Direction Selectivity of Synaptic Inputs in Visual Cortical Neurons:: A Diversity of Combinations Produces Spike Tuning. *Neuron*, 37(4):663–680, 2003. ISSN 0896-6273.

[112] V. Mountcastle. Modality and topographic properties of single neurons of cat's somatic sensory cortex. *J Neurophysiol*, 20(4):408–434, 1957.

[113] Y. Mu and M. Poo. Spike timing-dependent LTP/LTD mediates visual experience-dependent plasticity in a developing retinotectal system. *Neuron*, 50(1):115–125, 2006. ISSN 0896-6273.

[114] R. Muller and J. Kubie. The effects of changes in the environment on the spatial firing of hippocampal complex-spike cells. *The Journal of neuroscience*, 7(7):1951, 1987. ISSN 0270-6474.

[115] R. Muller, J. Kubie, and J. Ranck. Spatial firing patterns of hippocampal complex-spike cells in a fixed environment. *The Journal of neuroscience*, 7(7):1935, 1987. ISSN 0270-6474.

[116] A. Nagahara, T. Otto, and M. Gallagher. Entorhinal-perirhinal lesions impair performance of rats on two versions of place learning in the Morris water maze. *Behavioral neuroscience*, 109(1):3, 1995. ISSN 0735-7044.

[117] J. O'Keefe and N. Burgess. Geometric determinants of the place fields of hippocampal neurons. *Nature*, 381(6581):425–428, 1996. ISSN 0028-0836.

[118] J. O'keefe and D. Conway. Hippocampal place units in the freely moving rat: why they fire where they fire. *Experimental Brain Research*, 31(4):573–590, 1978. ISSN 0014-4819.

[119] J. O'Keefe and J. Dostrovsky. The hippocampus as a spatial map. Preliminary evidence from unit activity in the freely-moving rat. *Brain research*, 34(1):171, 1971.

[120] J. O'Keefe and N. L. The Hippocampus as a Cognitive Map. 1978.

[121] J. O'Keefe and M. Recce. Phase relationship between hippocampal place units and the EEG theta rhythm. *Hippocampus*, 3(3):317–330, 1993. ISSN 1098-1063.

[122] J. O'Keefe and A. Speakman. Single unit activity in the rat hippocampus during a spatial memory task. *Experimental Brain Research*, 68(1):1–27, 1987. ISSN 0014-4819.

[123] D. O'Malley, J. Sandell, and R. Masland. Co-release of acetylcholine and GABA by the starburst amacrine cells. *Journal of Neuroscience*, 12(4):1394, 1992.

[124] A. Peters and B. Payne. Numerical relationships between geniculocortical afferents and pyramidal cell modules in cat primary visual cortex. *Cerebral Cortex*, 3(1):69, 1993. ISSN 1047-3211.

[125] G. Quirk, R. Muller, and J. Kubie. The firing of hippocampal place cells in the dark depends on the rat's recent experience. *The Journal of Neuroscience*, 10(6):2008, 1990. ISSN 0270-6474.

[126] J. Rauschecker and W. Singer. The effects of early visual experience on the cat's visual cortex and their possible explanation by hebb synapses. *The Journal of physiology*, 310(1):215, 1981.

[127] A. Redish. *Beyond the cognitive map: Contributions to a computational neuroscience theory of rodent navigation*. PhD thesis, Tech Report CMU-CS-97-166, Carnegie Mellon University, School of Computer Science, 1997.

[128] A. Redish, E. Rosenzweig, J. Bohanick, B. McNaughton, and C. Barnes. Dynamics of hippocampal ensemble activity realignment: time versus space. *The Journal of Neuroscience*, 20 (24):9298, 2000. ISSN 0270-6474.

[129] R. Reid and J. Alonso. Specificity of monosynaptic connections from thalamus to visual cortex. *Nature*, 378(6554):281–283, 1995. ISSN 0028-0836.

[130] B. Richards, O. Voss, and C. Akerman. GABAergic circuits control stimulus-instructed receptive field development in the optic tectum. *Nature Neuroscience*, 2010. ISSN 1097-6256.

[131] E. Rolls, S. Stringer, and T. Elliot. Entorhinal cortex grid cells can map to hippocampal place cells by competitive learning. *Network: Computation in Neural Systems*, 17(4):447–465, 2006. ISSN 0954-898X.

[132] J. Rubin, D. Lee, and H. Sompolinsky. Equilibrium properties of temporally asymmetric Hebbian plasticity. *Physical Review Letters*, 86(2):364–367, 2001. ISSN 1079-7114.

[133] A. Samsonovich and B. McNaughton. Path integration and cognitive mapping in a continuous attractor neural network model. *Journal of Neuroscience*, 17(15):5900, 1997.

[134] F. Sargolini, M. Fyhn, T. Hafting, B. McNaughton, M. Witter, M. Moser, and E. Moser. Conjunctive representation of position, direction, and velocity in entorhinal cortex. *Science*, 312(5774):758, 2006. ISSN 0036-8075.

[135] A. Saul and A. Humphrey. Spatial and temporal response properties of lagged and nonlagged cells in cat lateral geniculate nucleus. *Journal of Neurophysiology*, 64(1):206, 1990. ISSN 0022-3077.

[136] F. Schenk and R. Morris. Dissociation between components of spatial memory in rats after recovery from the effects of retrohippocampal lesions. *Experimental Brain Research*, 58(1): 11–28, 1985. ISSN 0014-4819.

[137] J. Schummers, J. Sharma, and M. Sur. Bottom-up and top-down dynamics in visual cortex. *Progress in Brain Research*, 149:65–81, 2005. ISSN 0079-6123.

[138] G. Sclar and R. Freeman. Orientation selectivity in the cat's striate cortex is invariant with stimulus contrast. *Experimental Brain Research*, 46(3):457–461, 1982. ISSN 0014-4819.

[139] W. Scoville and B. Milner. Loss of recent memory after bilateral hippocampal lesions. *Journal of Neurology, Neurosurgery & Psychiatry*, 20(1):11, 1957. ISSN 1468-330X.

[140] W. Senn and N. Buchs. Spike-based synaptic plasticity and the emergence of direction selective simple cells: Mathematical analysis. *Journal of Computational Neuroscience*, 14(2):119–138, 2003. ISSN 0929-5313.

[141] J. Sharma, A. Angelucci, and M. Sur. Induction of visual orientation modules in auditory cortex. *Nature*, 404(6780):841–847, 2000. ISSN 0028-0836.

[142] H. Sherk and M. Stryker. Quantitative study of cortical orientation selectivity in visually inexperienced kitten. *Journal of Neurophysiology*, 39(1):63–70, 1976.

[143] A. Shon and R. Rao. Learning temporal patterns by redistribution of synaptic efficacy. *Neurocomputing*, 52:13–18, 2003. ISSN 0925-2312.

[144] A. Shon, R. Rao, and T. Sejnowski. Motion detection and prediction through spike-timing dependent plasticity. *Network: Computation in Neural Systems*, 15(3):179–198, 2004. ISSN 0954-898X.

[145] A. Sillito. The contribution of inhibitory mechanisms to the receptive field properties of neurones in the striate cortex of the cat. *The Journal of physiology*, 250(2):305, 1975. ISSN 0022-3751.

[146] B. Skottun, A. Bradley, G. Sclar, I. Ohzawa, and R. Freeman. The effects of contrast on visual orientation and spatial frequency discrimination: a comparison of single cells and behavior. *Journal of Neurophysiology*, 57(3):773, 1987. ISSN 0022-3077.

[147] T. Solstad, E. Moser, and G. Einevoll. From grid cells to place cells: a mathematical model. *Hippocampus*, 16(12):1026–1031, 2006. ISSN 1098-1063.

[148] D. Somers, S. Nelson, and M. Sur. An emergent model of orientation selectivity in cat visual cortical simple cells. *The Journal of neuroscience*, 15(8):5448, 1995. ISSN 0270-6474.

[149] H. Sompolinsky and R. Shapley. New perspectives on the mechanisms for orientation selectivity. *Current Opinion in Neurobiology*, 7(4):514–522, 1997. ISSN 0959-4388.

[150] S. Song and L. Abbott. Cortical development and remapping through spike timing-dependent plasticity. *Neuron*, 32(2):339–350, 2001. ISSN 0896-6273.

[151] S. Song, K. Miller, and L. Abbott. Competitive Hebbian learning through spike-timing-dependent synaptic plasticity. *nature neuroscience*, 3(9):919–926, 2000.

[152] R. Soodak, R. Shapley, and E. Kaplan. Linear mechanism of orientation tuning in the retina and lateral geniculate nucleus of the cat. *Journal of neurophysiology*, 58(2):267, 1987. ISSN 0022-3077.

[153] B. Stafford, A. Sher, A. Litke, and D. Feldheim. Spatial-temporal patterns of retinal waves underlying activity-dependent refinement of retinofugal projections. *Neuron*, 64(2):200–212, 2009. ISSN 0896-6273.

[154] K. Tanaka. Organization of geniculate inputs to visual cortical cells in the cat. *Vision Research*, 25(3):357–364, 1985. ISSN 0042-6989.

[155] T. Troyer, A. Krukowski, N. Priebe, and K. Miller. Contrast-invariant orientation tuning in cat visual cortex: thalamocortical input tuning and correlation-based intracortical connectivity. *Journal of Neuroscience*, 18(15):5908, 1998.

[156] T. Troyer, A. Krukowski, and K. Miller. LGN input to simple cells and contrast-invariant orientation tuning: an analysis. *Journal of neurophysiology*, 87(6):2741, 2002. ISSN 0022-3077.

[157] T. Tsumoto, W. Eckart, and O. Creutzfeldt. Modification of orientation sensitivity of cat visual cortex neurons by removal of GABA-mediated inhibition. *Experimental Brain Research*, 34(2):351–363, 1979. ISSN 0014-4819.

[158] S. Van Hooser, J. Heimel, S. Chung, S. Nelson, and L. Toth. Orientation selectivity without orientation maps in visual cortex of a highly visual mammal. *Journal of Neuroscience*, 25(1): 19, 2005.

[159] N. Van Strien, N. Cappaert, and M. Witter. The anatomy of memory: an interactive overview of the parahippocampal–hippocampal network. *Nature Reviews Neuroscience*, 10(4):272–282, 2009. ISSN 1471-003X.

[160] T. Vidyasagar and J. Urbas. Orientation sensitivity of cat LGN neurones with and without inputs from visual cortical areas 17 and 18. *Experimental Brain Research*, 46(2):157–169, 1982. ISSN 0014-4819.

[161] T. Vidyasagar, X. Pei, and M. Volgushev. Multiple mechanisms underlying the orientation selectivity of visual cortical neurones. *Trends in neurosciences*, 19(7):272–277, 1996. ISSN 0166-2236.

[162] R. Vislay-Meltzer, A. Kampff, and F. Engert. Spatiotemporal specificity of neuronal activity directs the modification of receptive fields in the developing retinotectal system. *Neuron*, 50 (1):101–114, 2006. ISSN 0896-6273.

[163] L. Von Melchner, S. Pallas, and M. Sur. Visual behaviour mediated by retinal projections directed to the auditory pathway. *Nature*, 404(6780):871–876, 2000. ISSN 0028-0836.

[164] L. Wang, K. Rangarajan, C. Lawhn-Heath, R. Sarnaik, B. Wang, X. Liu, and J. Cang. Direction-specific disruption of subcortical visual behavior and receptive fields in mice lacking the $\beta 2$ subunit of nicotinic acetylcholine receptor. *The Journal of Neuroscience*, 29(41):12909, 2009. ISSN 0270-6474.

[165] A. Watson and A. Ahumada. Model of human visual-motion sensing. *Optical Society of America, Journal, A: Optics and Image Science*, 2:322–342, 1985. ISSN 0740-3232.

[166] O. Wenisch, J. Noll, and J. Hemmen. Spontaneously emerging direction selectivity maps in visual cortex through STDP. *Biological cybernetics*, 93(4):239–247, 2005. ISSN 0340-1200.

[167] L. White, D. Coppola, and D. Fitzpatrick. The contribution of sensory experience to the maturation of orientation selectivity in ferret visual cortex. *Nature*, 411(6841):1049–1052, 2001.

[168] T. Wiesel, D. Hubel, et al. Single-cell responses in striate cortex of kittens deprived of vision in one eye. *J Neurophysiol*, 26(1003):17, 1963.

[169] T. Wiesel, D. Hubel, D. Lam, et al. Autoradiographic demonstration of ocular-dominance columns in the monkey striate cortex by means of transneuronal transport. *Brain Res*, 79(2): 273–279, 1974.

[170] M. Wilson and B. McNaughton. Dynamics of the hippocampal ensemble code for space. *Science*, 261(5124):1055, 1993.

[171] S. Wimbauer, O. Wenisch, K. Miller, and J. Van Hemmen. Development of spatiotemporal receptive fields of simple cells: I. Model formulation. *Biological Cybernetics*, 77(6):453–461, 1997. ISSN 0340-1200.

[172] M. Wong-Riley. Changes in the visual system of monocularly sutured or enucleated cats demonstrable with cytochrome oxidase histochemistry. *Brain Research*, 171(1):11–28, 1979. ISSN 0006-8993.

[173] H. Xu, H. Chen, Q. Ding, Z. Xie, L. Chen, L. Diao, P. Wang, L. Gan, M. Crair, and N. Tian. The Immune Protein CD3 [zeta] Is Required for Normal Development of Neural Circuits in the Retina. *Neuron*, 65(4):503–515, 2010. ISSN 0896-6273.

[174] Y. Yamada, A. Koizumi, E. Iwasaki, S. Watanabe, and A. Kaneko. Propagation of action potentials from the soma to individual dendrite of cultured rat amacrine cells is regulated by local GABA input. *Journal of neurophysiology*, 87(6):2858, 2002. ISSN 0022-3077.

[175] H. Yao, Y. Shen, and Y. Dan. Intracortical mechanism of stimulus-timing-dependent plasticity in visual cortical orientation tuning. *Proceedings of the National Academy of Sciences of the United States of America*, 101(14):5081, 2004.

[176] K. Yoshida, D. Watanabe, H. Ishikane, M. Tachibana, I. Pastan, and S. Nakanishi. A key role of starburst amacrine cells in originating retinal directional selectivity and optokinetic eye movement. *Neuron*, 30(3):771–780, 2001. ISSN 0896-6273.

[177] L. Zhang, H. Tao, C. Holt, W. Harris, and M. Poo. A critical window for cooperation and competition among developing retinotectal synapses. *Nature*, 395(6697):37–44, 1998. ISSN 0028-0836.

[178] J. Zheng, S. Lee, and Z. Zhou. A developmental switch in the excitability and function of the starburst network in the mammalian retina. *Neuron*, 44(5):851–864, 2004. ISSN 0896-6273.